NASA CONTRACTOR REPORT NASA CR-62085

GEOS-II C-BAND RADAR SYSTEM PROJECT FINAL REPORT SPECTRAL ANALYSIS AS RELATED TO C-BAND RADAR DATA ANALYSIS

STUDIES PERFORMED UNDER CONTRACTS NAS6-1467 AND NAS6-1628

By:
Wolf Research and Development Corporation
Range Engineering Department
Riverdale, Maryland
And:
RCA Corporation
Missile and Surface Radar Division
Moorestown, New Jersey

Prepared for:
NATIONAL AERONAUTICS AND SPACE ADMINISTRATION
WALLOPS STATION
WALLOPS ISLAND, VIRGINIA 23337

October 1972

GEOS-II C-BAND RADAR
SYSTEM PROJECT

FINAL REPORT

SPECTRAL ANALYSIS AS RELATED TO C-BAND RADAR DATA ANALYSIS

STUDIES PERFORMED
FOR
NASA/WALLOPS STATION
UNDER
CONTRACTS NAS6-1467 AND NAS6-1628
NASA Technical Monitor - H.R. Stanley

BY
WOLF RESEARCH AND DEVELOPMENT CORPORATION
Range Engineering Department
Riverdale, Maryland

and

RCA CORPORATION
Missile and Surface Radar Division
Moorestown, New Jersey

October 1972

TABLE OF CONTENTS

LIST OF FIGURES

LIST OF FIGURES (Cont.)

LIST OF FIGURES (Cont.)

LIST OF TABLES

1.0 INTRODUCTION

1.1 SUMMARY

This report describes the work performed on spectral analysis of data from the C-Band radars tracking GEOS-II and on the development of a data compaction method for the GEOS-II C-Band radar data.

The purposes of the spectral analysis study were to determine the optimum data recording and sampling rates for C-Band radar data and to determine the optimum method of filtering and smoothing the data. The optimum data recording and sampling rate is defined as the rate which includes an optimum compromise between serial correlation and the effects of frequency folding. The goal in development of a data compaction method was to reduce to a minimum the amount of data stored, while maintaining all of the statistical information content of the non-compacted data.

A digital computer program for computing estimates of the power spectral density function of sampled data was used to perform the spectral analysis study. See Section 1.3.1 and Section A-2 of Appendix A for details. The spectral analysis was performed on raw data, before any filtering or data correction operations were performed, so that the data analyzed contained signal and noise components unmodified by data processing.

The first study performed, described in Section 2.1.1, determined the signal cut-off frequency. It was determined

that for range, azimuth, and elevation data on tracks of GEOS-II, the signal component of the data is concentrated in frequencies below .05 Hertz. The second study on spectral content of the data, described in Sections 2.1.2 and 2.1.3, was conducted to define the spectral characteristics of the noise content of the data, at frequencies above .05 Hertz. The results are summarized in Section 3.1.1.

Based on the results of the spectral analysis studies, it was determined that low-pass linear digital filtering of the raw data would reduce the noise content of the data significantly while not degrading the signal content. A digital computer program to implement this approach was used to conduct studies on the properties of filtered data. The approach and the computer program are discussed in Section 1.3.2 and in Section A-3 of Appendix A.

The data studies conducted using the filtering and compaction program are discussed in Section 2.2. These studies consisted of orbital reductions, using both filtered and unfiltered data, and a comparison of the orbits and of the data residuals from the two sets of data. The major conclusions to be drawn from these studies are that filtering improves the precision of the data, as demonstrated by the RMS of the short arc reductions or by examining the residual plots, and that filtering does not significantly affect the accuracy of the data, as demonstrated by comparison of the orbital elements and by data extrapolation. Details of these conclusions are given in Section 3.1.2.

Studies to determine the possible serial correlation of filtered and unfiltered data were conducted using a program to compute the auto-covariance function, as described in Section 2.3. Two sets of data with known abnormalities were investigated, the ship test data study as described in Section 2.3.2 and the PMRMR1 data as described in Section 2.3.3. These studies indicate that calculations of the auto-covariance function can be used to investigate abnormal data. The investigation of the auto-covariance function of residuals from short-arc orbits, using both filtered and unfiltered data, is reported in Section 2.3.4. The results indicate that serial correlation of short arc residuals is not dramatically affected by data filtering.

In order to implement the digital studies described, computer programs designed for the purpose were developed. These programs are described, in general, in Appendix A, and in Reference 2, and the detailed theory used is given in Reference 1.

1.2 STUDY GOALS

The goals of this segment of the effort are:

a) Evaluation and analysis of the spectral content of the radar data.

b) Development, implementation and documentation of a data compaction and reformatting scheme suitable for supplying C-Band data to the National Space Science Data Center.

1.2.1 Spectral Analysis

The first goal of this effort was to determine the spectral content of the Wallops AN/FPQ-6 and AN/FPS-16

radar measurement channels. Determination of spectral content, or power spectral density estimation, is concerned with decomposition of the time domain signal from a particular channel into periodic components, as a function of frequency, and determining the average power in each component. The term "power" used in this context refers to the mean squared amplitude of the component, in analogy to the mean squared amplitude of a sinusoidal voltage passed through a unit resistance. Spectral analysis is based on the mathematical principle that a set of data points representing a function of time can be transformed into a set of data representing a function of frequency. The frequency domain representation of the data is called the spectrum, or the spectral representation, of the time domain representation. The process of transforming data from the time domain to the frequency domain, and then evaluating the spectral characteristics, is called spectral analysis. The process of transformation from one domain to another does not add or subtract any information from the data. The information content of the frequency domain data is the same as that of the time domain data.

Frequency domain analysis is a valuable tool when we wish to consider the effects of an additive measurement error. The radar data we are considering is the result of the measurement of a continuous physical process, and the measurements have had random errors added to them in the measurement process. In frequency domain terminology, which was derived from communications engineering, the error-free measurements are referred to as the signal and the additive errors are called noise. Each time domain point contains both the signal and noise components. In the frequency domain, however, the signal component tends

to be concentrated in the low frequency portion of the data, while the noise is spread over a wider range of the frequency band. To the extent that this is true, it is possible to distinguish between signal and noise in the frequency domain and to define methods for eliminating the noise.

Spectral analysis is worth doing when the frequency domain representation can tell us more about the data than we can obtain from the time domain function. This condition is true when we are dealing with data which has been passed through a time invariant linear system. The effect of a time invariant linear system on each frequency component of the spectral representation of a function is multiplication by a constant phase angle. Since a radar instrument can be approximated by a time invariant linear system, spectral analysis of radar data can help in analyzing the effects of the radar on the data, and help to predict the effects of further data processing.

Another piece of information to be obtained from spectral analysis involves the tradeoffs in the choice of a sampling interval for data. The power spectrum of a data array and autocorrelation function of the data are a Fourier transform pair. That is, the power spectrum is the frequency domain representation of the autocorrelation function. If the power spectrum of the noise has a cutoff at a frequency f_c, the sampling theorem says that data sampled at an interval of more than $1/(2f_c)$ is subject to aliasing or frequency folding. For a very narrow band signal, this aliasing does not degrade the data if the sampling interval is less than $1/f_c$. This is a frequency domain constraint on the sampling interval. The time domain constraint on the sampling interval is based on the autocorrelation

function. Many methods of statistical data reduction, including orbit determination methods, contain error estimates based on an assumption of zero (or negligible) serial correlation between data points. On this basis, the sampling interval should be the time for which the autocorrelation is sufficiently small.

1.2.2 Data Compaction

For much geodetic work, such as the estimation of geopotential coefficients or the recovery of station positions, long arcs of data must be processed. At the normal sampling rate for most radars of ten observations per second an excessive number of observations must be processed. The solution is not simply to discard data. A method based on simply selecting each Nth point and discarding N-1 of every N points will throw away information with the discarded points. In the frequency domain representation, this method of data compaction introduced aliasing or frequency foldover of the higher frequency noise components of the spectrum. For example, if data containing a 1 hz noise component is sampled at 1/second, the 1 hz component becomes a bias error.

A data smoothing or filtering scheme must be used so that the frequency of observations, or sampling rate, is significantly reduced while the majority of the original information is retained. The design goal is to reduce to a minumum the amount of data that is necessary to maintain the statistical information content of the non-compacted data. The filtering operation must decrease the bandwidth of the noise content of the data, so that

the cut-off frequency f_c is reduced. Then the data selection interval can be chosen to avoid frequency foldover effects and to minimize serial correlation of the data.

1.3 TECHNICAL APPROACH

1.3.1 Power Spectrum Estimation by Fourier Methods

The power spectrum is an idealized mathematical concept and in the strictest sense is defined only for an infinite set of data. From any given finite set of data we can only obtain an estimate of the power spectrum of a hypothetical set of infinite data from which the finite set is a sample.

An intuitive, non-mathematical, definition of the power spectrum is based on the concept of passing the function through a parallel array of very narrow band pass filters. Each filter is an idealized perfect filter, with unit gain and zero phase shift in a narrow band, and zero gain outside that band. The pass bands of the set of filters are non-overlapping, and cover the frequency band from zero to infinity. Then the output of each filter is squared, and the average power over time is obtained by integrating and obtaining a time average. If the band width of each filter is allowed to approach zero, and the time over which the power is averaged approaches infinity, the resulting output is the power spectrum of the input function.

Two approaches have been used in the past to obtain spectral density estimates from sampled data. The

direct approach uses the digital Fourier transform to obtain a spectral representation of the data, then obtains the estimate of power spectral density by squaring the spectrum and averaging to smooth the estimated power spectrum. Various methods of smoothing of the power spectrum are used. Smoothing or averaging of the spectrum is necessary because the unsmoothed squared spectral function, or periodogram, is a statistically unstable estimator of the spectral density.

The indirect method of obtaining an estimated power spectrum is the method most widely described in the literature, because it was the most widely used until a few years ago. The indirect method consists of obtaining an estimate of the auto-covariance function of the data by taking mean lagged products, then Fourier transforming the estimated auto-covariance function to obtain an estimated power spectral density function. The indirect method is based on a theorem of Fourier analysis which states that the auto-covariance function and the power spectral density are a Fourier transform pair.

The reason for the widespread use of the indirect method is not that it is theoretically better, because the indirect and the direct methods are theoretically equivalent. The indirect method was used because, before discovery of the fast Fourier transform, the direct method involved much too much computing time. Since the use of the fast Fourier transform has become widespread, the indirect method is being used less.

For this project, the direct method was used. The calculation of the periodogram is implemented by use of

the fast Fourier transorm method. Two types of smoothing of the periodogram were programmed and used, a linear smoothing to increase resolution on the signal components of the data and a quadratic smoothing to decrease the variance of the estimation of the noise components. The theory of the methods used is discussed in Reference 1.

1.3.2 Data Compaction Using Digital Filtering

The method selected for use in preparing input data for data compaction was the use of linear digital filters. In the following discussion, the term "digital filter" rather than "linear digital filter" will often be used, but in general, the reference is to linear digital filters.

This distinction is made because any mathematical operation which changes the frequency content of a set of data can be considered to be a digital filter. For example, if an orbit is computed using measured range, azimuth and elevation data and then the (R, A, E) variables are computed from that orbit at the measurement times, those computed variables can be considered to be the result of filtering the original data by use of the orbital equations.

The decision to use linear digital filters for the data compaction method, rather than use a more elaborate "filter" such as a short arc orbit or a state variable dynamic model, was based on a desire not to introduce a priori assumptions into the analysis at this early stage. Any sophisticated data filtering method such

as fitting to an orbit involves deciding on a system model which can in any case only approximate the actual dynamics of the system being observed. The approximations introduced into the model can produce trends and biases into the resulting data. For example, the effects of station survey errors and gravity model errors can introduce trends and biases into an orbit reduced from the data. An investigator desiring to use the data at a later date would not be able to remove these trends and biases if he desired to use a different dynamic model.

The use of a linear digital filter in data preparation involves only a very simple model of the data which is valid over a much shorter time interval than an orbital pass. That model is contained in the assertion that the signal portion of the data is concentrated in the low frequency part of the spectrum, and that the high frequency part of the spectrum is all noise. Then a low pass filter, which acts as an identity operator on the low frequency components and effectively removes all high frequency components, will remove much of the noise without changing the signal.

A linear digital filter operates on an input sequence x to produce an output sequence y. If the previously values of y are used in the computation of the next value, the filter is called recursive. If only input sequence values are used in computing each value of the output sequence, the filter is non-recursive.

For the applications in which we will be interested, non-recursive filters have the most general use. Recursive filters are more generally applicable to real time applications, in simulation or in digital control systems.

We are concerned here with a data processing application, in which the data to be filtered is stored in an array, with no distinction between "past", "present" or "future". In this situation, non-recursive filters can be used and are more versatile and general in application than recursive filters.

The specific use for the digital filters will be as low-pass filters, to eliminate the noise component of the data while retaining the signal component. The filters to be used must be highly selective, with a very sharp cut-off above a specified frequency. In order to attain this high selectivity with a very narrow band low-pass filter, a large number of data input points must be filtered to obtain each output point. The method used to implement these filters employs the Fourier Convolution theorem. The process of applying a non-recursive digital filter to a set of data is mathematically equivalent to obtaining the convolution of the filter coefficients with the set of data. The Fourier Convolution theorem states that the convolution of two functions is the inverse Fourier transform of the products of the Fourier transforms of the two functions. This method is used for digital filtering because the employment of the fast Fourier transform algorithm makes it much more efficient than the direct convolution.

A disadvantage in the use of non-recursive filters is loss of data points at both ends of the data span. The non-recursive filter can also be regarded as a weighting function, consisting of a symmetric array of coefficients which are multiplied by the input data points to produce one output data point at the center of the array. It is

impossible to obtain output data at the ends of the input data array because the weighting function must be applied to the input data symmetrically about the output data point. The number of data points lost in the filtering process is one half of the number of points in the filter minus one. The disadvantage of loss of data points is increased because the number of coefficients in the filter is dependent on the shaprness of the required cut-off. To a close approximation, the minimum number of points in the filter is inversely proportional to the cut-off frequency desired. Thus a tradeoff between cut-off frequency and data points lost must be considered. Such a trade-off is described in Section 3.2.

1.3.3 Use of Finite Fourier Transform

The theory of the methods used for power spectrum estimation and for computation of digital filters is based on the digital Fourier transofrm, which has been known and used for many years. The actual numerical methods used are based on a special way of calculating the digital Fourier transform, which was developed only a few years ago and which is called the fast Fourier transform. The fast Fourier transform algorithm is only a very efficient method of calculating the digital Fourier transform, and does not add anything the the theory of what can be done. In practice, because of the great decrease of computing time brought about by its use, the fast Fourier transform actually makes possible the application of Fourier analysis methods to routine problems.

2.0 RADAR DATA STUDIES PERFORMED

The computer programs described in Appendix A were used to perform studies on the C-Band radar data. Most of the radar data used as inputs to the programs was taken from the GEOS-II tracking records. However, since the GEOS-II tracking data is almost all beacon track, data from other satellites was used for some of the studies of skin track characteristics.

2.1 SPECTRAL ANALYSIS STUDIES

The spectral analysis studies were carried out using the SPECDEN program, described in Appendix A. The goal of these studies was to determine the spectral characteristics of the radar measurement data from the Wallops AN/FPQ-6 and AN/FPS-16 radars. All of the spectral analysis studies were carried out on data containing both signal and noise. The data was not filtered or modified in order to remove the signal component before analyzing the noise characteristics. The basis of the decision not to prefilter the data in any fashion, before spectral analysis, was the desire to avoid any possibility that the spectral content of the data had been modified by the filtering process. The investigation was divided into two phases, first, to define as well as possible the cut-off frequency of the signal component of the data, and second to obtain the spectral characteristics of the noise component of the data.

2.1.1 Signal Cut-Off Determination

The spectral analysis of any data containing both signal and noise must be planned on the basis of some knowledge of the characteristics of the data. This is a

seeming paradox: that the analysis cannot proceed until the results of the analysis are known. The paradox must be resolved by performing some preliminary analysis based on general knowledge of the data to be analyzed. The signal cut-off determination studies reported here were part of that preliminary analysis.

It was known that the signal component of the data was very large by comparison with the noise component. The signal component is of the order of magnitude of 10^7 meters; the noise of the order of magnitude of 1 meter. It was also known that the signal component is concentrated at the low end of the frequency spectrum. Based on these two facts, a linear smoothing, or spectral window, as described in Appendix A, Section A.2.1, must be applied to the spectrum to prevent spectral leakage of the signal component into the higher frequency spectral bands.

A series of test runs on actual range data, similar to those performed on simulated data and discussed in Section A.2.2, were performed to determine the amount of smoothing required. The linear smoothing selected was the application of the hanning window, three times. For these runs quadratic smoothing, by averaging of spectral estimates over a frequency band, was not used because the highest possible resolution on the spectrum was desired, at the expense of a large variance in the spectral estimates of the noise content. (Appendix A, Section A.2.1 and Lecture 5 of Reference 1 present more detail on the effects of linear and quadratic smoothing of spectral estimates).

Data runs were then made using the selected smoothing method on data from 23 satellite passes, to determine the effective signal cut-off frequency. Figures 1, 2, and 3 present typical results of the computations. From each satellite pass, 3000 data points at 10/second were used in the spectral estimate, yielding a frequency resolution of .00333 hertz. Only the first .333 hertz of the total frequency range (0 - 5 hertz) is plotted, as the region of interest in the determination of signal cut-off is at low frequencies. Figure 1 presents range data, Figure 2 elevation data and Figure 3 azimuth data from GEOS Rev 5050, taken by the Wallops AN/FPQ-6 radar (NWALI3).

The spectral density estimate for the range data, plotted in Figure 1 shows a well defined signal peak at 0 frequency, about 125 db. The signal peak drops off smoothly, and at about .05 Hz merges with an apparent white noise at a level of -20 to -30 db. The spectral estimates of the noise are what would be expected from the the method used, which is not designed for optimum estimation of noise characteristics. The noise data scatter, almost 30 db, is in agreement with theory. The apparent short period trends are evidence of the serial correlation caused by application of the linear window function.

All of the spectral density estimates for range data, performed using the above methods, showed the same characteristics. The cut-off frequency varied between .033 hertz and .05 hertz, and the average level of the noise spectrum varied at most 3 db, among the data taken from beacon track records. Spectral estimates performed on range data from a skin track mission, using the same computational methods show similar results, as shown in Figure 4. The noise level

FIGURE 1

POWER SPECTRAL DENSITY VS FREQUENCY
RANGE DATA, GEOS REV 5050, NWALI3
SIGNAL CUT-OFF DETERMINATION

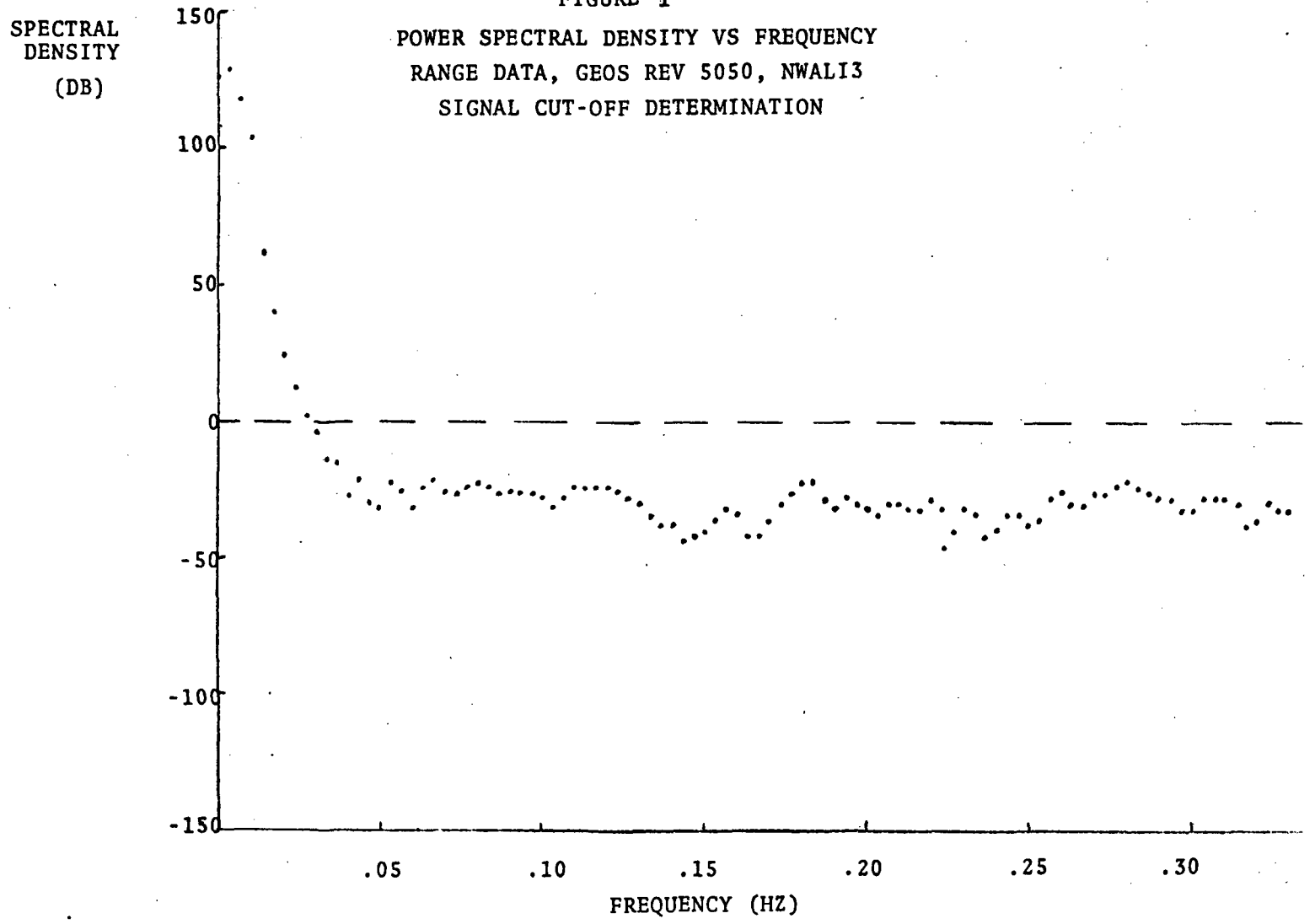

FIGURE 2

POWER SPECTRAL DENSITY VS FREQUENCY
ELEVATION DATA, GEOS REV 5050, NWALI3
SIGNAL CUT-OFF DETERMINATION

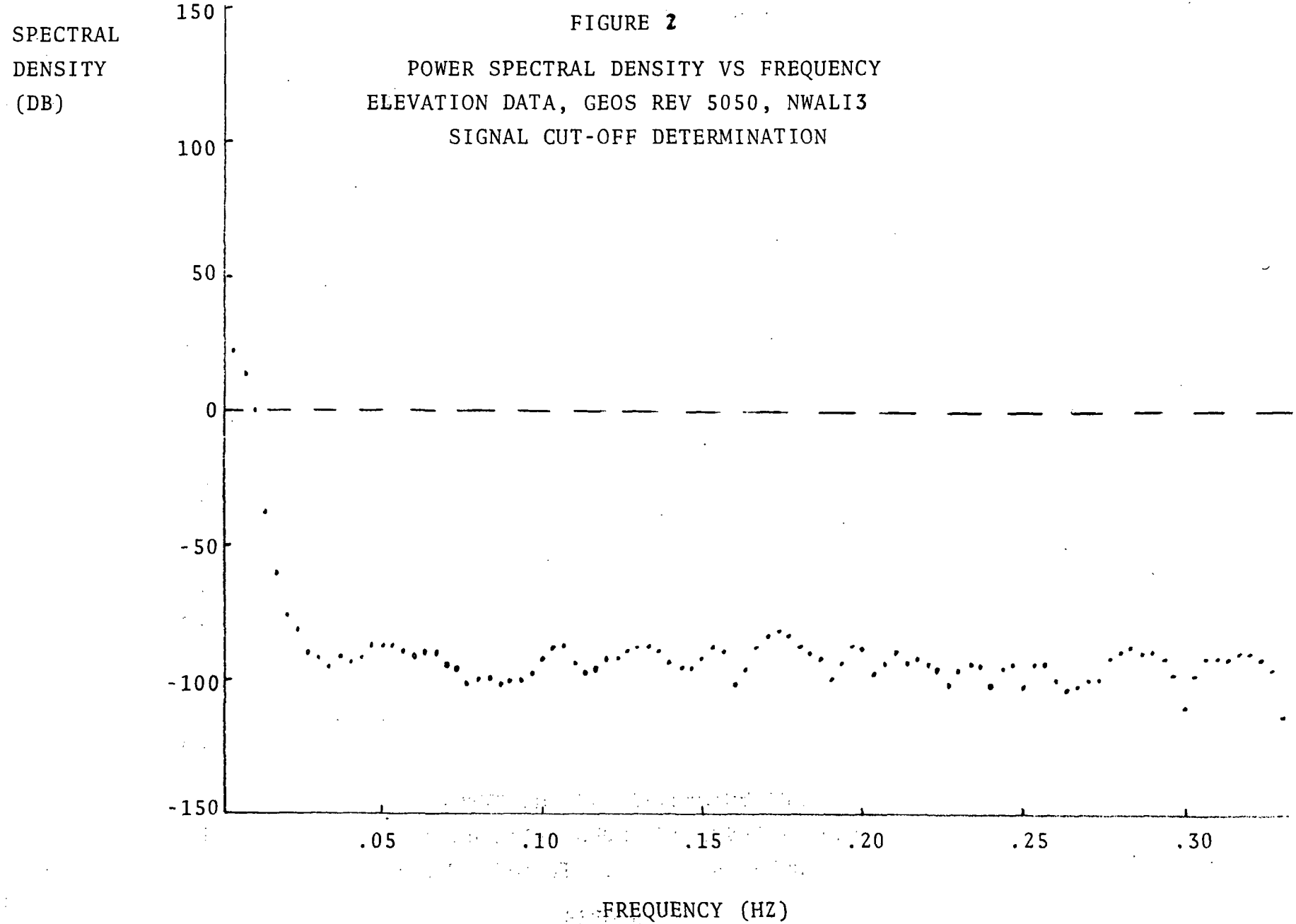

FIGURE 3

POWER SPECTRAL DENSITY VS FREQUENCY
AZIMUTH DATA, GEOS REV 5050, NWALI3
SIGNAL CUT-OFF DETERMINATION

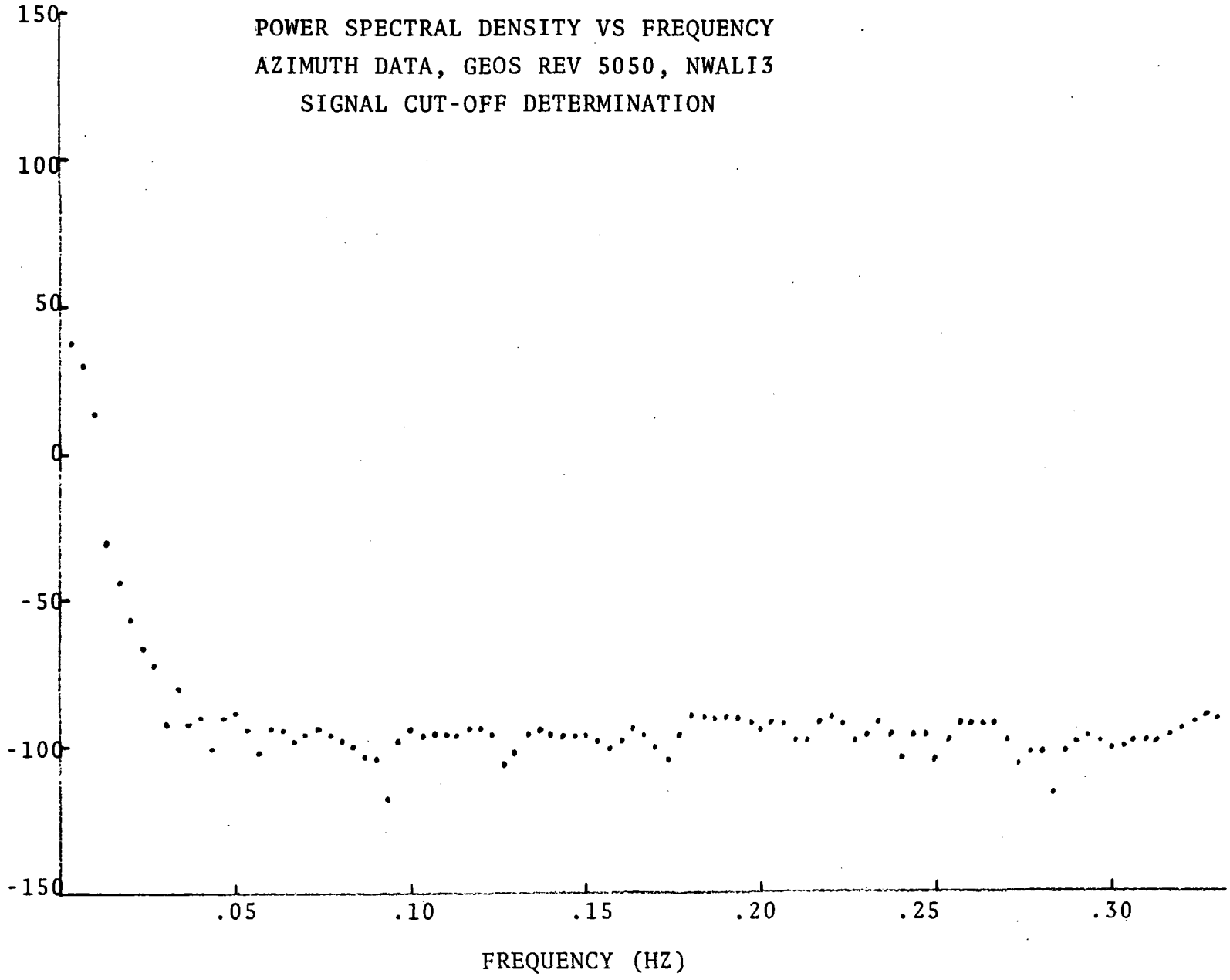

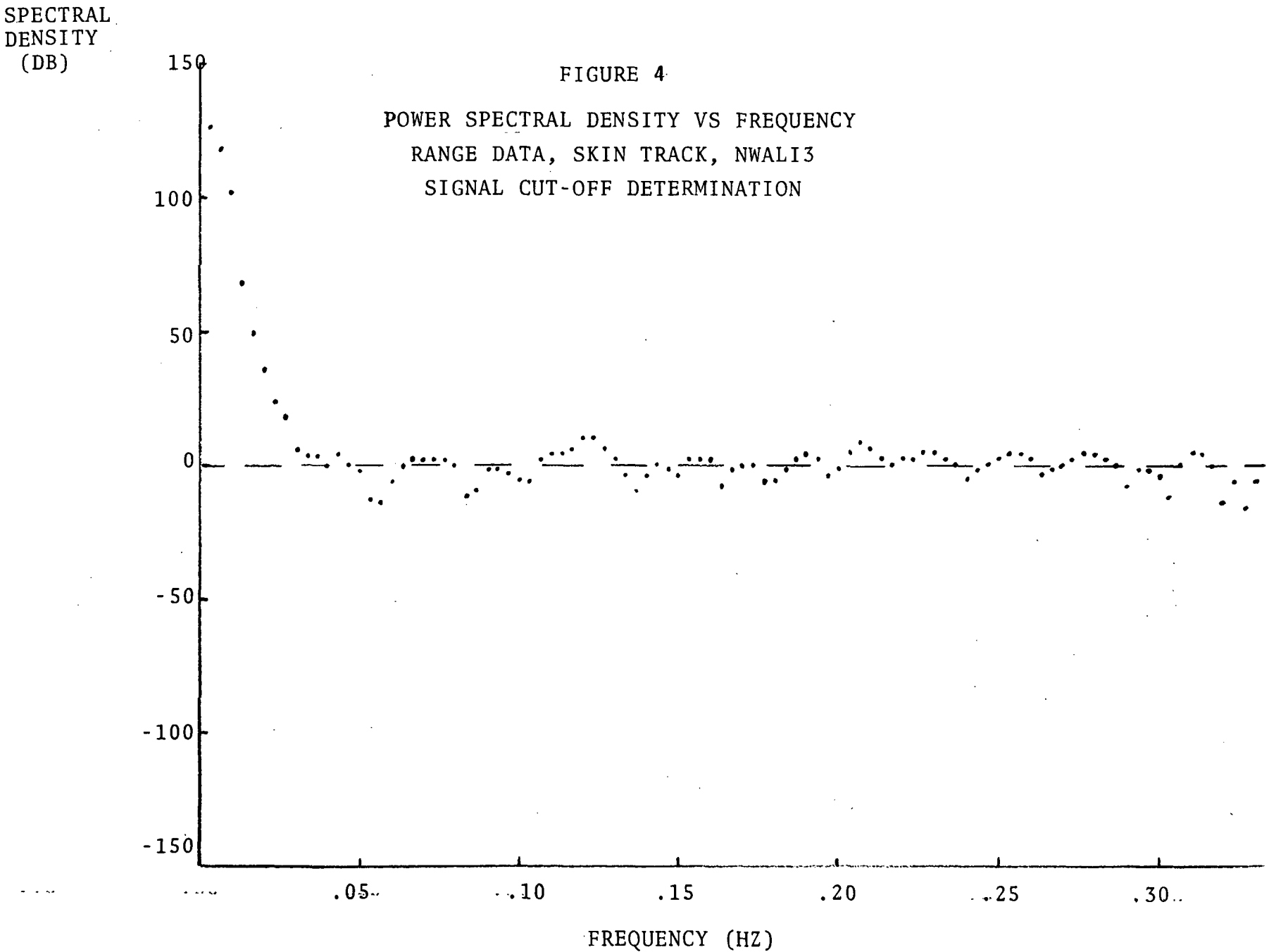

FIGURE 4

POWER SPECTRAL DENSITY VS FREQUENCY
RANGE DATA, SKIN TRACK, NWALI3
SIGNAL CUT-OFF DETERMINATION

is about 30 db higher than that of the beacon track, and the signal cut-off frequency is about .033 hertz.

Spectral density estimates of the elevation data and azimuth data, as shown in Figures 2 and 3 show a signal cut-off at about .033 hertz and a noise level of -90 to -110 db. These results are also typical of all of the data examined.

The conclusion to be drawn from this study is that the signal content of the data is effectively contained in frequencies below .05 hertz. It is possible, and indeed probable, that this conclusion is conservative. Since the windowing or linear smoothing method used has the effect of broadening any spectral peak, the signal cut-off frequency can be as much as .01 hertz less than that shown.

2.1.2 Beacon Track Spectral Analysis

The studies described above led to adoption of a standard method for obtaining power spectral density estimates from the radar measurement data. The method is as follows:

a) 3000 data points, sampled at 10/second, were used for all spectral estimates. The nyquist, or folding frequency, is 5 hertz for data sampled at 10/second, and the frequency resolution of the raw periodogram is .00333 hertz.

b) The data was not prefiltered to remove the signal content. Three successive applications of the hanning frequency window were done, to decrease spectral leakage from the signal component of the data.

c) The raw periodogram was smoothed to reduce noise variance by averaging over 15 adjacent points. This reduced the spectral resolution (interval between data points on the frequency axis) to .05 hertz. The number of degrees of freedom of the estimate of each spectral point is 30, and the spread, in db, including 80% of the data points is about 3 db. (See Reference 1, page 5-18).

Data from 20 revolutions of GEOS-II, taken from measurements by the Wallops AN/FPQ-6 and AN/FPS-16 radars, were reduced by this method. The results for GEOS rev 5050 are plotted on Figure 5 through 10.

The power spectral density of the range measurements on rev 5050, from the Wallops AN/FPQ-6, are plotted on Figure 5. The plot shows the signal spectral peak at 0 db and the noise spectrum essentially flat from .1 hz to 5.0 hz. This spectrum is typical of all of those examined. The similar spectral density estimate for range data from the AN/FPS-16 is shown on Figure 8.

Figure 6 shows the spectral density estimate for the elevation data from the Wallops AN/FPQ-6. This plots shows a noise spectrum falling off linearly about 10 db between .05 hertz and 2 hertz, then decreasing another 3 db out to 5 hertz. Two frequency spikes appear at exactly 2 and exactly 4 hertz. It has been determined that these spikes are caused by an eccentricity in the elevation encoder mechanism, which creates errors with a fundamental frequency of 8 hertz, plus harmonics at 16, 24 and 32 hertz. The 8 and 32 hertz components fold to 2 hertz, and the

FIGURE 5

POWER SPECTRAL DENSITY VS FREQUENCY
RANGE DATA, GEOS REV 5050, NWALI3

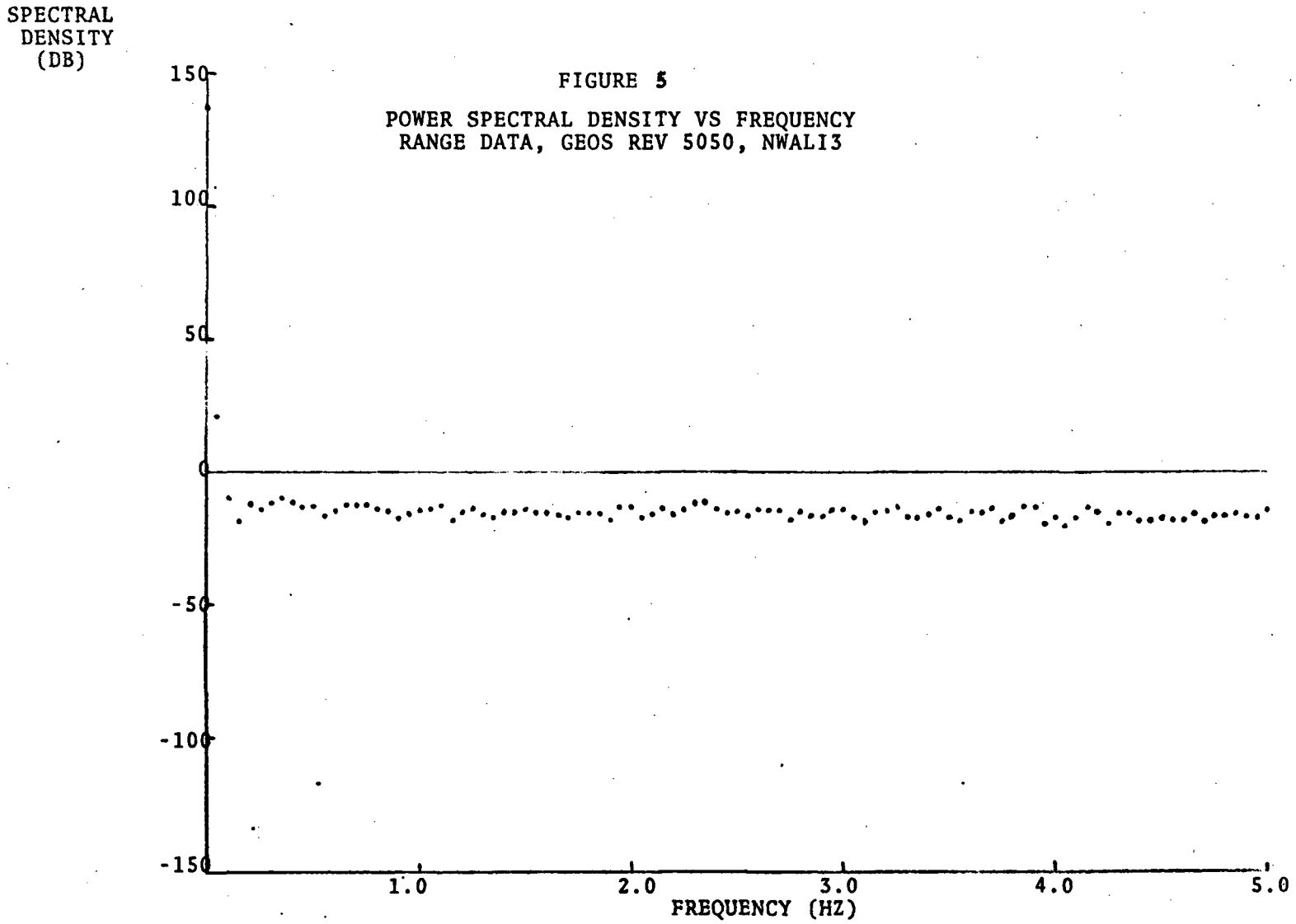

FIGURE 6

POWER SPECTRAL DENSITY VS FREQUENCY
ELEVATION DATA, GEOS REV 5050 NWALI3

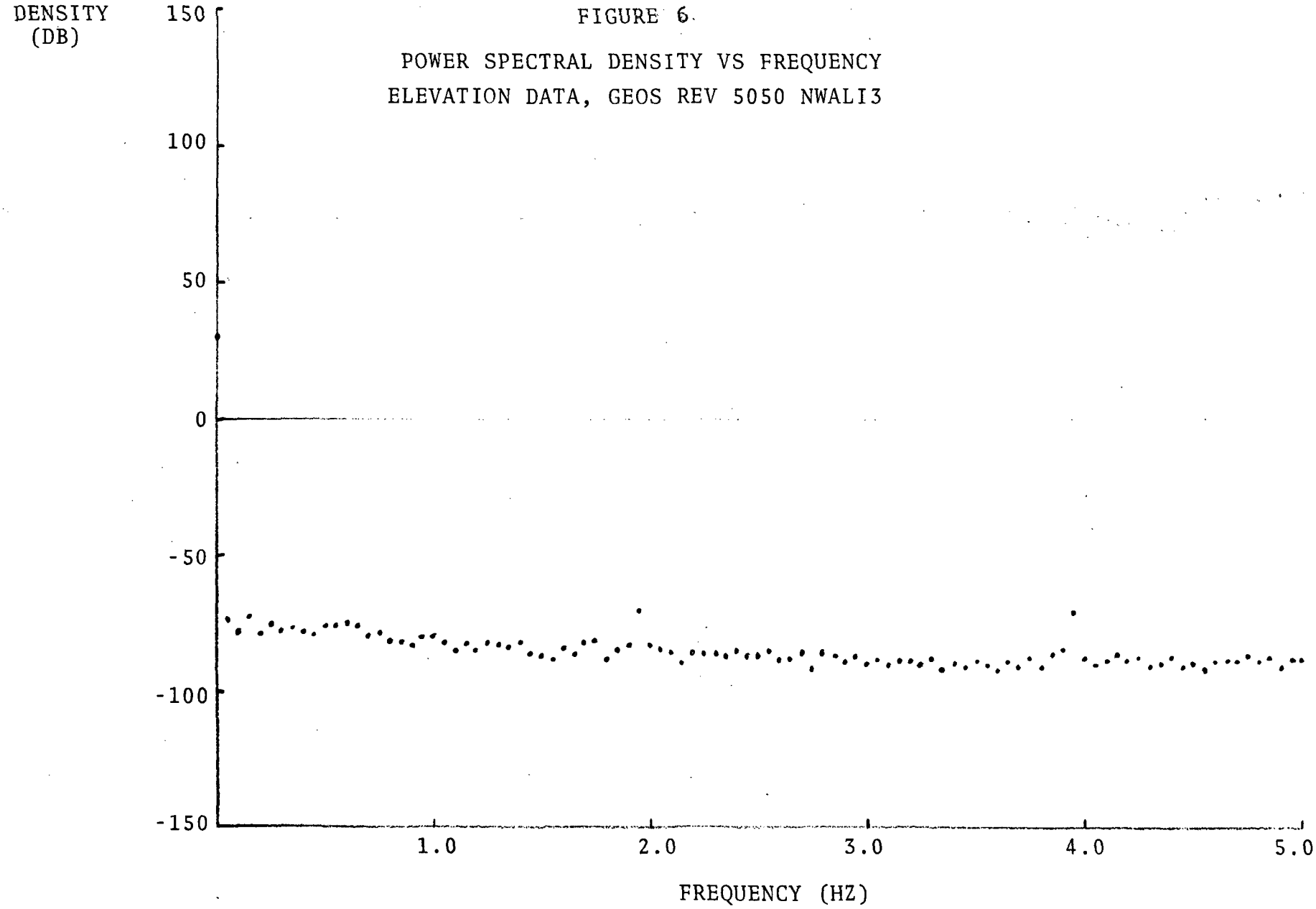

FIGURE 7

POWER SPECTRAL DENSITY VS FREQUENCY
AZIMUTH DATA, REV 5050 NWALI3

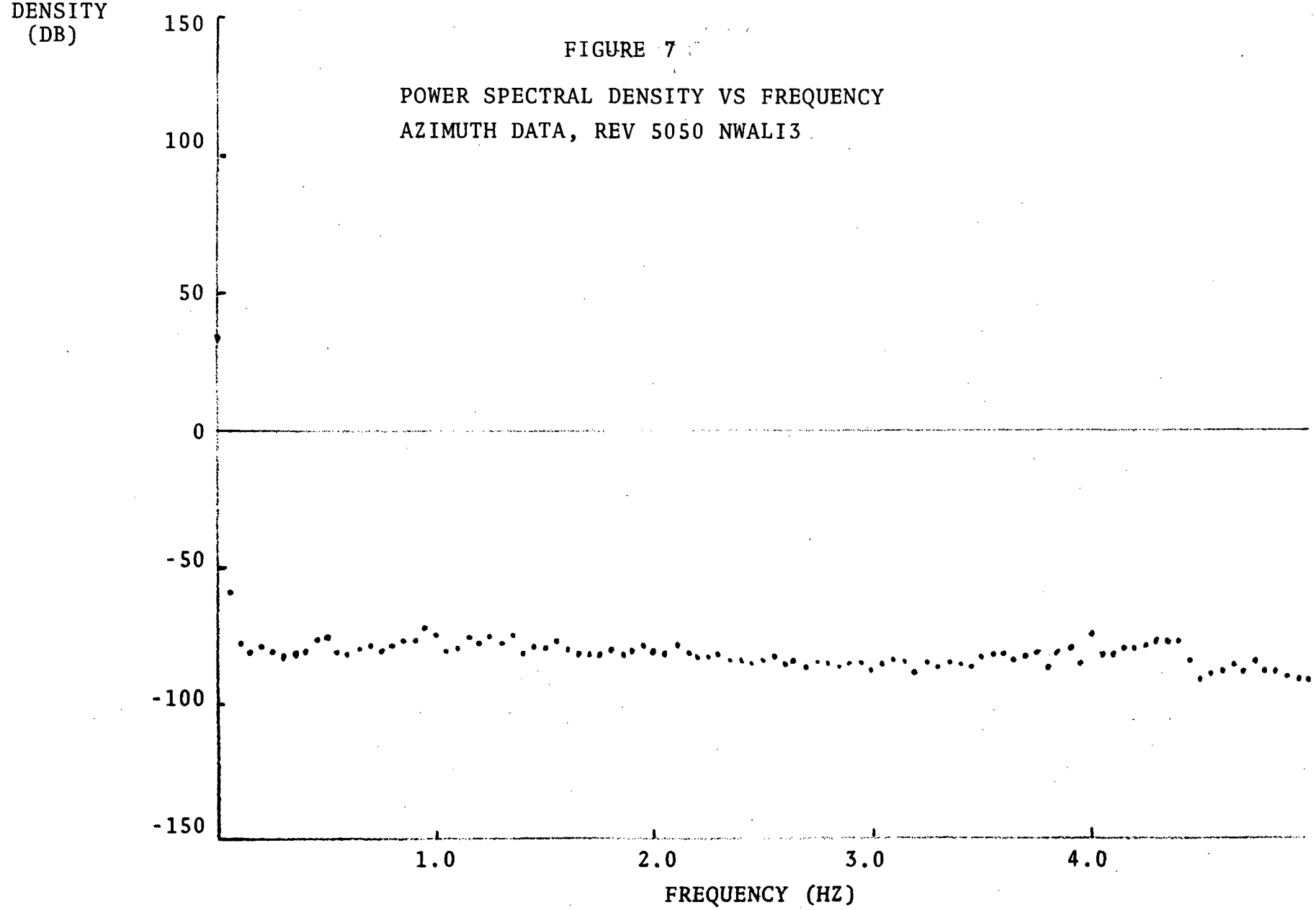

FIGURE 8

POWER SPECTRAL DENSITY VS. FREQUENCY

RANGE DATA, GEOS REV 5050, NWALI8

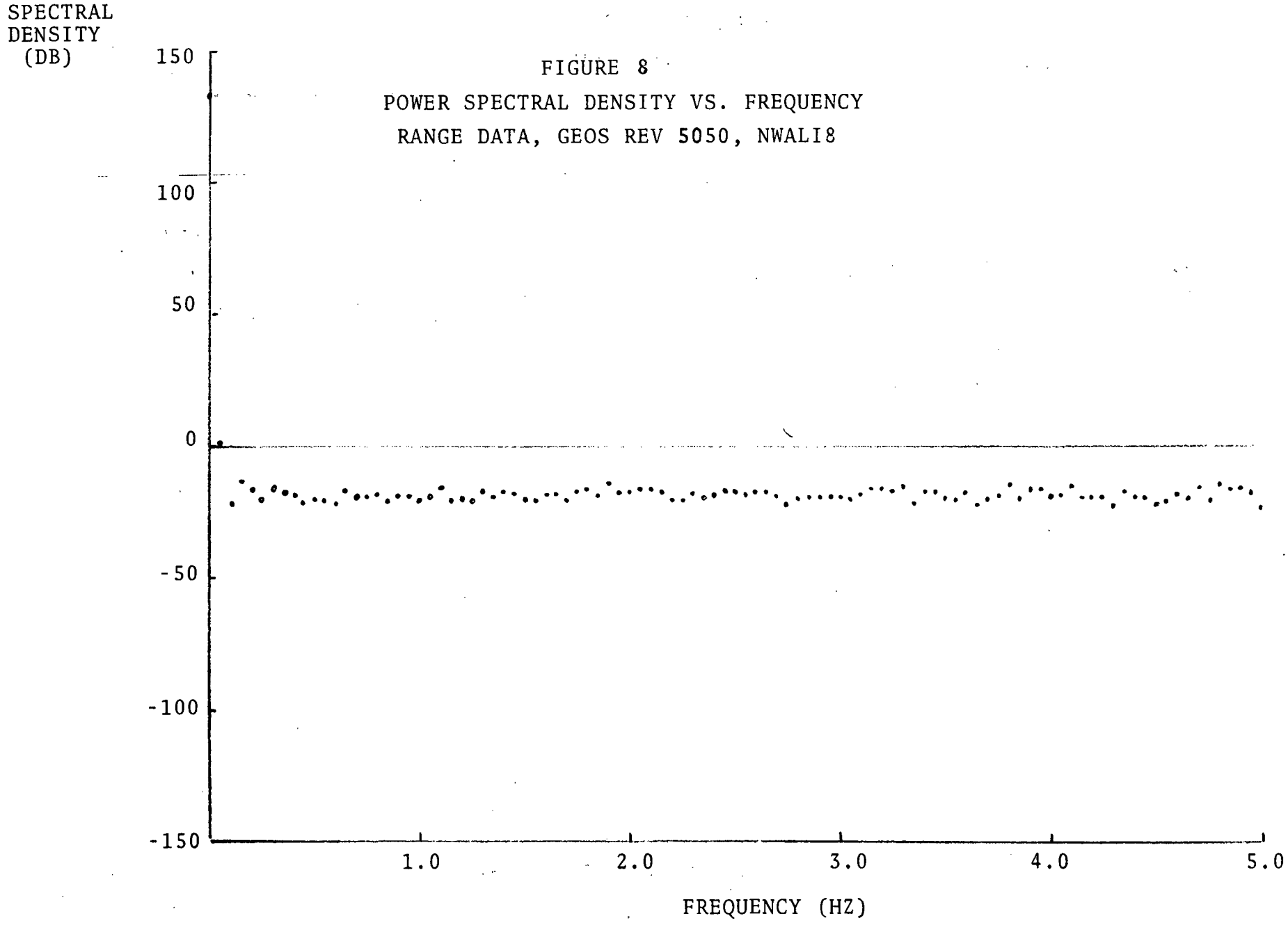

FIGURE 9

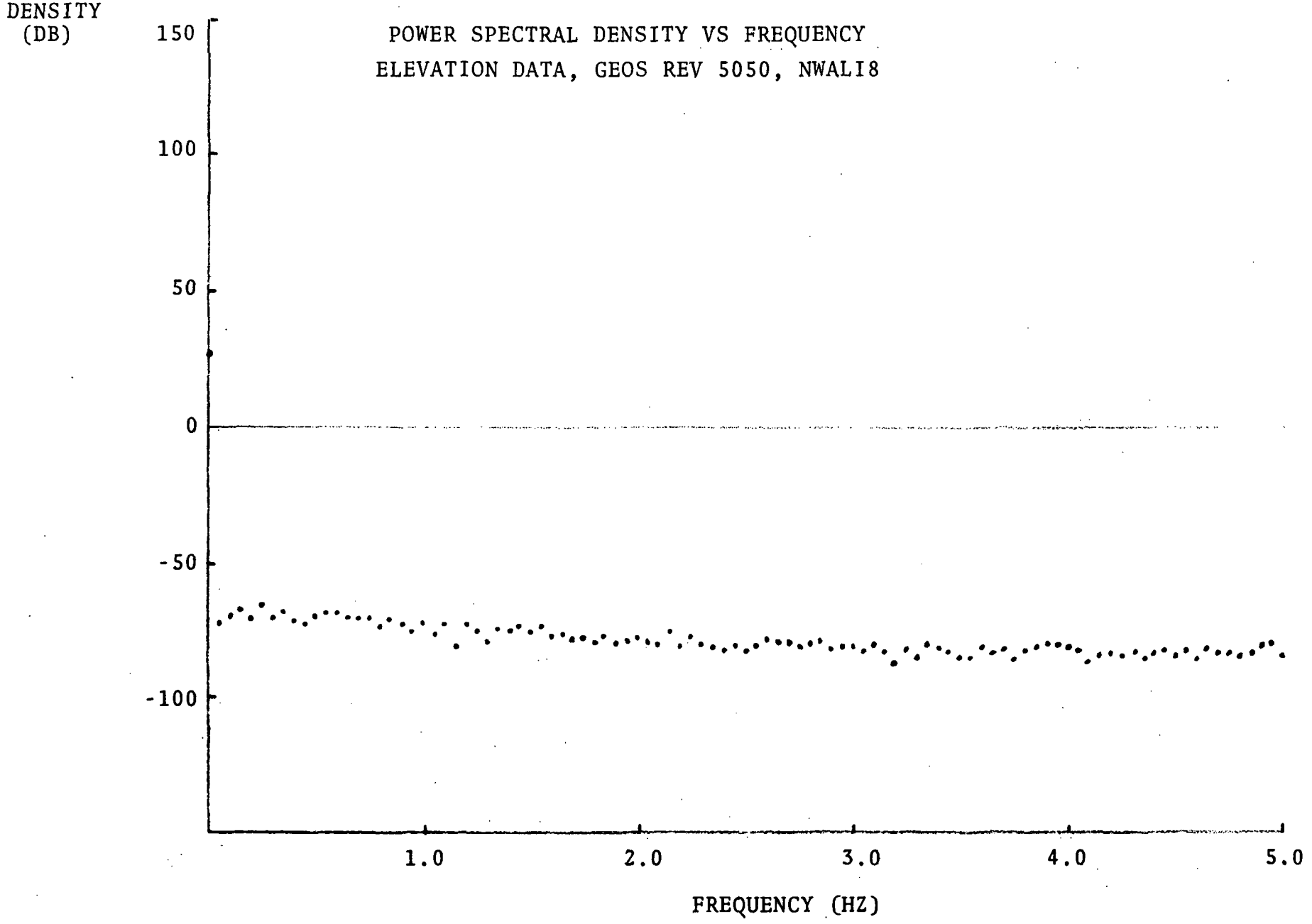
SPECTRAL DENSITY (DB)
POWER SPECTRAL DENSITY VS FREQUENCY
ELEVATION DATA, GEOS REV 5050, NWALI8
150
100
50
0
-50
-100
1.0
2.0
3.0
4.0
5.0
FREQUENCY (HZ)

FIGURE 10

POWER SPECTRAL DENSITY VS FREQUENCY
AZIMUTH DATA, GEOS REV 5050 NWALI8

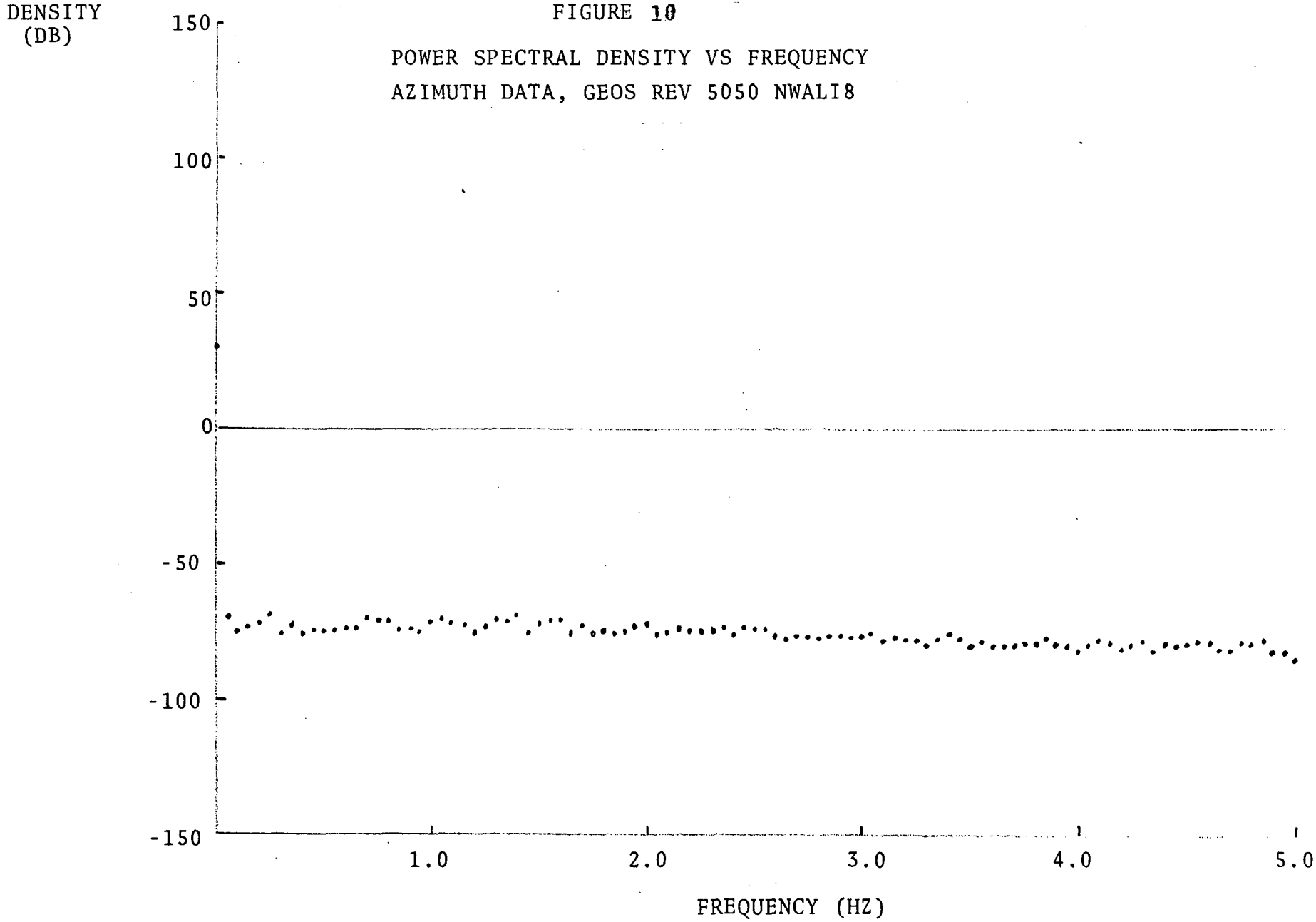

16 and 24 hertz components fold to 4 hertz in the sampled data. The spectral density estimate for elevation data from the Wallops AN/FPS-16, shown on Figure 9, is similar in general nature, but does not show the frequency spikes. The spectrum of the azimuth data from the Wallops AN/FPQ-6 is shown on Figure 7, and that from the AN/FPS-16 on Figure 10.

2.1.3 Skin Track Data Spectral Analysis

Since essentially all of the GEOS-II data was taken in beacon track, no skin track data from the GEOS-II was analyzed. Data was selected from skin track measurements by the Wallops AN/FPQ-6 on Object 1314, and the spectral estimates were obtained by the method described in the previous section.

A plot of the spectral density of the skin track range data is shown on Figure II. This spectrum shows a pronounced peak in the noise spectrum at .2 hertz. The noise level drops off about 20 db between .2 hertz and 1.2 hertz, then remains essentially level out to 5 hertz. It is assumed that the object, which is a large booster motor, might be tumbling or precessing with a period of about 5 seconds, causing a peak at about .2 hertz in the noise spectrum.

2.2 DATA COMPACTION STUDIES

The data compaction studies were carried out using the COMPACT program which is described in Appendix A. The goal of these studies was to investigate the properties of the filtered and compacted data, to better determine an optimum method for data compaction.

FIGURE 11

POWER SPECTRAL DENSITY VS FREQUENCY

RANGE DATA, OBJECT 1314, NWALIS

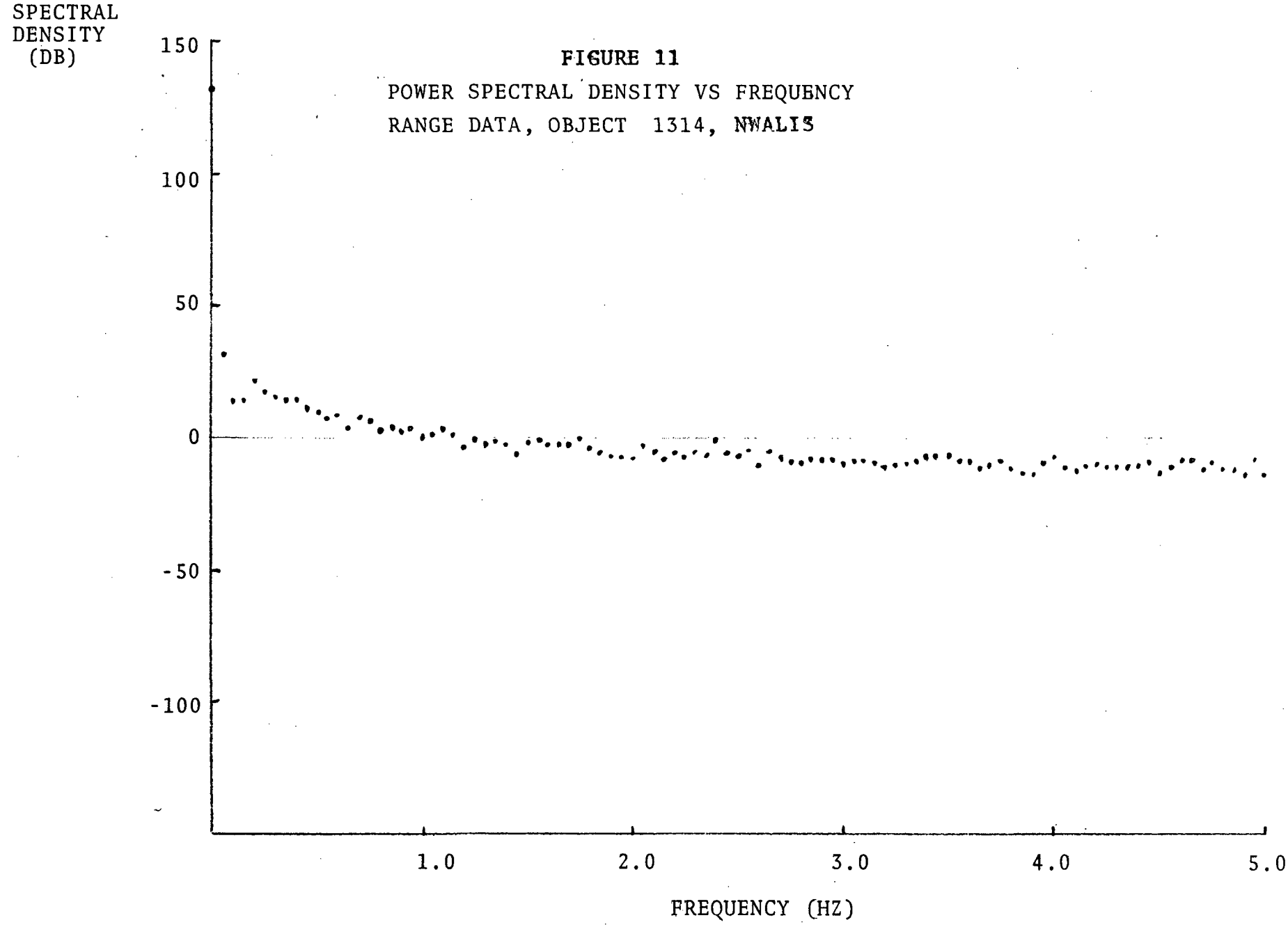

2.2.1 GEOS-II Rev No. 5462

In this test computation, data from the Wallops AN/FPQ-6 on Rev 5462 was filtered but not compacted. The data was kept at 10/sec. for analysis purposes. The filter used was a 401 point (40 second) non-recursive low-pass filter with nominal cut-off at .15 Hz. The number of data points, N, the cut-off frequency, f_c, and the sampling interval T are related by the equation

$$N - 1 = \frac{6}{f_c T}$$

given in Section A.3.1. The cut-off frequency f_c = .15 hertz is not optimum from the sense of removing all noise from the data. The spectral analysis studies reported above indicate that f_c = .05, with N = 1201, would be the best choice, if it is desired to eliminate essentially all noise while retaining the signal intact. However, N - 1201 means the loss of two minutes of data, one minute at the start and one minute at the end of the data span. It was recommended by Wallops personnel that a higher cut-off frequency be selected to reduce the amount of data lost. The question of optimum interval selection is discussed further in Section 3.2.

In order to obtain a comparison between filtered and unfiltered data, the unfiltered range data was used in an A/OMEGA run to determine an orbit and obtain residuals. For this run, the range RMS was .75 meters. The smoothed range data were then used through one iteration of A/OMEGA, with the orbit elements determined from the unsmoothed data, to obtain residuals on the smoothed data. The RMS of residuals of the smoothed range data from the orbit obtained from the unsmoothed data was .43 meters.

A complete plot of the approximately 9000 residuals was not made.

Figure 12 is a plot of the residuals of the smoothed (filtered) range data with respect to the reference orbit, on a compressed time scale. Every 50th data point (one every 5 seconds) was plotted on Figure 12. Figure 12 gives an idea of the noise left in the data after filtering and shows a low frequency trending of the data. Figure 13 shows the corresponding unsmoothed residuals.

Figure 14, 15 and 16 are plots of short segments of the filtered and unfiltered residuals vs. time, plotted 10/second on an expanded time scale. Figure 14 shows data just after acquisition, Figure 15, near PCA, and Figure 16 near end of track.

On these plots, the filtered data shows jumps of almost half a meter at the two ends of the tracking span, but is very smooth near PCA. Examination of the A/OMEGA run shows that the jumps appear when the seconds column of the time tag changes by one in the fourth decimal place. Also, the size of the jumps is almost exactly one one-thousandth of the range difference taken over one-tenth of a second. The changes in the time tags are caused by transit time corrections, and the time is carried on the input tape to only four decimal places. The jump occurs because the computed value of the range is computed at a time which is in error in the fifth decimal place, compared to the time at which the measurement was made.

FIGURE 12

RESIDUALS OF FILTERED RANGE DATA
WITH RESPECT TO REFERENCE ORBIT
Rev 5462 AN/FPQ-6

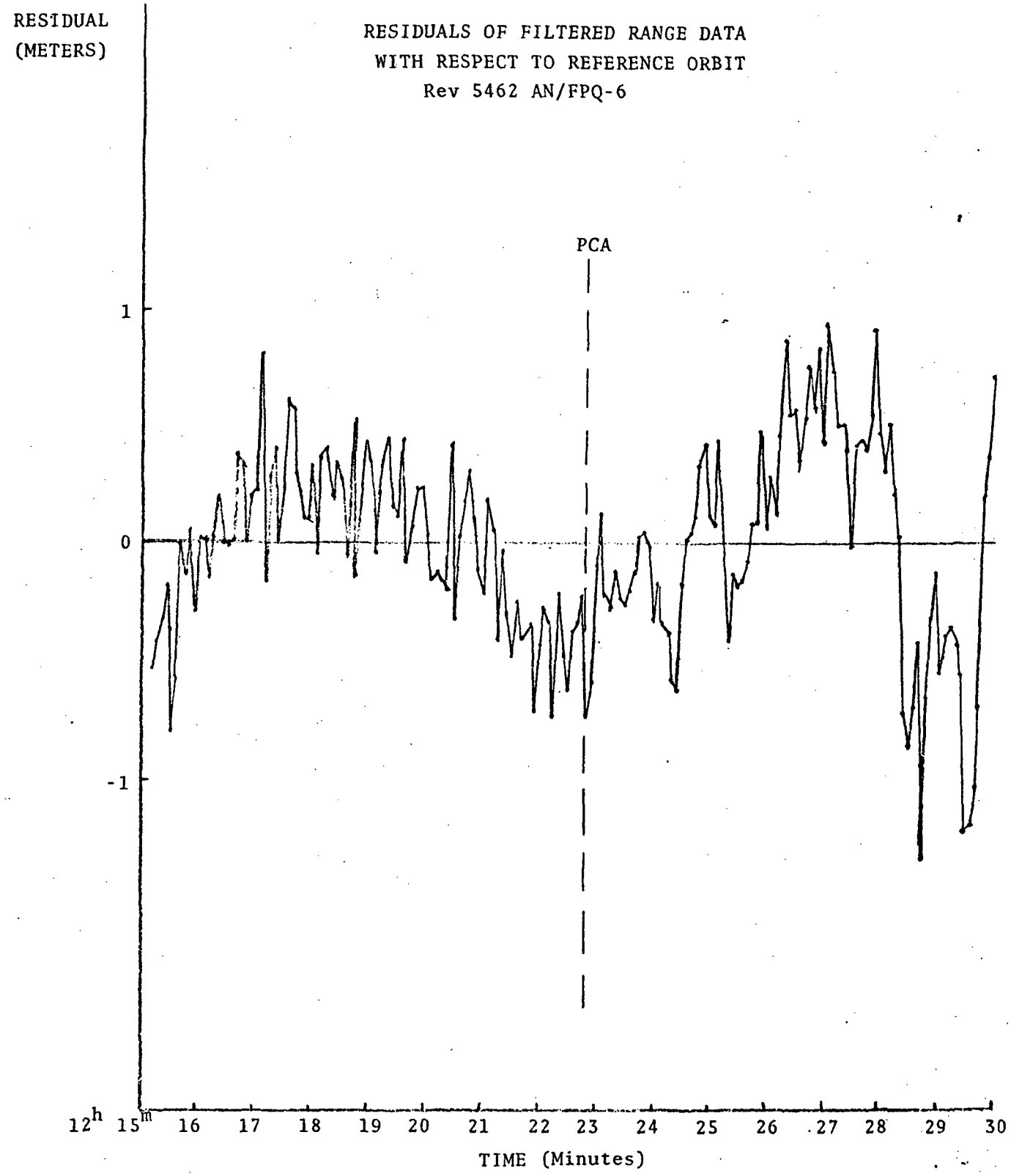

FIGURE 13
RESIDUALS OF UNFILTERED RANGE DATA
WITH RESPECT TO REFERENCE ORBIT
REV 5462, AN/FPQ-6

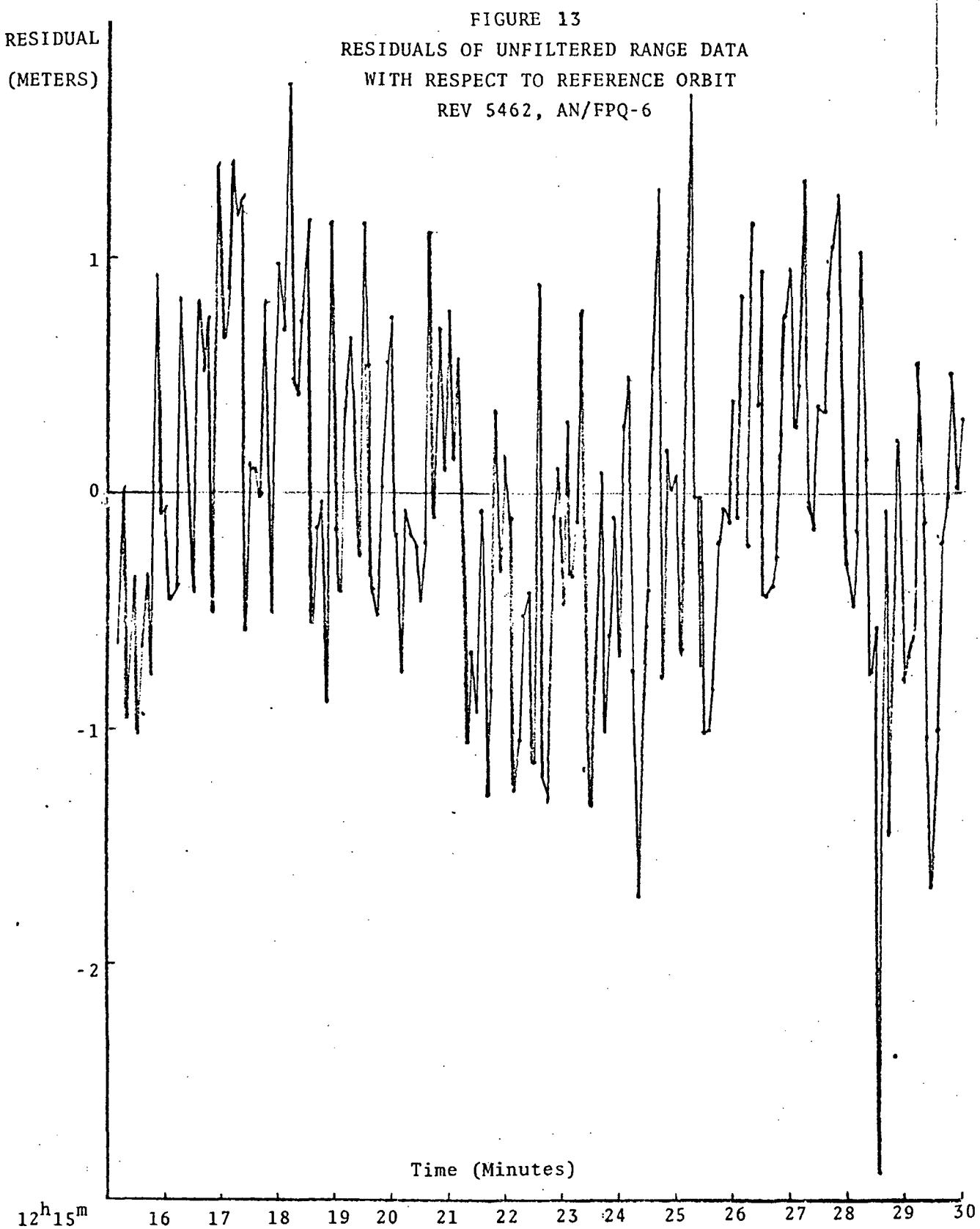

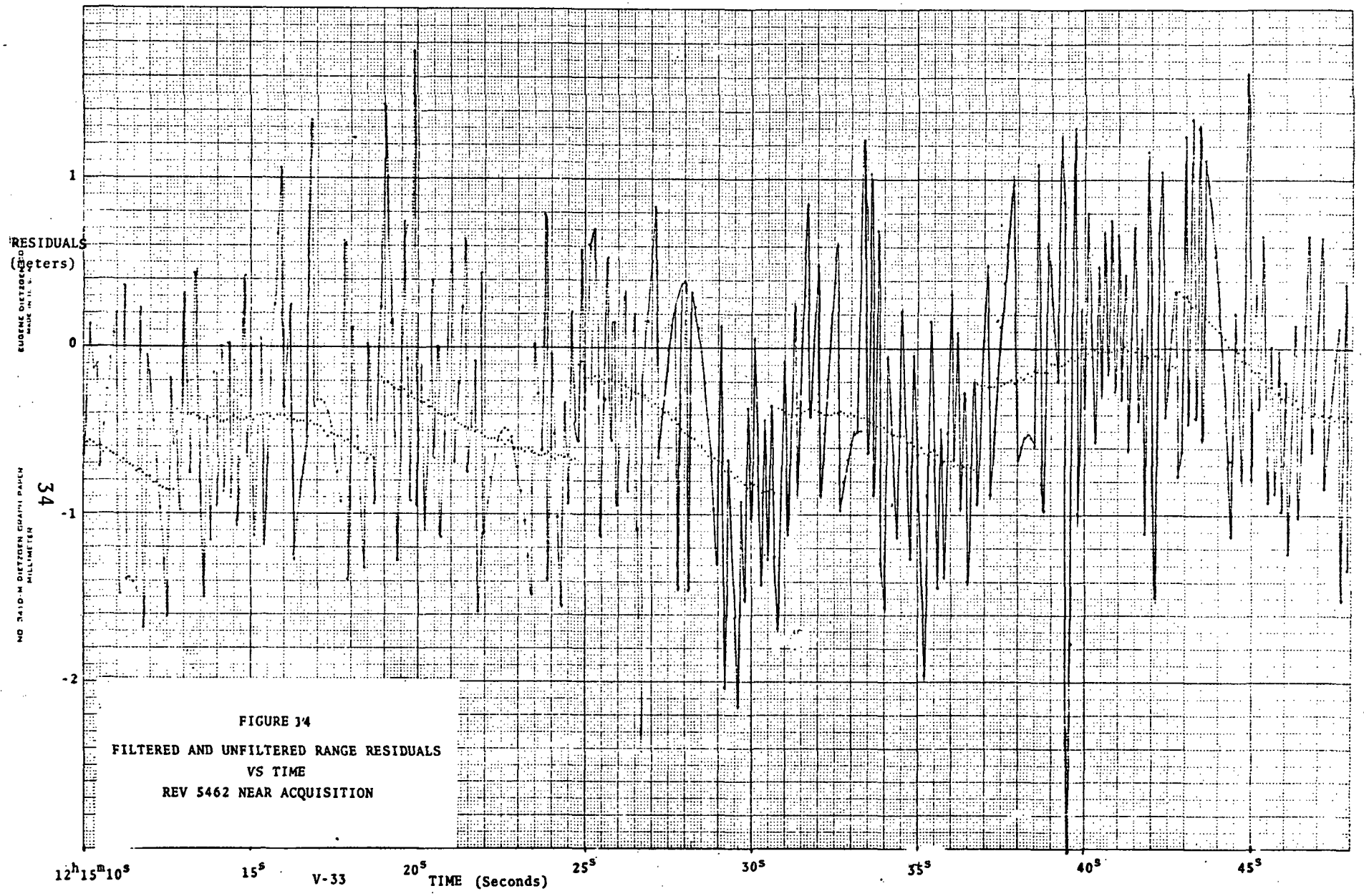

FIGURE 14

FILTERED AND UNFILTERED RANGE RESIDUALS
VS TIME
REV 5462 NEAR ACQUISITION

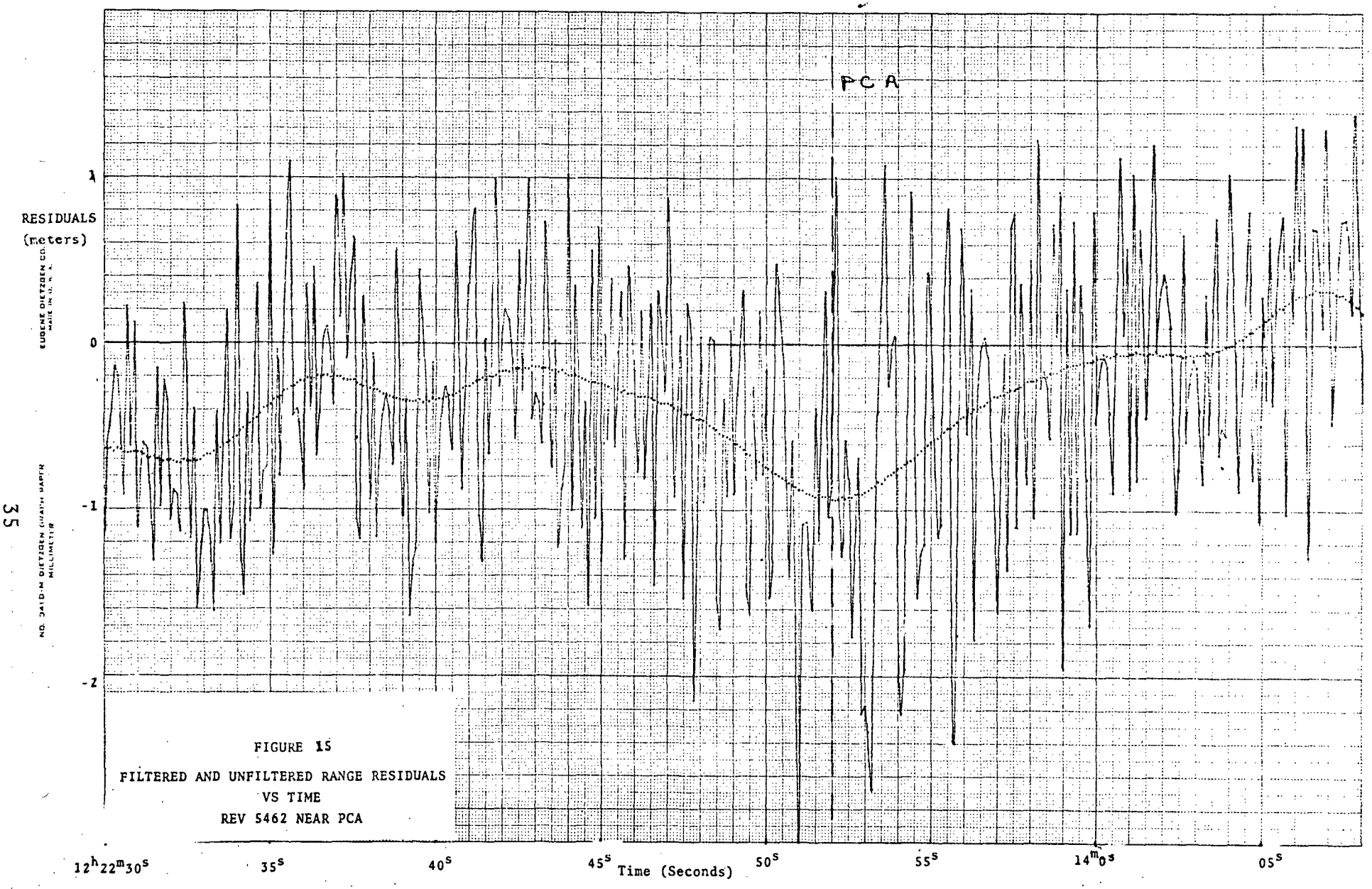

FIGURE 15

FILTERED AND UNFILTERED RANGE RESIDUALS
VS TIME
REV 5462 NEAR PCA

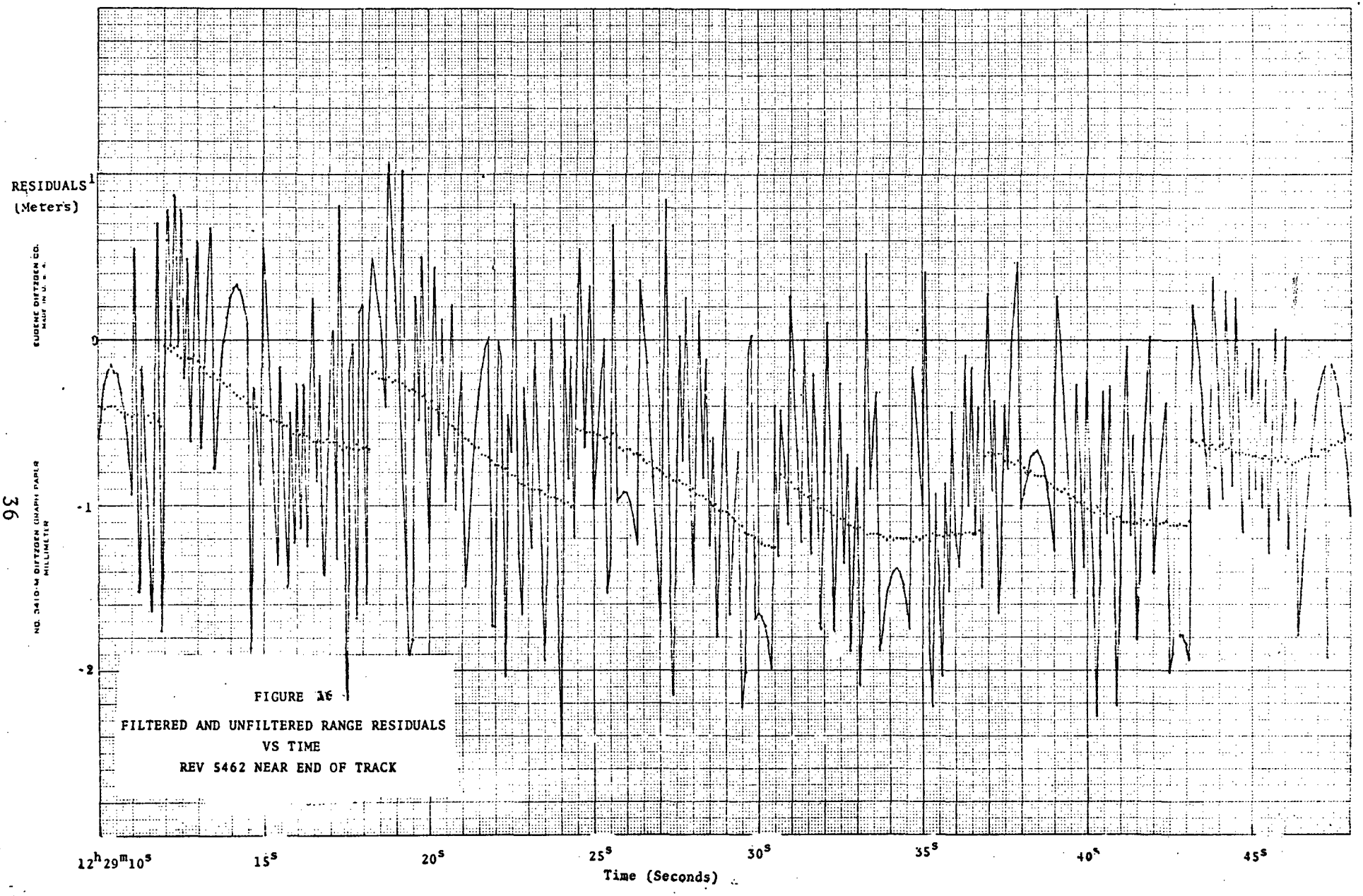

FIGURE 16

FILTERED AND UNFILTERED RANGE RESIDUALS
VS TIME
REV 5462 NEAR END OF TRACK

These jumps result in an error which is locally non-random and has a variance of one-twelfth of the mean square value of the jumps. This error is probably negligible when compared to the other errors in the data. See, for example, Figure 15, and note that the noise on the data seems to be about as big near PCA, where no jumps occur, as it does near the ends of the plot, where the jumps are the largest.

The jumps can be prevented in one of two ways. The first is to change the data format to carry five decimals on the seconds of time. The second is to compute the transit time correction in A/OMEGA, in double precision, and input non-transit-time-corrected time.

The plot of residuals of filtered data with respect to the reference orbit, in Figure 12, shows a systematic or low frequency component with a period of about 7 minutes and amplitude of .5 meter. In order to determine whether this might represent some actual satellite motion, rather than a low frequency radar noise, data was reduced from the Wallops AN/FPS-16 on the same pass, using the same method. The residuals of the filtered range data using a reference orbit obtained from the unfiltered range data are shown on Figure 17. The low frequency component which appears in the AN/FPQ-6 data is not apparent in the AN/FPS-16 data. The tentative conclusion is that it is caused by low frequency noise in the radar range system.

In the course of examining the residuals of the unfiltered range data from the orbit; plotted in Figures 14, 15, and 16, an apparent short term systematic pattern was observed.

FIGURE 17
RESIDUALS OF FILTERED RANGE DATA
FROM REFERENCE ORBIT (FPS-16)
AN/FPS-16 DATA

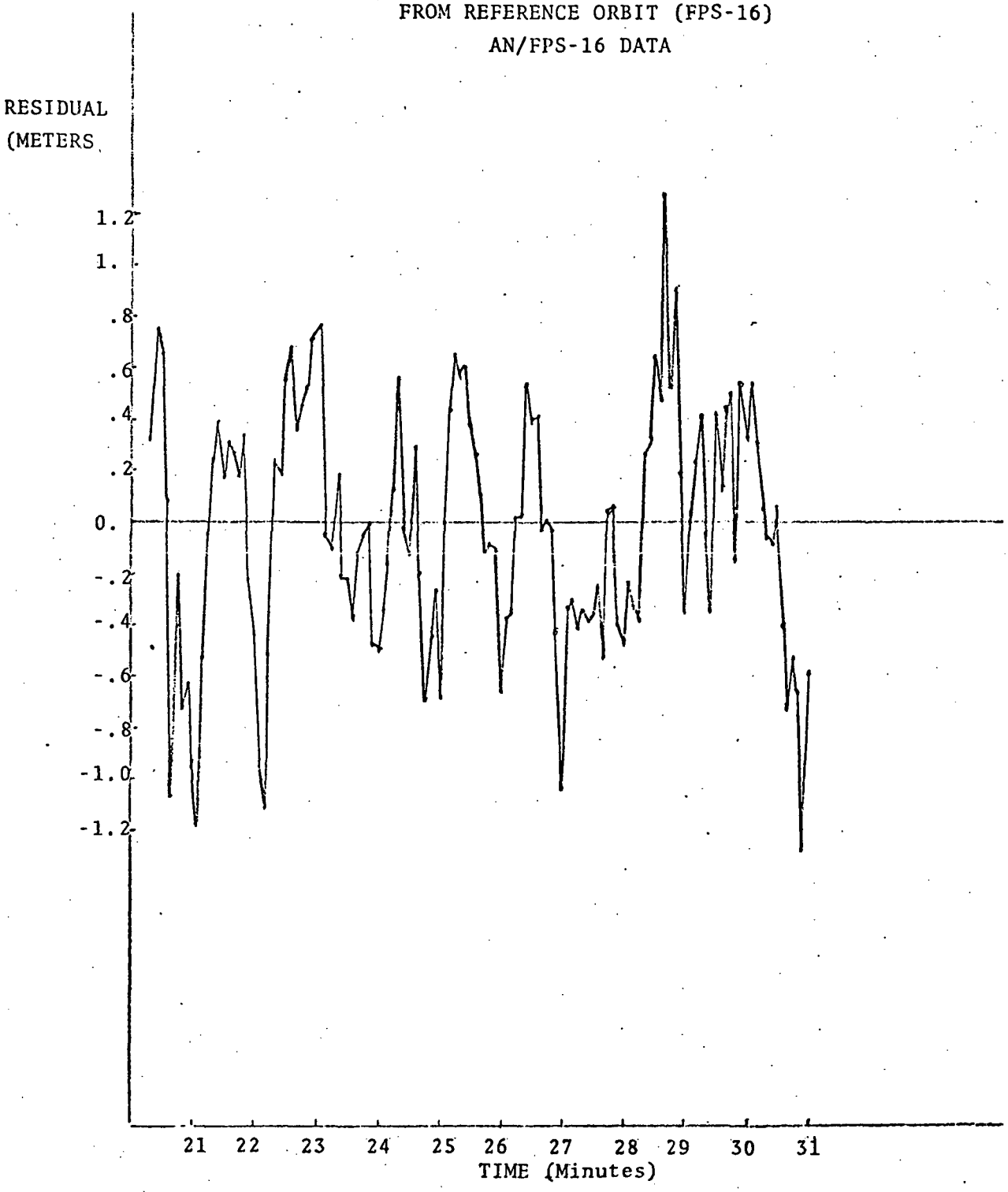

The same pattern appeared in the residuals obtained by differencing the unfiltered data and the filtered range data. Figures 18, 19 and 20 show the distinctive pattern of the differences between filtered and unfiltered range data, when plotted vs time. Instead of plotting 9000 data points, three ten second intervals (100 points each) were plotted as typical examples. One set near acquisition, one near PCA and one near loss of track. was plotted. All three plots show points with a nearly linear distribution between plus and minus one meter, with sporadic wild points outside those limits. In addition, the first and third of the three show a pattern in the successive data points.

The linear distribution and the patterns shown can both be explained by assuming that the predominant source of error in the range data is granularity caused by the low order bit size. This granularity or truncation error would be linearly distributed about the mean.

When the range rate is almost constant, as it is at the two ends of the track, the successive errors will follow a pattern of a saw-tooth curve with slope depending on the velocity and slowly changing as the $\dot{R}$ changes. When the $\dot{R}$ is exactly a multiple of the granularity, the errors will become nearly constant for a few points; then as the $\dot{R}$ changes, the sawtooth pattern resumes. Near PCA, the range acceleration is great enough that these patterns do not form.

As a test of the explanation, the effect of data granularity was simulated by computing the exact range to the computed orbit, at 10/second over a 6 second period, then introducing the granularity caused by a low order bit weight of

FIGURE 18

RANGE DIFFERENCE
(FILTERED MINUS UNFILTERED)
VS TIME
10 SECONDS NEAR ACQUISITION

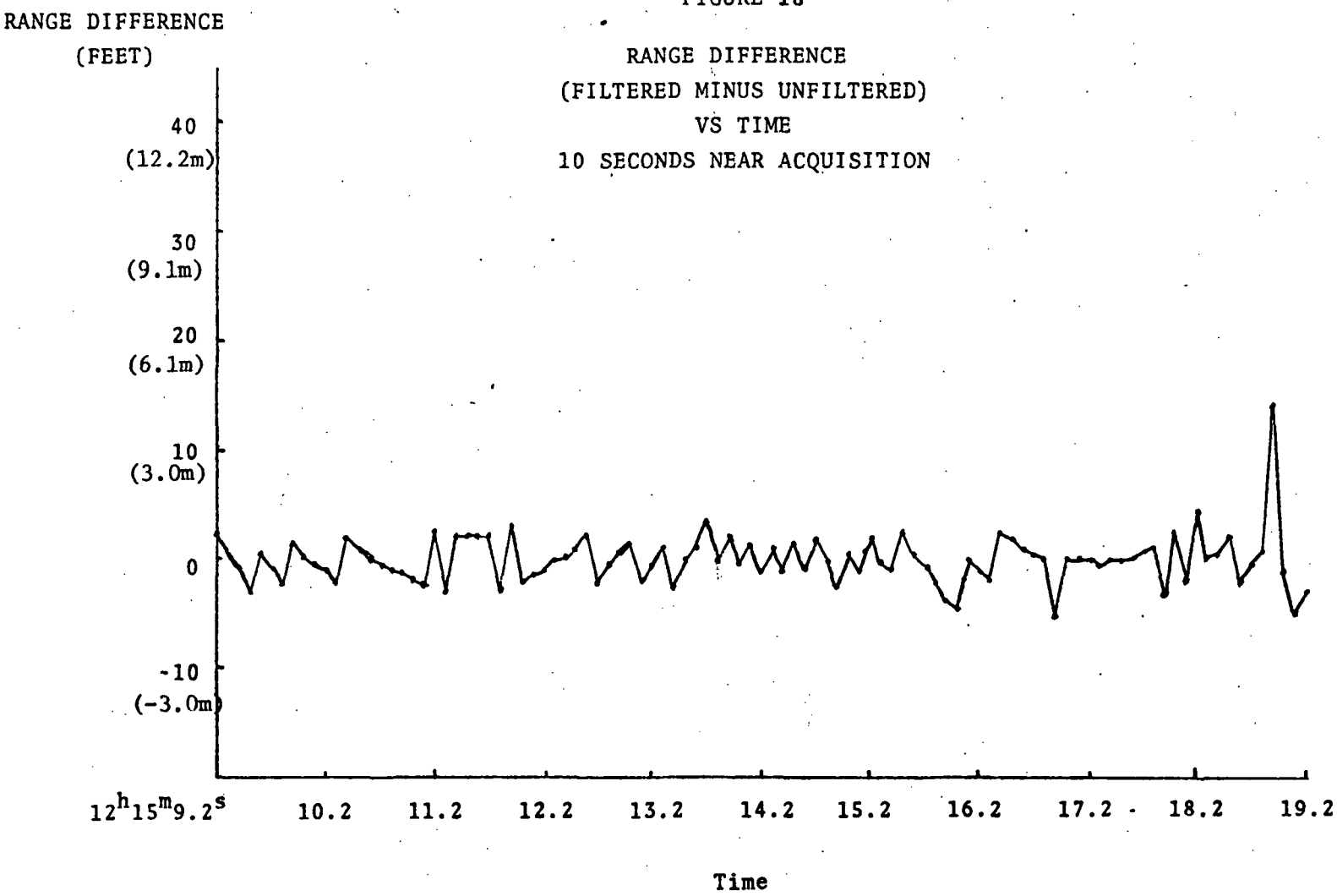

FIGURE 19

RANGE DIFFERENCE
(FILTERED MINUS UNFILTERED)
VS TIME
10 SECONDS NEAR PCA

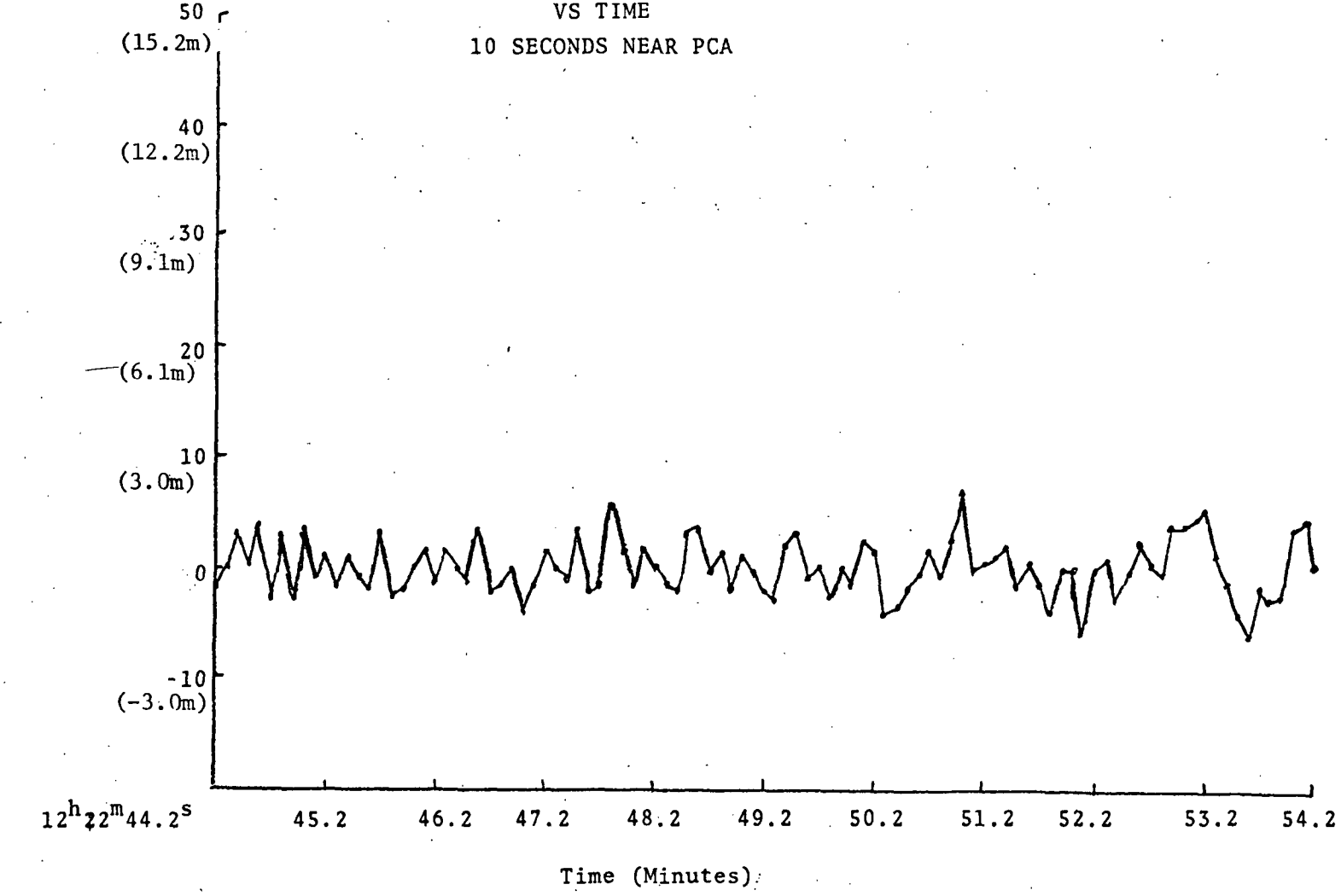

FIGURE 20

RANGE DIFFERENCE

(FILTERED MINUS UNFILTERED)

VS TIME

10 SECONDS NEAR END OF TRACK

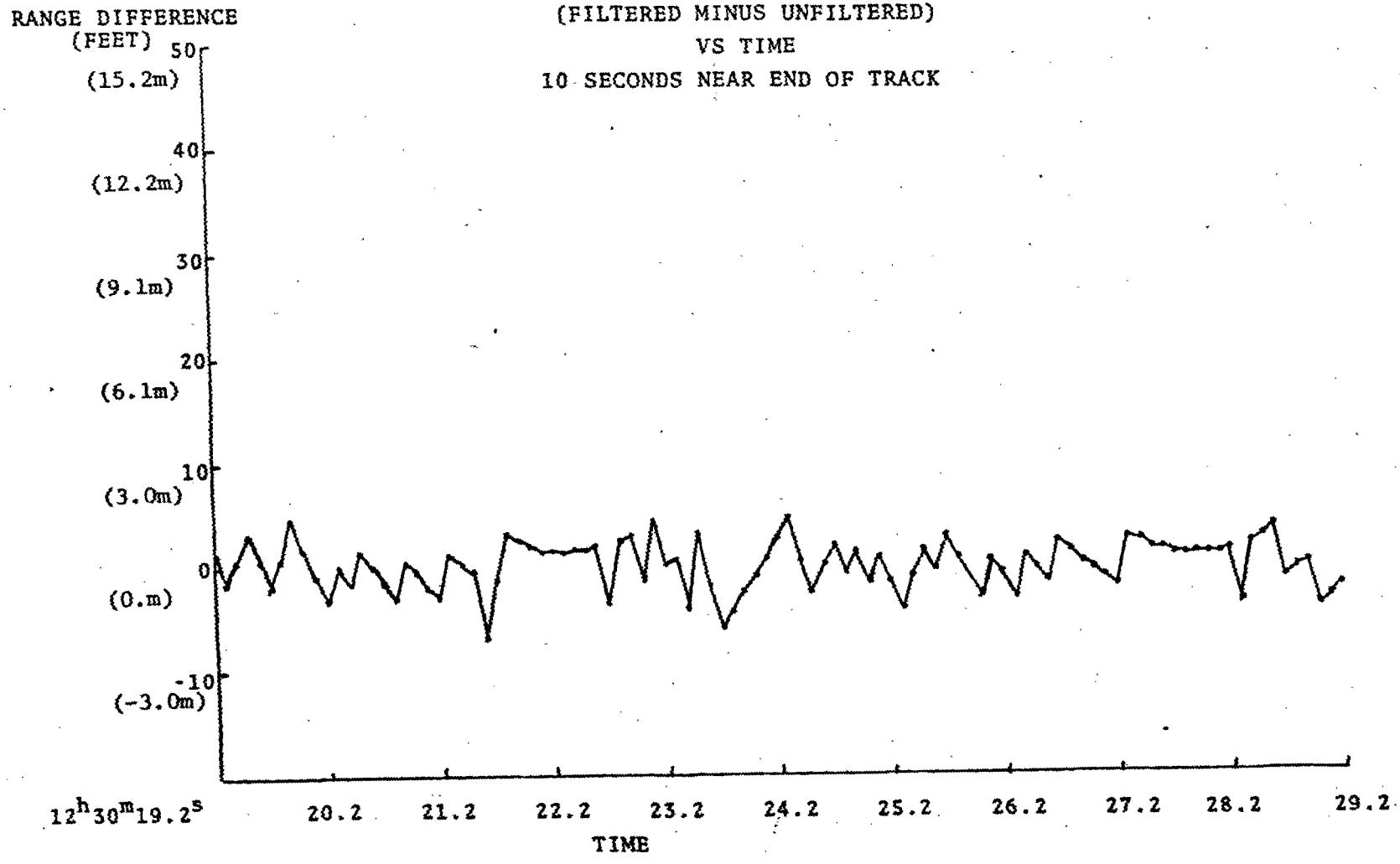

1.786 meters. The residuals obtained are plotted on Figure 21, along with the actual residuals from the orbit.

The similarity in the short period trending in the two curves is apparent. The differences, for example in the interval from 22.4 to 23.0 seconds, are caused by a bias in the level at which granularity occurs. If one bit weight is added to the simulated residuals in that interval, the curves will be similar.

2.2.2 Data Analysis on WICE Test 80

In order to further investigate the possibility of detection of orbital variations with periods of the order of a few minutes, another reduction was made, using data from both the AN/FPQ-6 and the AN/FPS-16 radars at Wallops Island, Range data from both radars, tracking WICE Test number 80, were filtered and compacted using the COMPACT program. The filter used was a 401 point (40 second) low pass filter with cut-off at 0.15 Hz. The filtered data were selected at every 5 seconds to eliminate serial correlation.

The filtered data were used in an A/OMEGA short arc reduction, with the AN/FPQ-6 data used to determine the orbit. Range residuals are plotted on Figure 22. The large range bias was also observed on the reduction of the normal WICE test data. From inspection of the plotted data, no correlation can be observed between results from the two radars. The conclusion is that there are no systematic effects which can be attributed to short period orbital variations.

FIGURE 21

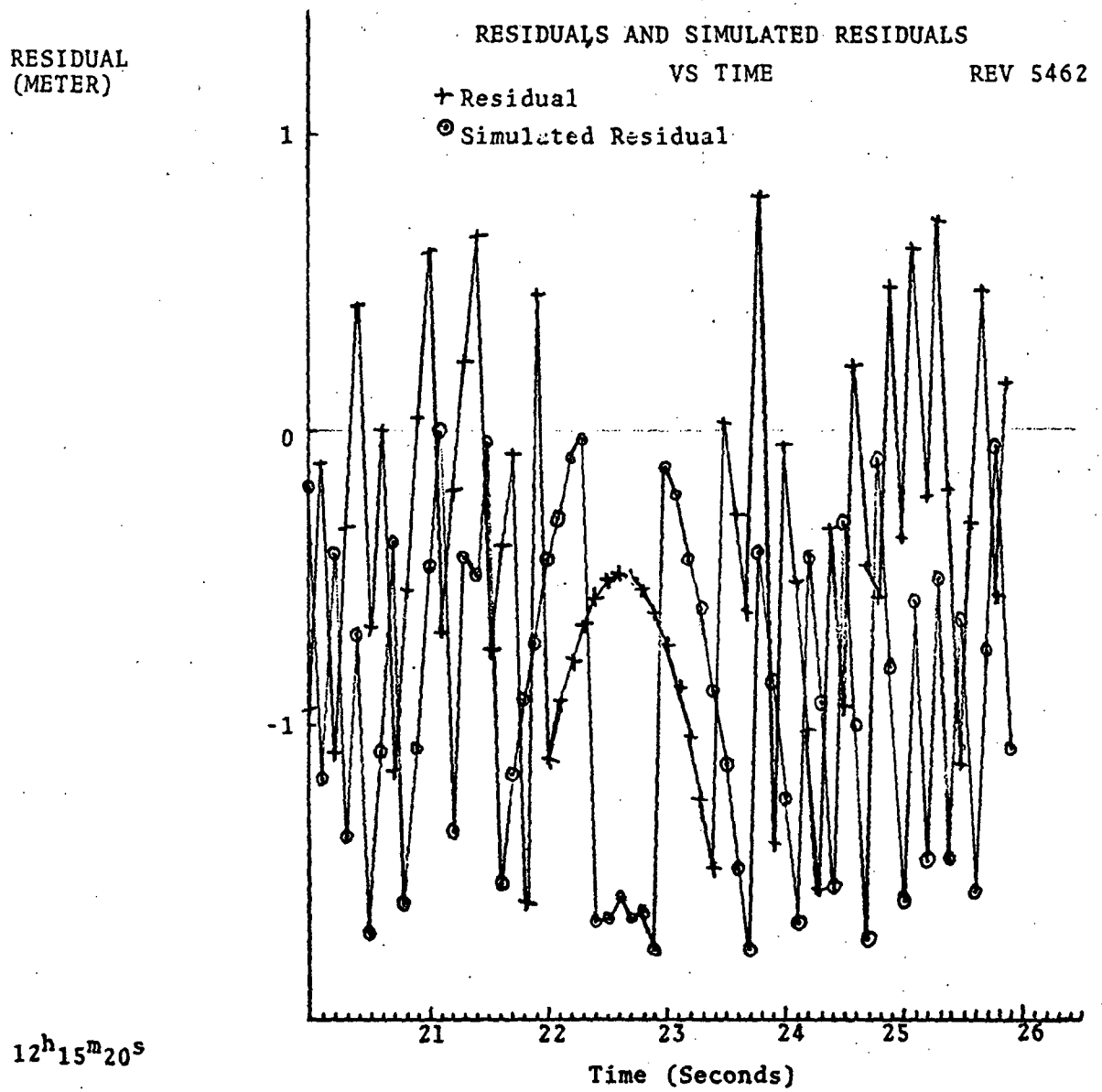
RESIDUALS AND SIMULATED RESIDUALS
VS TIME
REV 5462
Residual
Simulated Residual
RESIDUAL (METER)
1
0
-1
21
22
23
24
25
26
Time (Seconds)
12h15m20s

FIGURE 22

RANGE RESIDUALS VS TIME
AN/FPQ-6 AND AN/FPS-16, WALLOPS ISLAND
WICE TEST 80

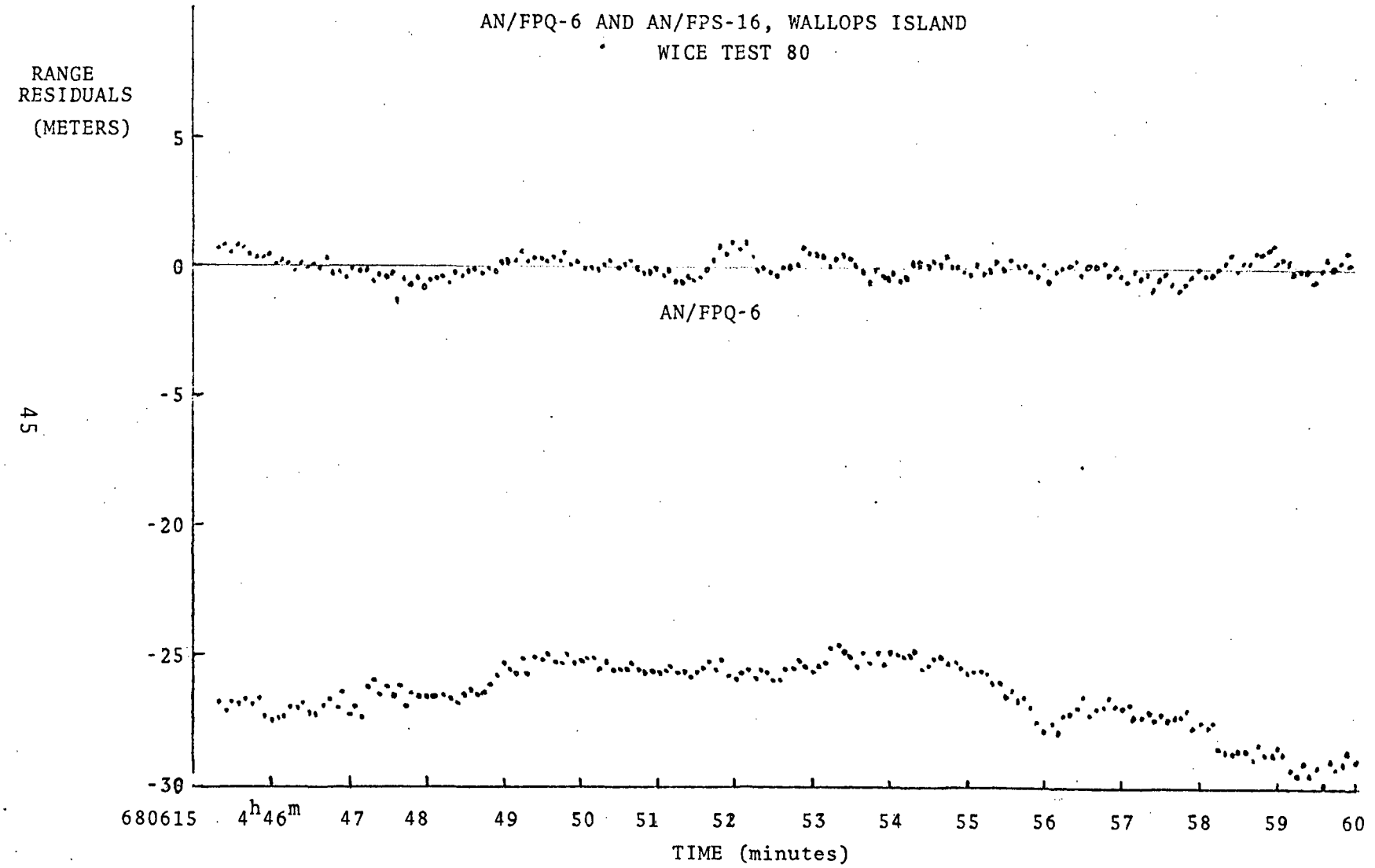

As a further comparison of filtered and unfiltered data, orbits were determined, using data from the AN/FPQ-6 radar only.

One orbit used the unfiltered range data, selected every five seconds. The other orbit used filtered range data, as described above, also selected every five seconds. The results are summarized in Table 1, which tabulates orbital elements from unfiltered data, filtered data, the differences of corresponding elements, and the estimated standard deviation of each element. The RMS of the residuals of range, azimuth and elevation for each orbit are also tabulated, along with the input a priori standard deviation of each variable. It is evident that the two sets of elements are in agreement to well within the estimated error limits.

2.2.3 NBER05 Data Comparisons

Range, azimuth and elevation data from NBER05 on two passes, Rev 4910 and Rev 5000 were filtered and compacted using the COMPACT program. The filter used was a 401 point (40 sec.) low pass filter with cut-off at .15 Hz. The filtered data were selected at 1/5 second, and included in a three week long arc reduction. Normally processed data from the same passes were included in another reduction. Residuals from the two reductions are plotted on Figures 23 to 28. The residuals of the filtered data from the reference orbit show essentially the same trends, but significantly less short period variation.

COMPARISON OF ORBITAL ELEMENTS DERIVED FROM FILTERED AND FROM UNFILTERED DATA FROM NWALI3 ON WICE TEST 80

	UNFILTERED DATA	FILTERED DATA	Δ	σ_{EST}
X(M)	-1624085.0	-1624101.5	-16.5	71.
Y(M)	-7366614.4	-7366606.8	7.6	30.
Z(M)	1691209.5	1691206.0	-3.5	23.
X(M/S)	-1671.3504	-1671.3260	.0244	.1368
Y(M/S)	1690.0173	1690.0135	.0038	.0219
Z(M/S)	6766.9897	6766.9991	-.0091	.0390
RMS(R) meters	.762	.388	$\frac{\sigma_{INPUT}}{2.0}$	
RMS(A) sec of arc	16.5	16.4	50.0	
RMS(E) sec of arc	21.6	20.0	50.0	

TABLE 1.

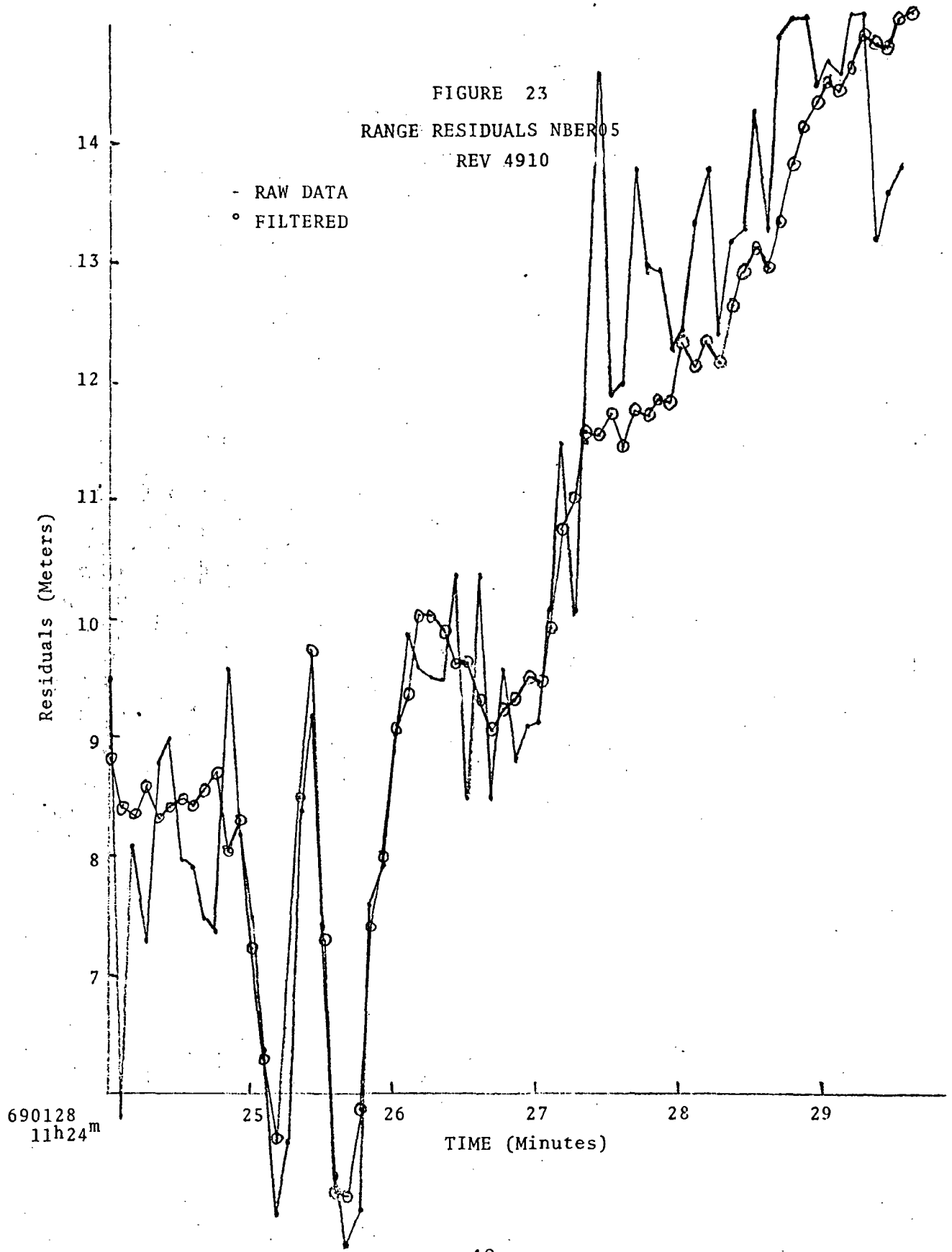
FIGURE 23
RANGE RESIDUALS NBER05
REV 4910
- RAW DATA
° FILTERED
Residuals (Meters)
14
13
12
11
10
9
8
7
690128
11h24m
25
26
27
28
29
TIME (Minutes)

FIGURE 24

ELEVATION RESIDUALS NBER05 REV 4910

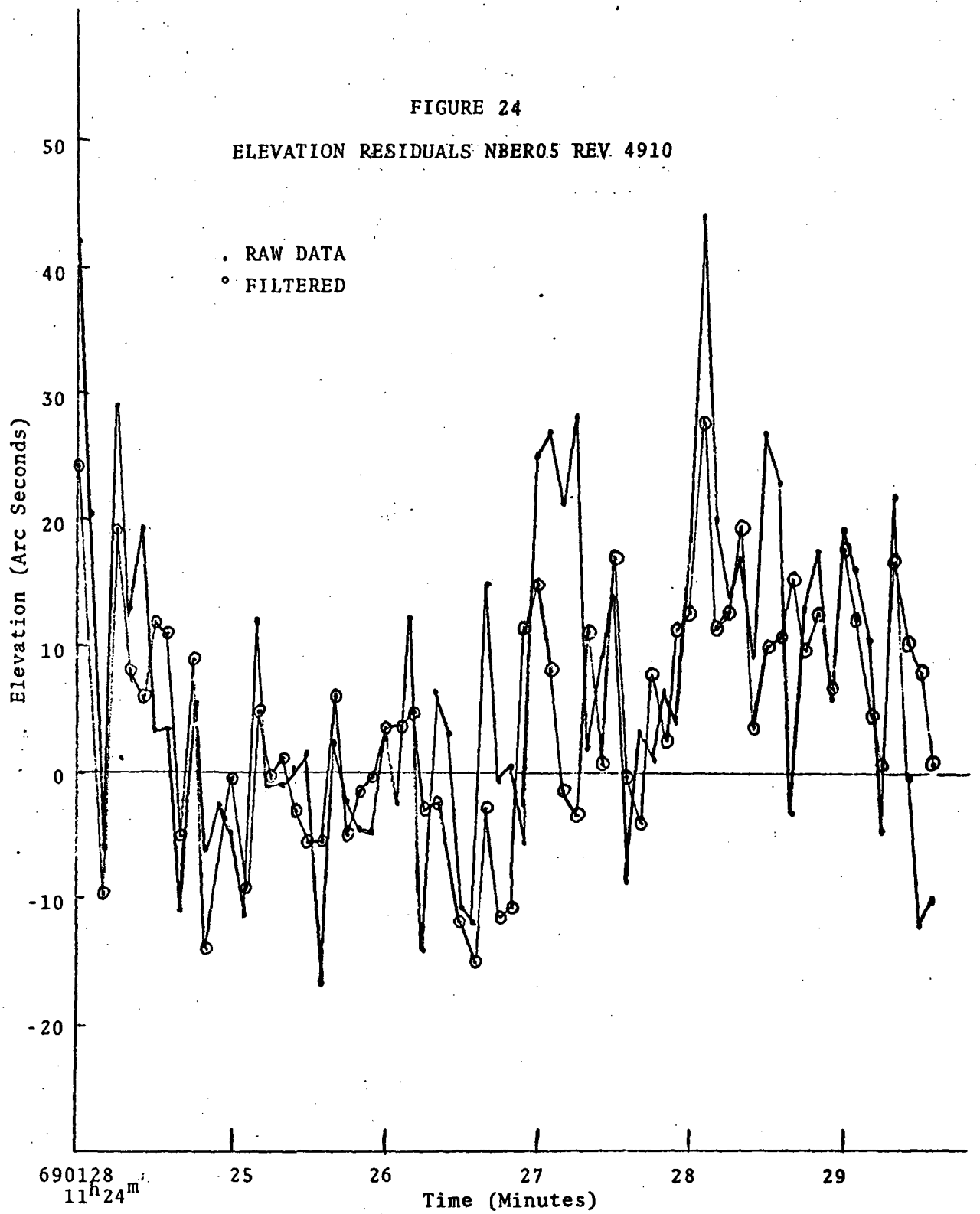

FIGURE 25

NBER05

REV 4910

AZIMUTH RESIDUALS

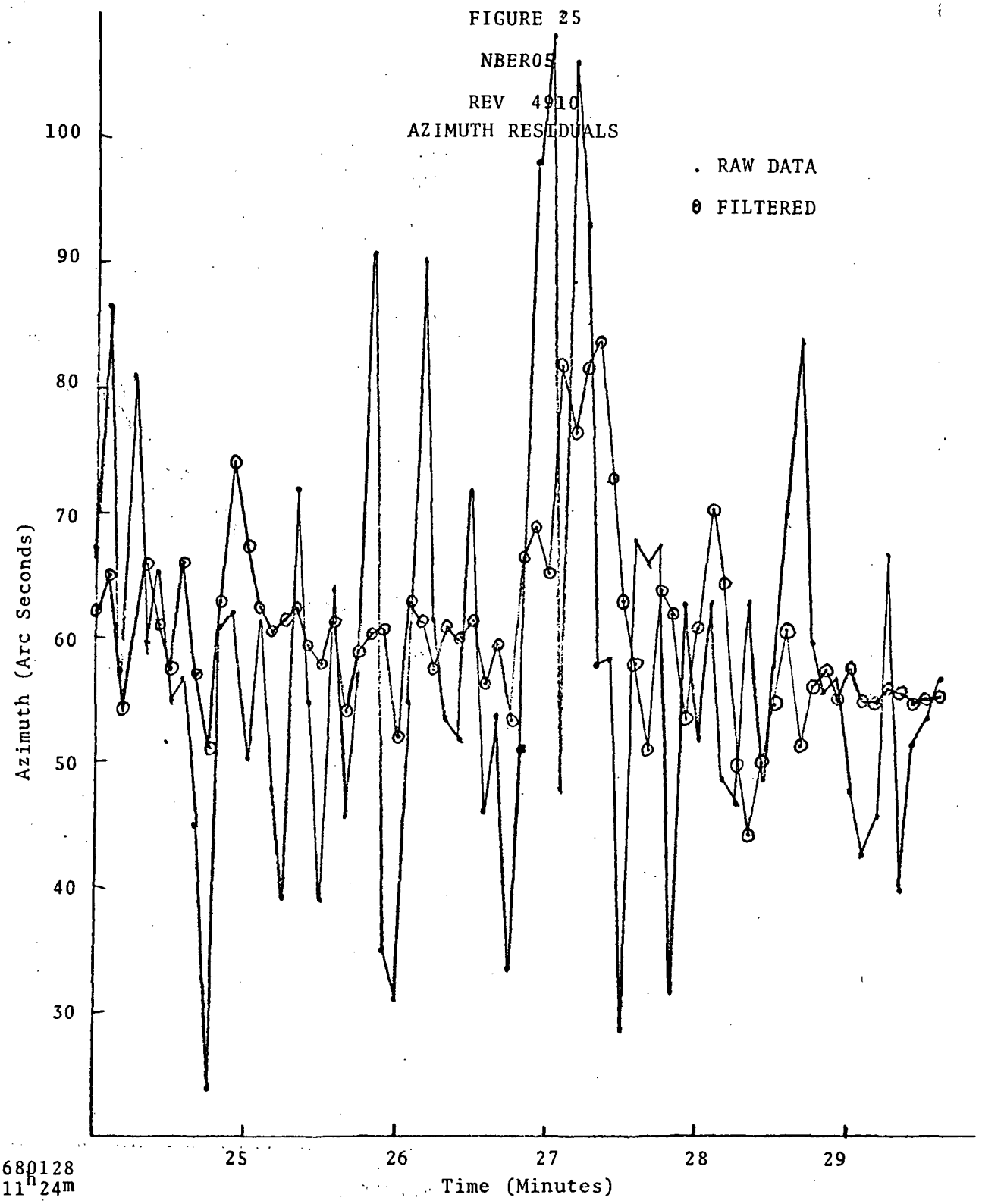

FIGURE 26

RANGE RESIDUALS NBER05
REV 5000

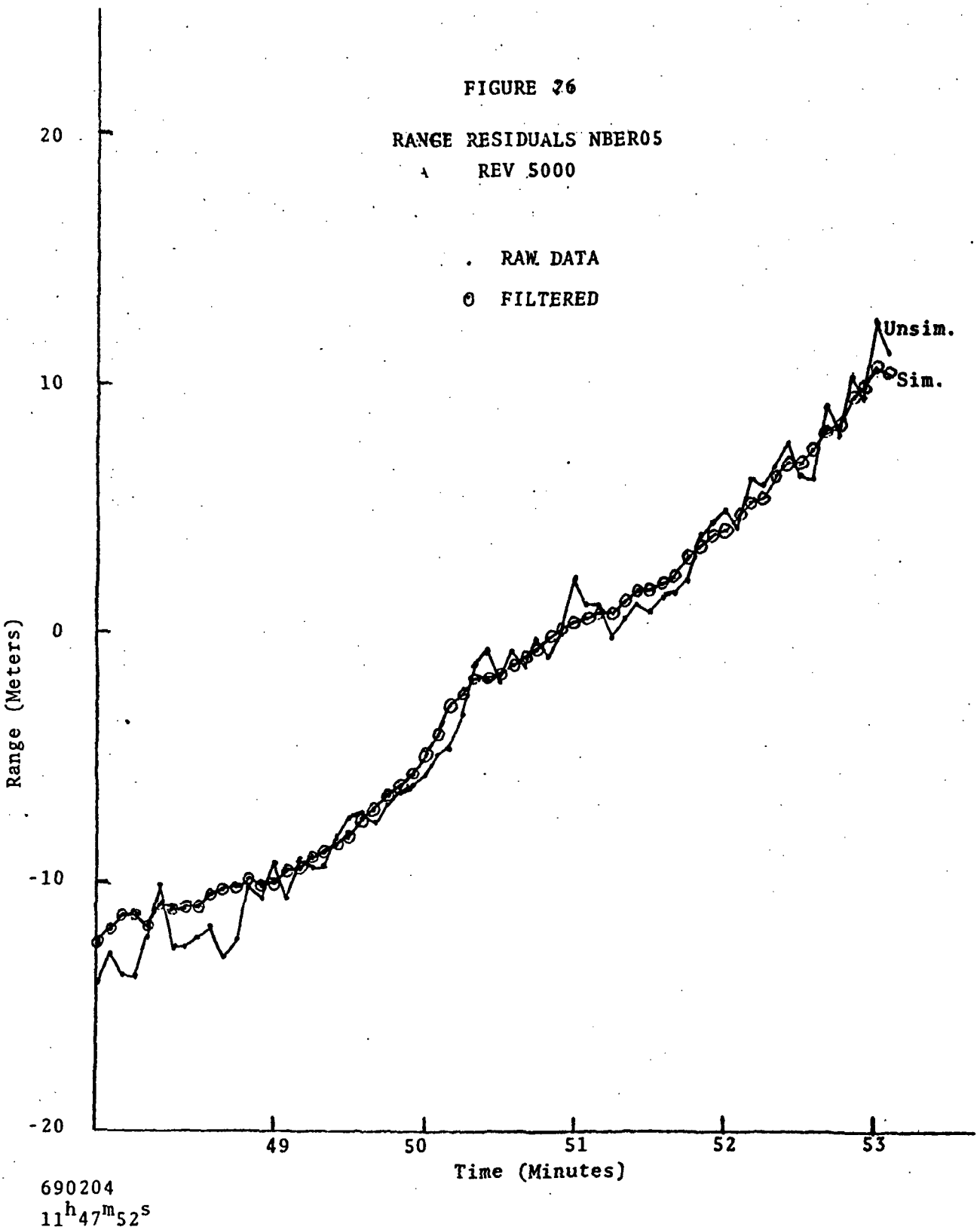

FIGURE 27
ELEVATION RESIDUALS NBER05 REV 5000

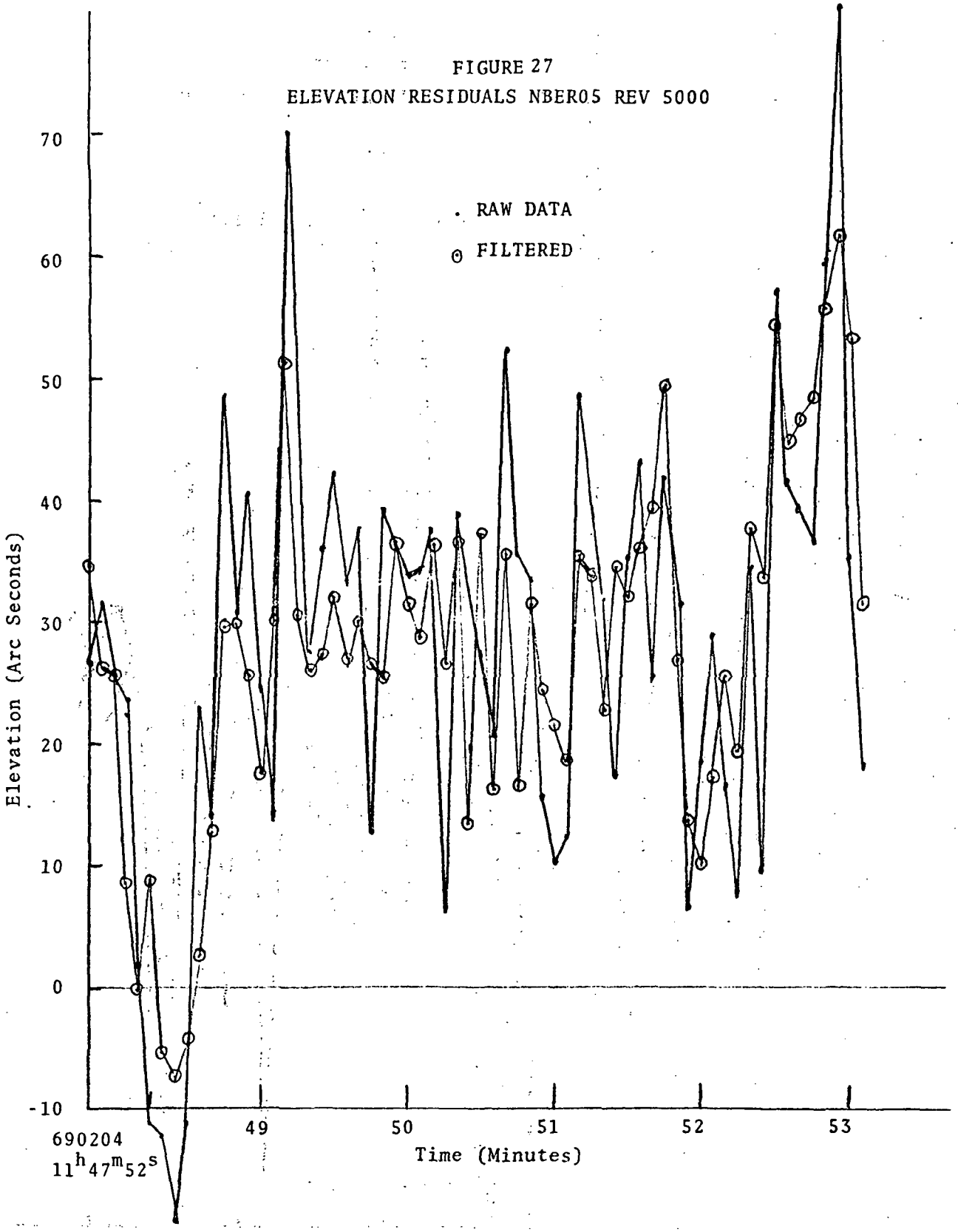

FIGURE 28
AZIMUTH RESIDUALS NBER05 REV 5000

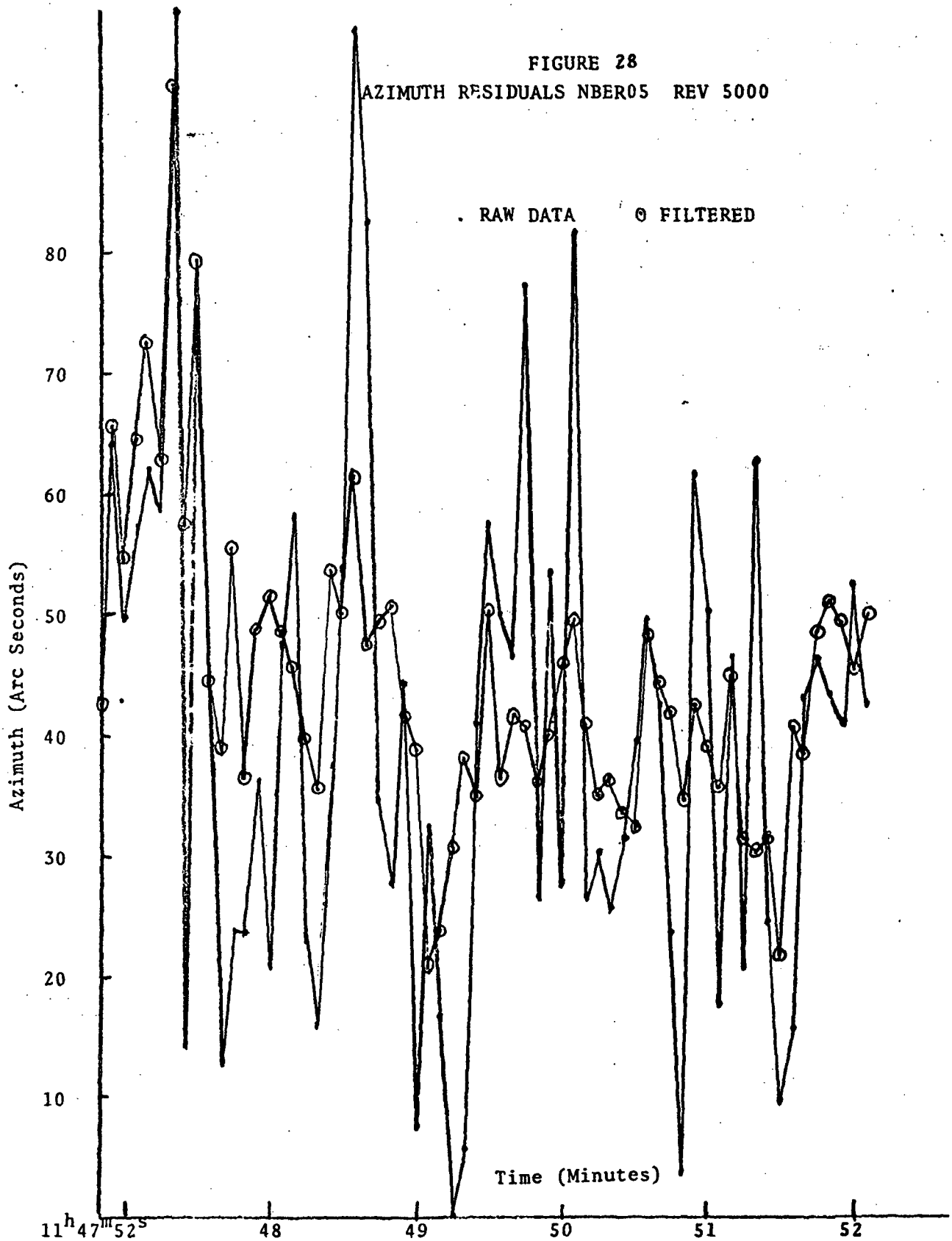

2.2.4 Long Arc Comparison

In order to examine the effects of use of filtering and compacting radar data on the orbital solution and the residuals obtained from the data, a long arc solution comparison was made. Data from seven GEOS-II passes over a period of slightly greater than 24 hours, as listed in Table 2, was reduced twice; once using filtered range data and once unfiltered range data. The filter used was a 601 point low pass filter, with cut-off frequency of .1 hertz. The filtered data was selected at 1 point per 10 seconds, then reduced in the nominal manner. The unfiltered data was also selected at 1 point per 10 seconds and reduced in the same manner.

In order to evaluate the accuracy of the orbital elements obtained by the two methods, the elements were used to predict measured values, and compared against actual measurements. For each set of elements, a 10 day orbit was computed, and data from 17 stations, a total of 9175 measurements, were used to compute residuals.

The RMS of residuals from the orbit determined by the unfiltered data was 180.8 meters, and from the orbit determined by the filtered data was 159.4 meters.

The indication is that the two orbit determinations are essentially the same. A true statistical comparison is difficult, because the effects of unmodelled errors prevents a valid estimate of what the standard deviation should be.

The orbital elements and the RMS residuals values are listed in Table 3.

Residuals of the unfiltered data are plotted on Figure 29, and those of the filtered data on Figure 30.

DATA USED IN FILTERED-UNFILTERED LONG ARC

STATION	REV	DATE	START TIME	STOP TIME
NBER34	4960	690201	085950	090620
NWALI3	4960	690201	090000	090620
NWALI3	4961	690201	104700	105420
NBER34	4961	690201	104650	105420
NWALI3	4967	690201	224140	224830
NWAL34	4967	690201	224150	224920
NWALI3	4973	690202	092110	092700

TABLE 2

COMPARISON OF ORBITAL ELEMENTS FROM FILTERED AND FROM UNFILTERED DATA ON LONG-ARC SOLUTION

	UNFILTERED DATA	FILTERED DATA	Δ
X(M)	-5541910.7	-5541934.7	-24.0
Y(M)	-3939388.2	-3939395.1	6.9
Z(M)	3942974.9	3942961.1	13.8
$\dot{X}$(M/S)	1331.5775	1331.5589	.0186
$\dot{Y}$(M/S)	3668.2914	3668.2816	-.0003
$\dot{Z}$(M/S)	5872.6921	5872.6874	.0047
RMS(M)	10.2	14.3	
RMS PREDICTED	180.8	159.4	

TABLE 3

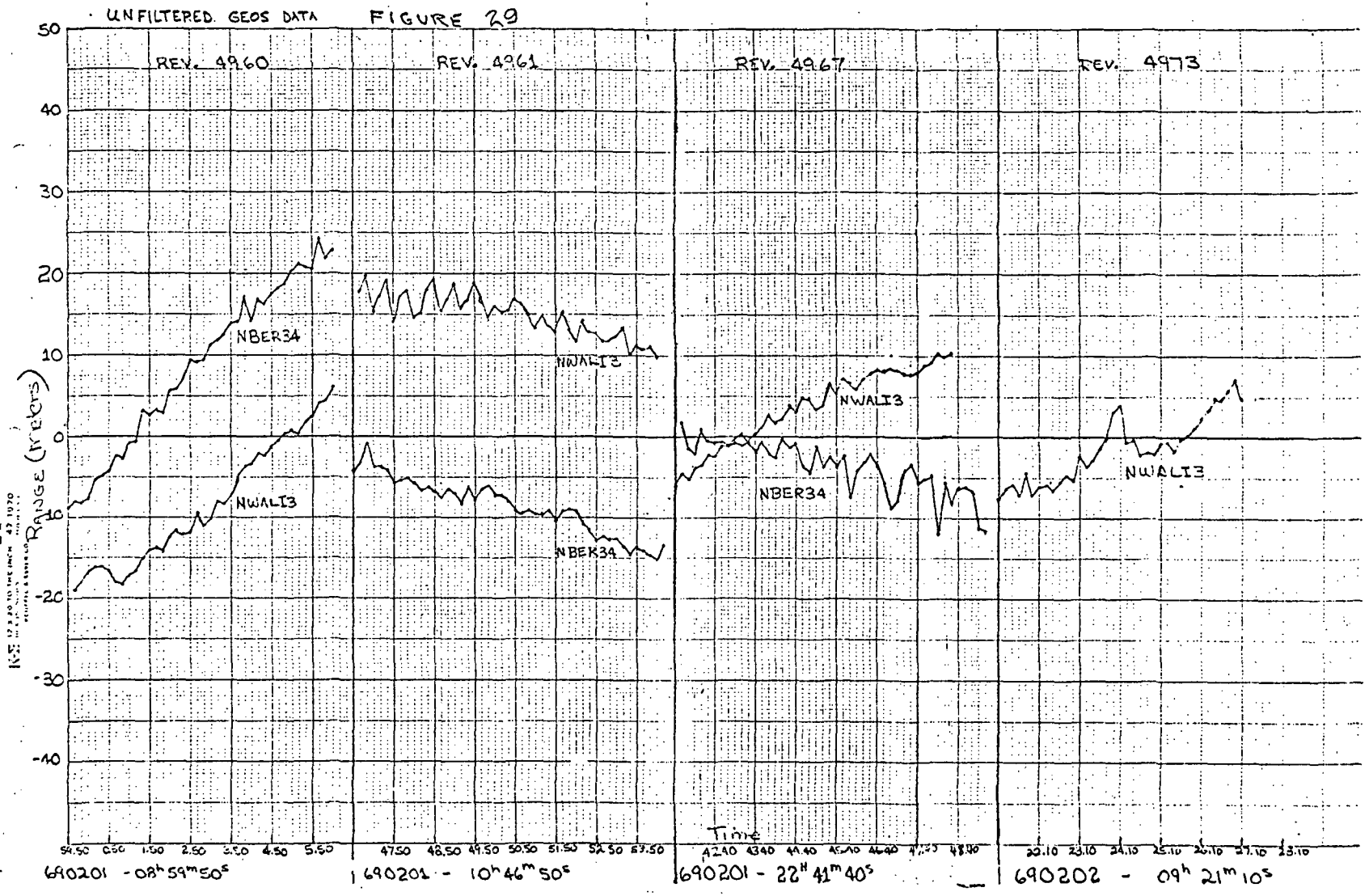
UNFILTERED GEOS DATA
FIGURE 29
REV. 4960
REV. 4961
REV. 4967
REV. 4973
NBER34
NWALI3
NWALI3
NBEK34
NWALI3
NBER34
NWALI3
RANGE (METERS)
50
40
30
20
10
0
-10
-20
-30
-40
Time
690201 - 08h 59m 50s
690201 - 10h 46m 50s
690201 - 22h 41m 40s
690202 - 09h 21m 10s

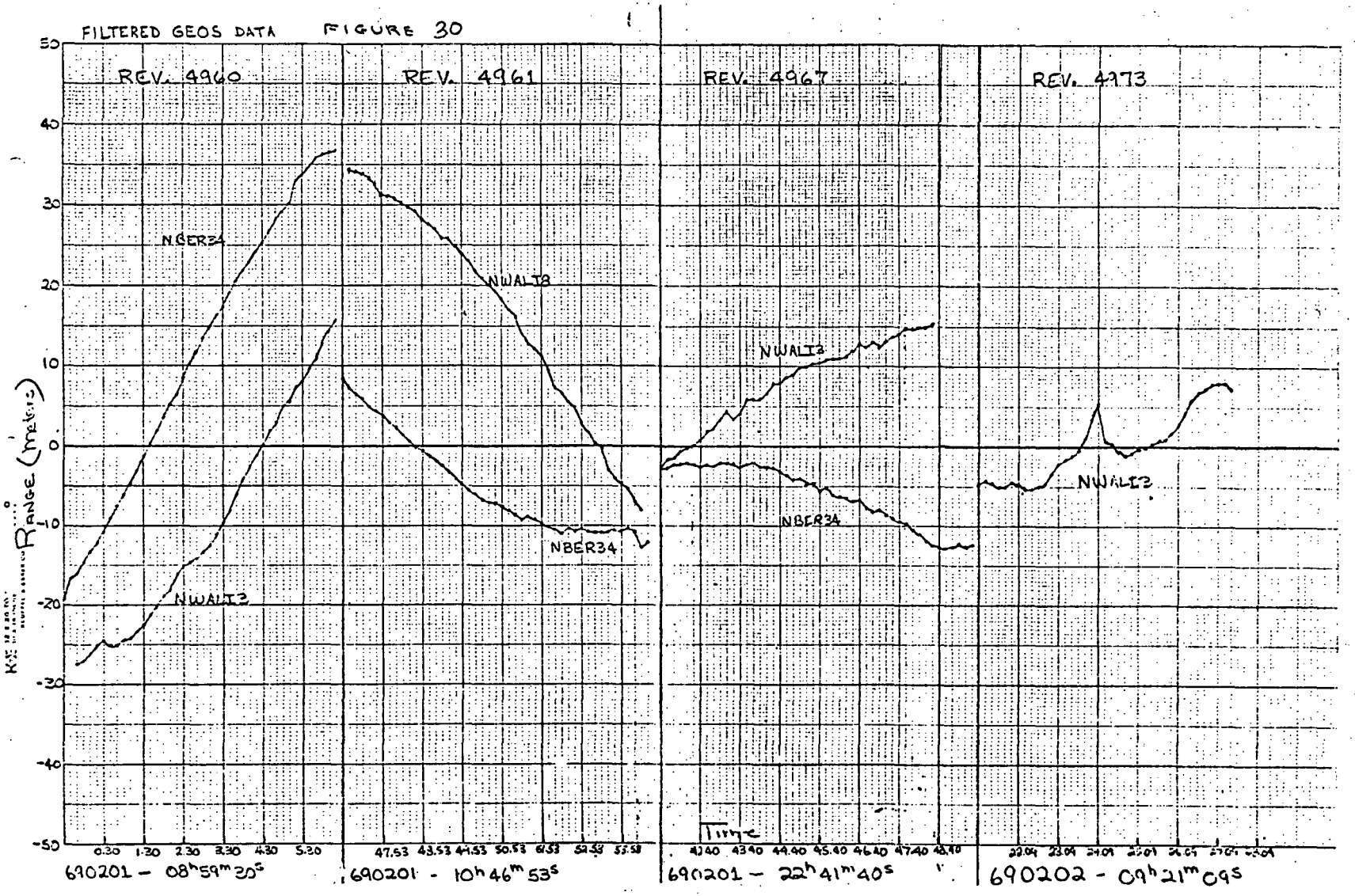
FILTERED GEOS DATA
FIGURE 30
REV. 4960
REV. 4961
REV. 4967
REV. 4973
NBER34
NWALI3
NWALI3
NBER34
NWALI3
NBER34
NWALI3
Range (meters)
50
40
30
20
10
0
-10
-20
-30
-40
-50
0.30 1.30 2.30 3.30 4.30 5.30
47.53 43.53 41.53 50.53 51.53 52.53 53.53
43.40 44.40 45.40 46.40 47.40 48.40
Time
690201 - 08h59m30s
690201 - 10h46m53s
690201 - 22h41m40s
690202 - 09h21m09s

2.2.5 CSP Studies on Wice Test 73

In connection with the CSP studies on WICE Test 73, the range rate values from the CSP unit were filtered, but not compacted, before computing the low-noise CSP ranges. The filter used was a 1201 point low-pass filter with cut-off at .05 hertz. The result was a reduction in RMS of fit to a 20 second orbit, from 7.6mm to 0.6mm.

2.3 AUTO-COVARIANCE FUNCTION STUDIES

Severval studies of the nature of the auto-covariance function of the residuals of unfiltered vs filtered range data were completed. The program used for these studies is subroutine FP9, (See Appendix A) which can be called as an option in the COMPACT program. FP9 produces a periodogram of a set of data, then Fourier transforms the periodogram to obtain the auto-covariance function of the data.

2.3.1 Auto-covariance Function of Normal Beacon Data

Data from NBER34 on Rev 4960 was processed by the COMPACT program, using a 601 point filter with cut-off at .1 hertz. The auto-covariance option was used. The periodogram computed was essentially featureless. A plot is not shown, because the periodogram contains over 1000 points and is a random scatter of points, above .1 hertz. Below .1 hertz the periodogram is essentially zero, since the residuals from wich the periodogram was taken have the frequencies from 0 .1 hertz filtered out. The auto-covariance function shows a spike of .477 meters^2 at zero lag, agreeing with the computed variance of the

residuals. All other points on the auto-covariance function are less than .04 in absolute value, and appear to be completely random.

2.3.2 Auto-covariance Results on The Ship Test Data

Data from the VANGUARD radar on Puerto Rican Trench Ship Test number 18 was treated in the fashion described above. 2000 points of range data at 10 per second were passed through COMPACT program with the option of computing the periodogram and auto covariance function. It was suspected that the autophasing mechanism was introducing spikes in the range system at one second intervals. The residuals did not conclusively show the spikes, as the general noise level tended to obscure them. The periodogram of the data did show frequency spikes, occurring at exactly 1., 2., 3. and 4. hertz, of almost equal amplitudes. The variance attributable the four spikes is .26 mtr.^{2} of a total variance of 4.78 mtr. It would appear that the error introduced by this effect is negligible with respect to the other contributing factors to the noise. The 1 per second spikes are quite apparent in the plot of the auto-covariance function of the residuals.

2.3.3 Auto-covariance Results on PMRMR1 Data

Power spectral density estimates on range data from PMRMR1 had indicated that some peculiarity would be found in the data. In addition, residuals from short arc data indicated periodic discontinuities in the data. Range data from Rev number 4989 were processed by the COMPACT program with option to compute the auto-covariance and periodogram.

The resulting residual plots showed discontinuities occurring approximately every 11.9 seconds. Figure 31 shows a 20 second sample of the residual plot. The periodogram, the low frequency part of which is plotted on Figure 32, shows spikes at the harmonics of this fundamental period. The fundamental, at .084 hertz, is relatively weak because of the action of the filter, which acts like a .1 hertz high-pass filter on the residuals. The auto-covariance function, plotted on Figure 33, clearly shows the periods of the fundamental and first harmonic.

2.3.4 Auto-covariance Results on Residuals from Short-Arc Data

A program, AUTOCORR, (See Appendix A) was written to read data from the A/OMEGA Plot output tape, and to apply FP9 to obtain the auto-covariance function and periodogram of the resulting data.

Raw range data at 10/second from the Wallops AN/FPQ-6 radar was reduced in a short-arc reduction and the resulting output tape representing residuals was used as input to AUTOCORR. Figures 34, 35 and 36 show the results.

The raw range data was then filtered by a 601 point low-pass filter, with cut-off at .1 hertz, and another short-arc reduction performed. The results of using the residuals of the filtered data as input to AUTOCORR are shown in Figures 37, 38 and 39.

The residuals of the unfiltered data, plotted on 34, show noise plus low frequency trending. The residuals of the filtered data, plotted on 37, show only the trending.

FIGURE 31

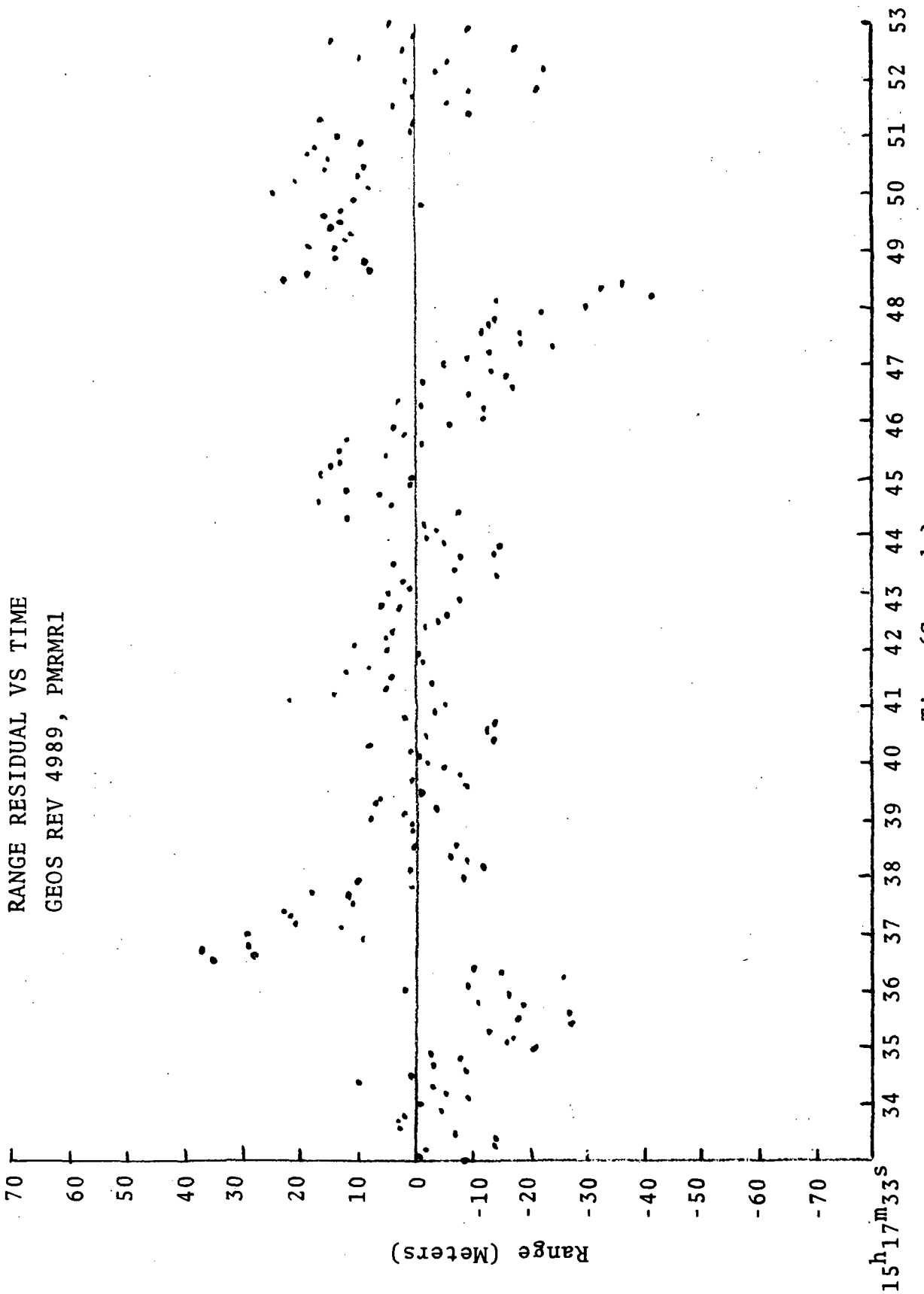
RANGE RESIDUAL VS TIME
GEOS REV 4989, PMRMR1
Range (Meters)
70
60
50
40
30
20
10
0
-10
-20
-30
-40
-50
-60
-70
15h17m33s
34
35
36
37
38
39
40
41
42
43
44
45
46
47
48
49
50
51
52
53
Time (Seconds)

FIGURE 32

POWER SPECTRAL DENSITY VS FREQUENCY
GEOS REV 4989, PMRMR1

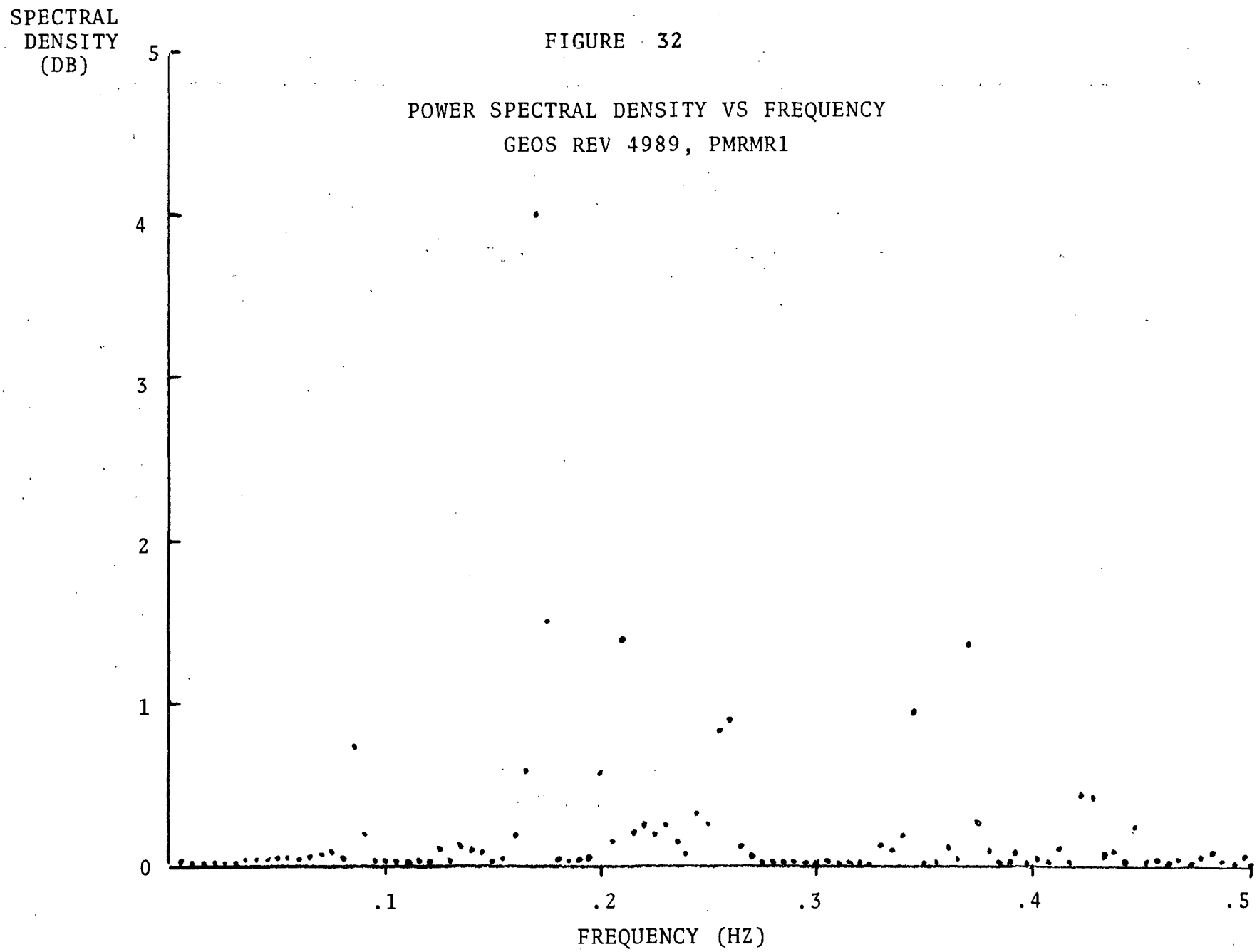

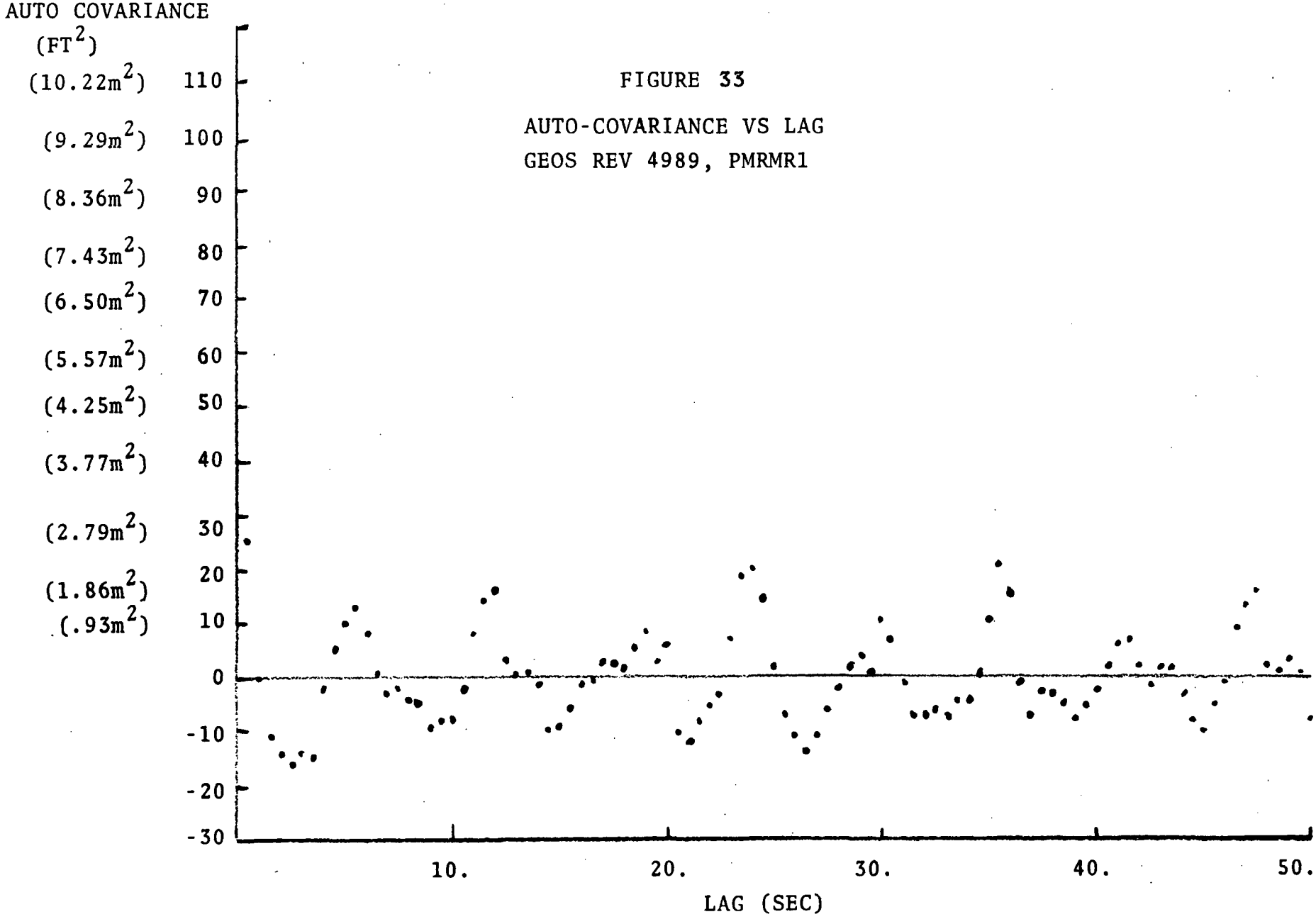

FIGURE 33

AUTO-COVARIANCE VS LAG
GEOS REV 4989, PMRMR1

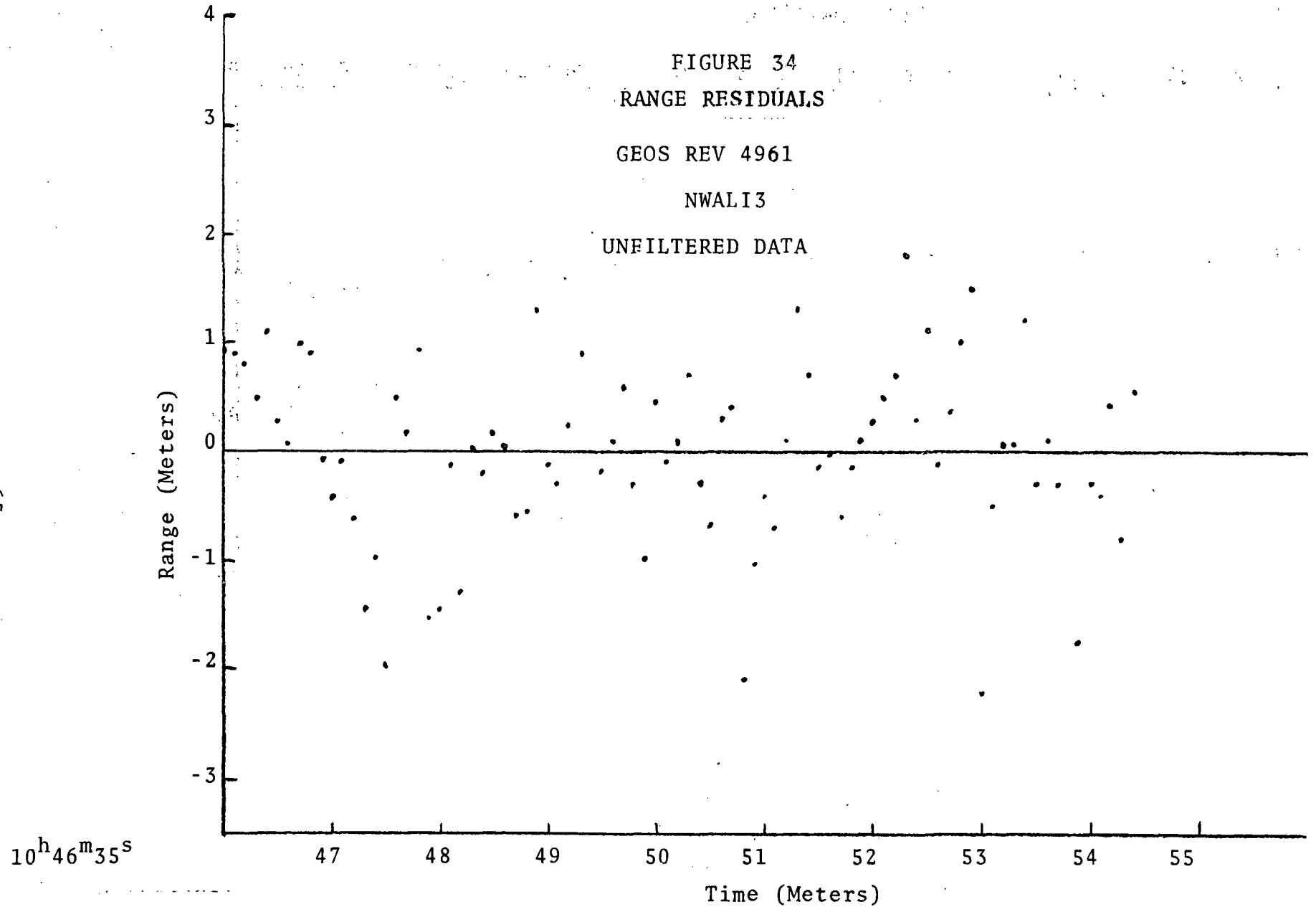
FIGURE 34
RANGE RESIDUALS
GEOS REV 4961
NWALI3
UNFILTERED DATA
Range (Meters)
4
3
2
1
0
-1
-2
-3
47
48
49
50
51
52
53
54
55
Time (Meters)
10h46m35s

FIGURE 35

POWER SPECTRAL DENSITY VS FREQUENCY

GEOS REV 4961, NWALI3

UNFILTERED DATA

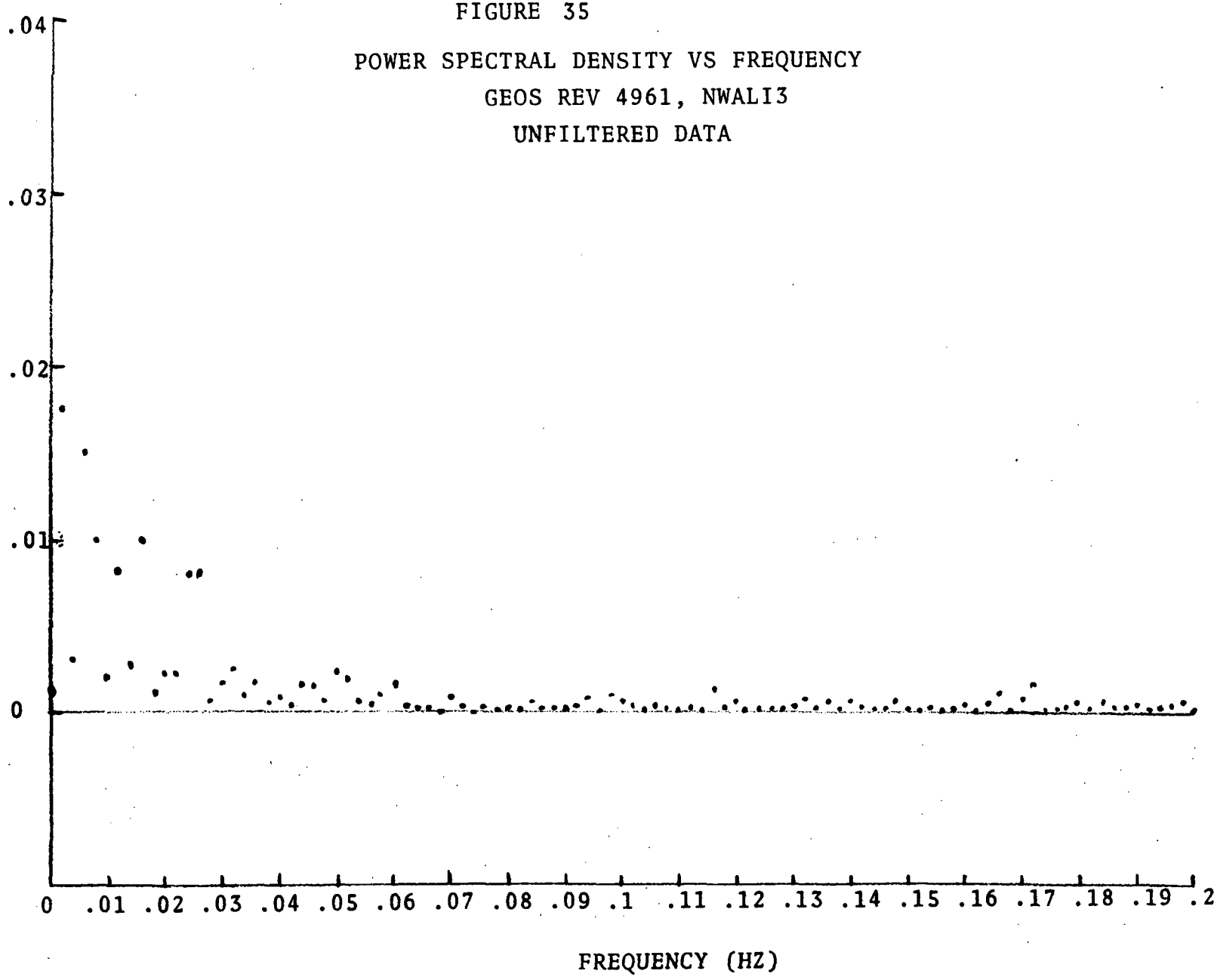

FIGURE 36

AUTO-COVARIANCE VS LAG

GEOS REV 4961, NWALI3

UNFILTERED DATA

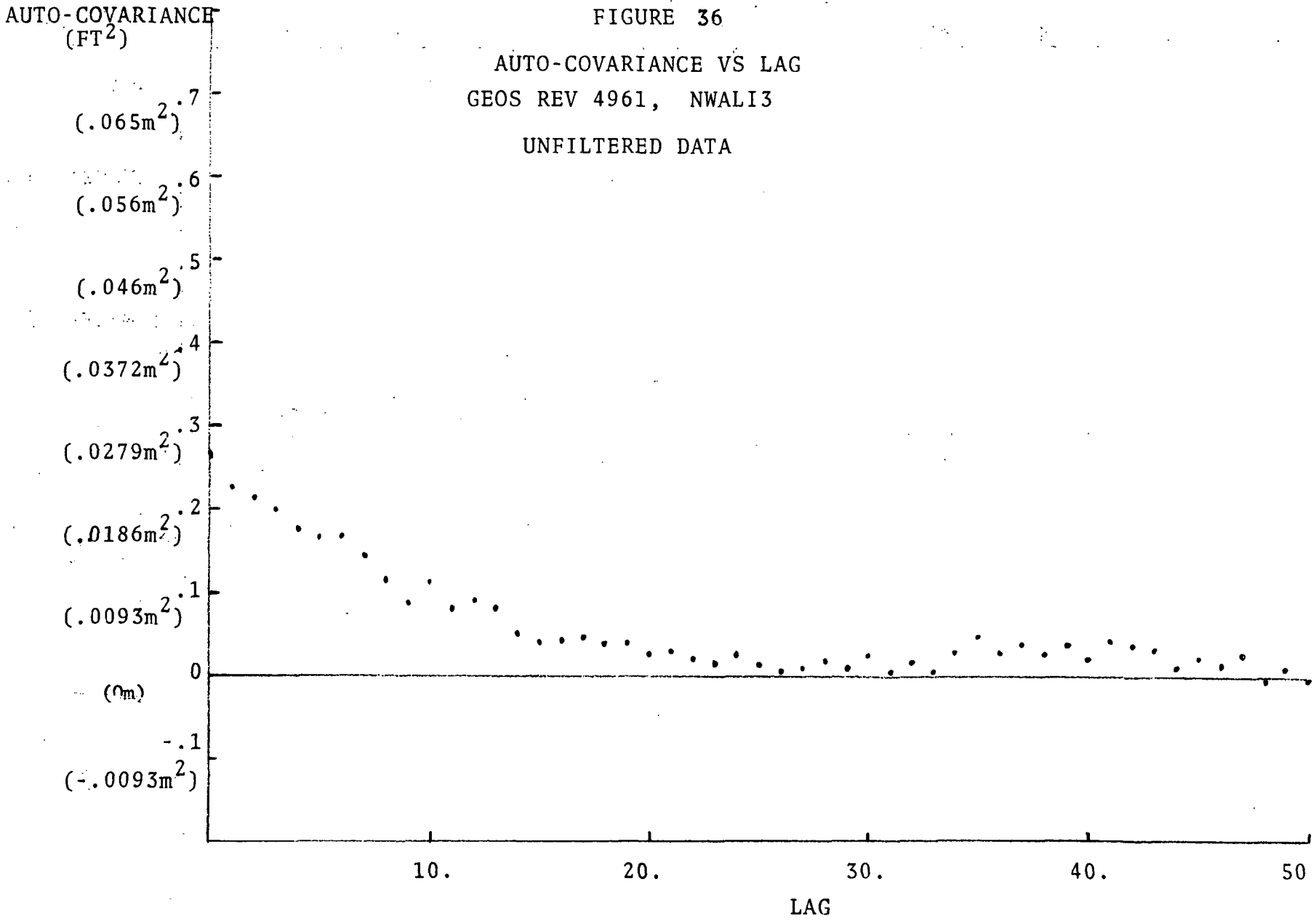

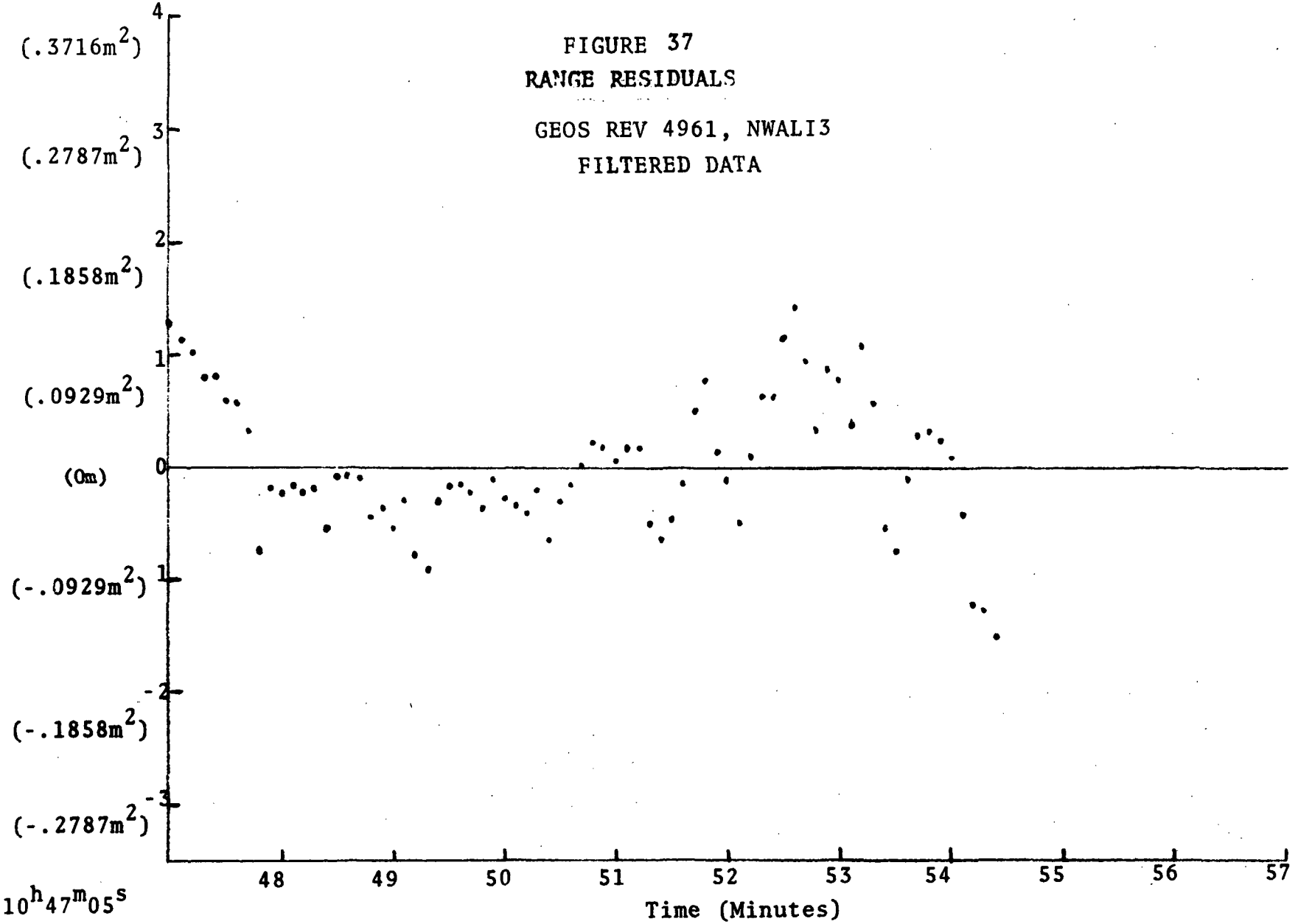
FIGURE 37
RANGE RESIDUALS
GEOS REV 4961, NWALI3
FILTERED DATA
4
(.3716m²)
3
(.2787m²)
2
(.1858m²)
1
(.0929m²)
0
(0m)
1
(-.0929m²)
2
(-.1858m²)
3
(-.2787m²)
48
49
50
51
52
53
54
55
56
57
10h47m05s
Time (Minutes)

FIGURE 38

POWER SPECTRAL DENSITY VS FREQUENCY
GEOS REV 4961, NWALI3
FILTERED DATA

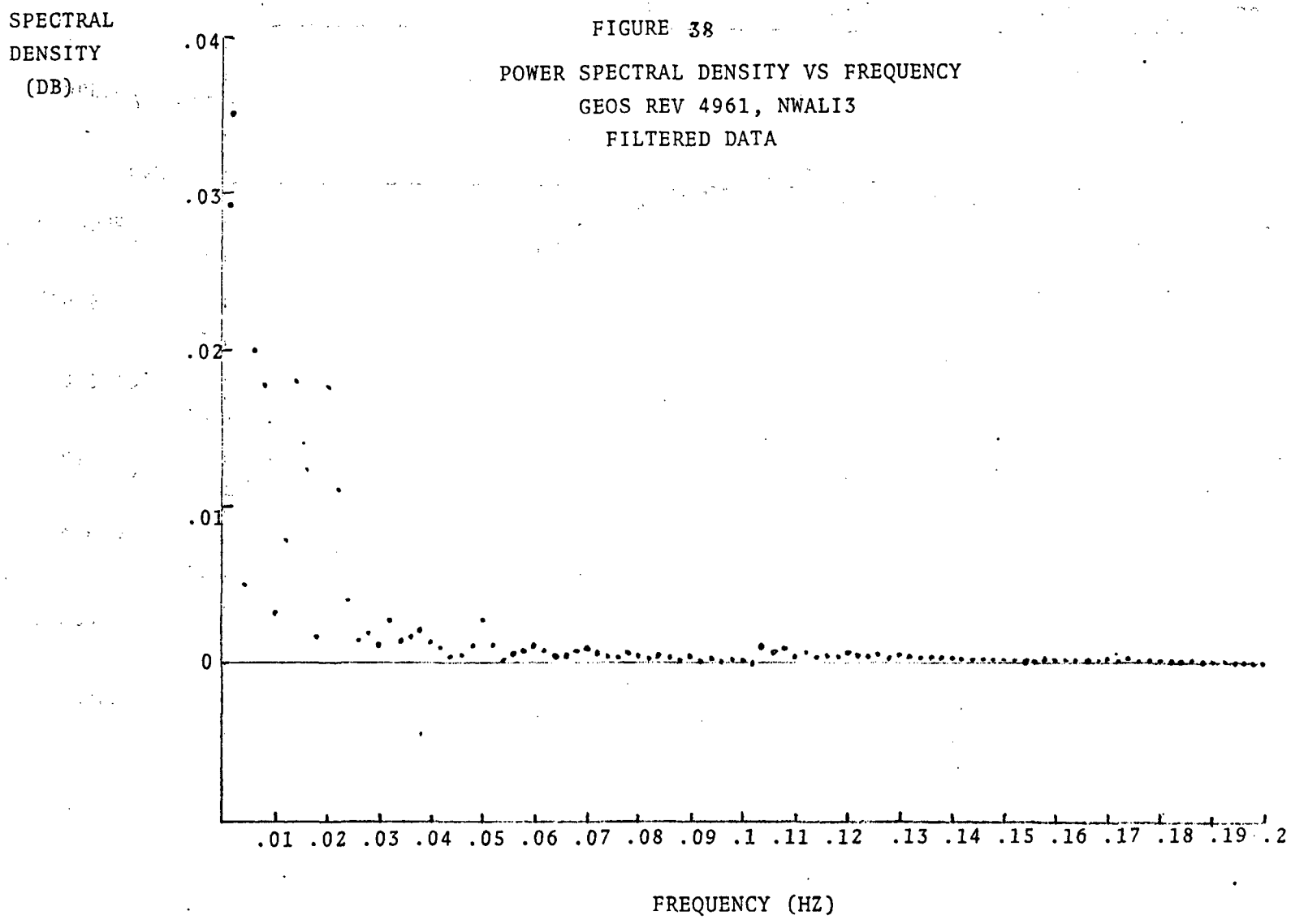

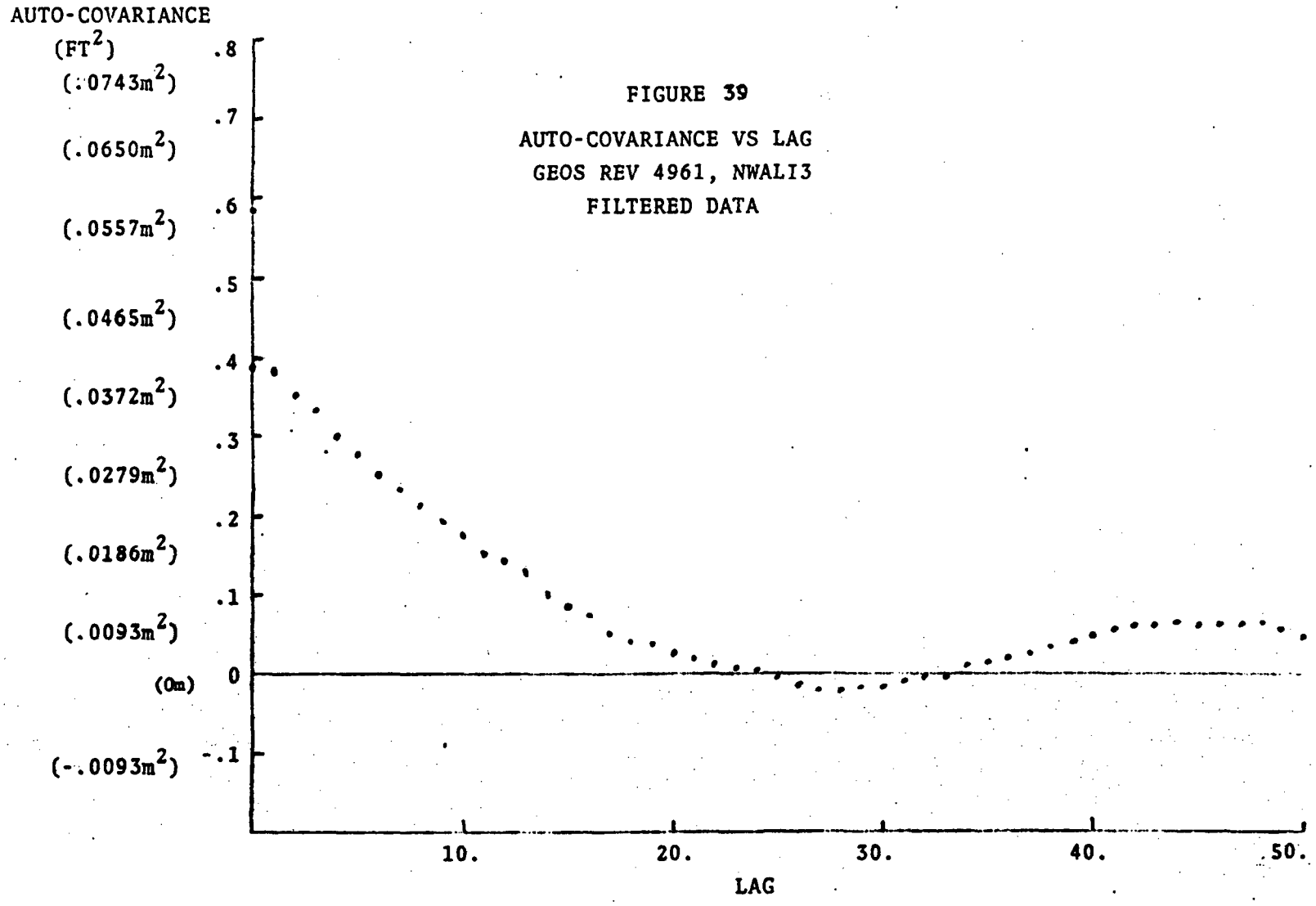

FIGURE 39

AUTO-COVARIANCE VS LAG
GEOS REV 4961, NWALI3
FILTERED DATA

The power spectrum (periodogram) of the residuals from unfiltered range data, Figure 35, shows the low frequency content cutting off at about .2 hertz, with white noise at higher frequencies. The periodogram of the residuals of filtered data, Figure 38, show about the same low frequency content but also show the white noise cut-off at about .1 hertz, caused by the filtering.

The auto-covariance functions of the two sets of data show a very similar overall structure. Both show a first zero crossing of about 25 seconds, which is compatible with a signal cut-off at about .02 hertz.

3.0 RESULTS AND CONCLUSIONS

3.1 RESULTS

3.1.1 Spectral Analysis

The major results of the investigation of the spectral content of the radar measurement channels are as follows:

a) The spectral density of the signal component of the data from range, azimuth and elevation measurement channels, tracking a satellite, is concentrated at frequencies lower than .05 hertz. A low-pass filter, with sharp cut-off at .05 hertz, will retain all signal content of the data, and reject almost all noise content.

b) The spectral density of the noise content of the range measurement channel is essentially flat from .05 hertz to 5 hertz, for 10/second data. Most of this noise content is caused by signal granularity, or low order bit truncation.

c) The spectral density of the noise content of the azimuth and elevation measurement channels are similar showing relatively flat noise to 1 hertz, and a decrease of about 10 db to 3 hertz, then flat noise to 5 hertz.

d) The spectral density from all satellite passes examined were consistent with each other. Variation from the described pattern always indicated bad data, either due to processing errors or radar malfunction.

3.1.2 Data Compaction

The major results of the investigation of techniques for data compaction of the radar data on GEOS tracking records are as follows:

a) Filtering before selection of data improves the RMS of the residuals to a short-arc fit, over simply selection of raw data. The example given in Table 1 is typical. In that test, data from WICE test 80, the RMS of the residuals from the unfiltered range data was .762 meters, and from the filtered range data, .388 meters. This implies that noise with an RMS value of .656 meters has been filtered out of the data. An RMS of .622 meters for the differences between filtered and unfiltered data was computed by the COMPACT program when the data was filtered.

b) The improvement of RMS is a non-linear function of the filter cut-off frequency. Because, as was shown by the spectral analysis studies, the power spectral density of the noise in the range channel is flat above .05 hertz, the pure noise variance will be directly proportional to the filter cut-off frequency. The variance of the unfiltered

data in the example is $.2323^2 = .0540m^2$. The variance of the filtered data is $.1183m^2 = .0140$ m^2. The remaining variance, .0400 m^2 is attributable noise uniformly distributed between .05 and 5 hertz. Figure 40 is a plot of the RMS of fit, vs filter cut-off frequency, based on these assumptions.

c) Filtering the data by non-recursive low-pass filters causes a data loss, on each end of the data span, inversely proportional to the filter cut-off frequency. Figure 41 is a plot of data loss vs cut-off frequency for 10/second data.

d) Data filtered before selection produces essentially the same orbital elements as data selected without filtering, for both short-arc and long-arc orbital reduction. This demonstrates that filtering does not change the statistical content of the data, and that the accuracy of the data is unaffected by filtering.

e) Short-arc orbital reductions using unfiltered range data show distinctive short period trends in range residuals caused by interaction of range rate with the data granularity caused by low order bit size.

f) Short-arc orbital reductions using filtered range data show low frequency trends, in the frequency range 0 to .025 hertz. Comparison of data on the same satellite pass, taken by adjacent radars, indicates that the low frequency trending in the residuals from different radars are dissimilar.

FIGURE 40

RMS ERROR VS FILTER CUTOFF
BASED ON DATA FROM WICE TEST 80
NWALI3 RANGE DATA

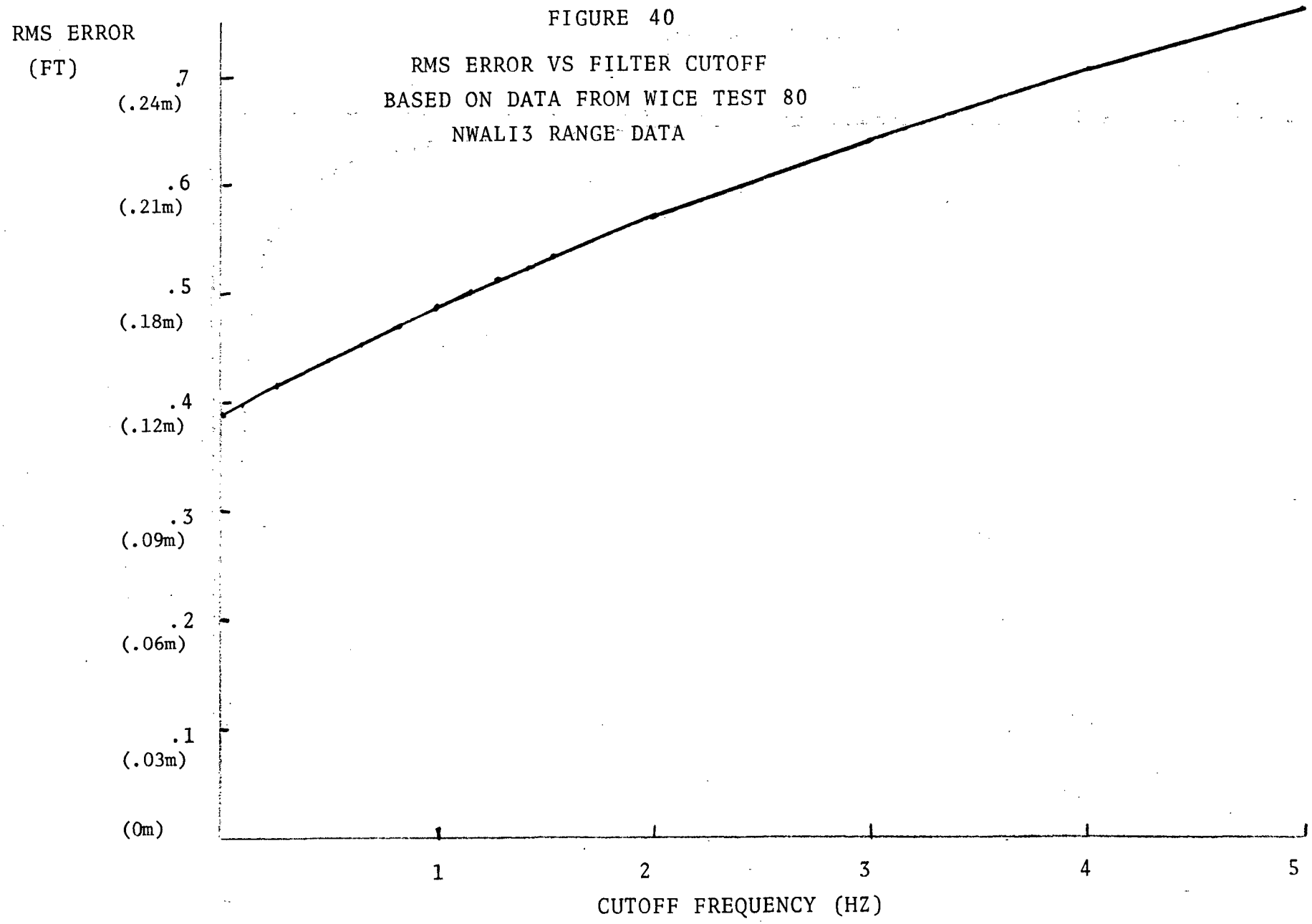

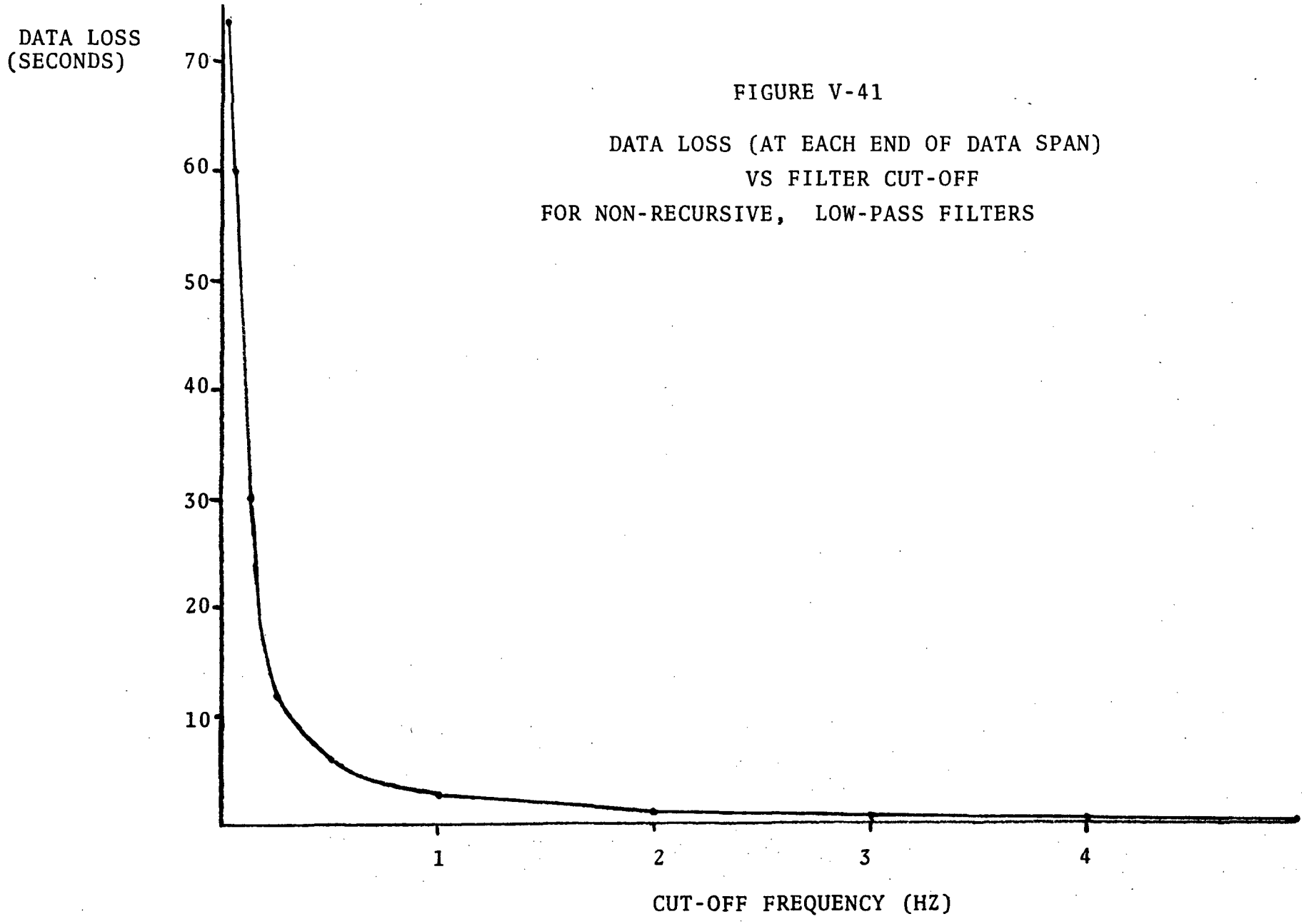

FIGURE V-41

DATA LOSS (AT EACH END OF DATA SPAN)
VS FILTER CUT-OFF
FOR NON-RECURSIVE, LOW-PASS FILTERS

This implies that the trends are caused by low frequency radar noise, not by orbit modelling errors or by data processing methods.

3.1.3 Serial Correlation and Frequency Folding

a) On the basis of theory, white noise with a cutoff frequency of f_c is uncorrelated when sampled at $1/(2f_c)$. On this basis, if the noise spectra of the radar data is essentially flat to 5 hertz, the noise is uncorrelated when sampled at 10/second. However, if the low frequency trending shown in the short-arc residuals is radar noise, then the total noise spectra of the radar cannot be considered to be flat, but is peaked at low frequencies.

b) Computation of the auto covariance function of residuals from short-arcs, indicates that zero correlation occurs at a lag of about 20 seconds, which is probably due to low frequency noise with cut-off at about .02 hertz.

c) Serial correlation of residuals is affected very little by fitlering of data. On the test described in paragraph 3.3.4, the lag for negligible serial correlation is approximately twenty seconds for both filtered and unfiltered data.

d) On unfiltered data, any sampling rate less than 10/second causes frequency folding. On filtered data, the sampling rate must be less than $1/(2f_c)$ to prevent frequency folding.

e) The theoretical optimum sampling rate to avoid both frequency folding and serial correlation is $1/(2f_c)$. This is applicable only to data with white noise having a cut-off frequency f_c.

3.2 RECOMMENDATIONS

3.2.1 Data Compaction Method

a) Based on the above results, it is recommended that the radar data which is to be stored for general scientific use be filtered with a low pass filter, with cut-off frequency at .1 hertz, then sampled at one sample per ten seconds. The .1 hertz filter is recommended to reduce the random noise content essentially to zero, and to provide for negligible error contribution caused by frequency folding or aliasing when the data is sampled at one per ten seconds. With this filter, 30 seconds of data will be lost at each end of each segment of data. This is considered acceptable in terms of total data content. Any lower frequency cut-off, with corresponding greater data loss, would not be acceptable. The one per ten second sampling is recommended as the largest interval which simultaneously

   1) Provides negligible serial correlation for short-arc residuals

   2) Provides negligible effects of frequency folding for a .1 hertz cut-off filter.

b) Data which is to be used only for long-arc reductions can be compacted by simply selecting data at 1 point per ten seconds or 1 point per 20 seconds. The slight increase in bias and low frequency error which can theoretically be expected to result

from frequency folding, apparently does not appreciably affect the orbital reduction.

c) Data should not be sampled at greater than 20 second intervals, pending further investigation, as the frequency folding of the low frequency noise might appreciably affect the data.

3.2.2 Spectral Analysis

a) The consistency of the spectral estimates is so good that it is recommended that a regular, standard check on radar operation should be an examination of the spectral density curves of the data. This check could be performed on raw data, before any reduction is done, and if done as a standard operational procedure would serve to identify instrument malfunctions early in the operation.

REFERENCES

1 Spectral Analysis Techniques Lecture Series, presented in Connection with Contract NAS6-1628, NASA/Wallops Station by Keith Guard, Wolf Research and Development Corporation, March 1972.

2 Spectral Analysis Subroutines Users Guide developed for Contract NAS6-1628, NASA/Wallops Station, by Keith Guard, Wolf Research and Development Corporation, March 1972.

APPENDIX A

COMPUTER PROGRAMS DEVELOPED

A.0 COMPUTER PROGRAMS DEVELOPED

A.1 SUBROUTINE PACKAGE

In order to implement the methods developed for Spectral Analysis and data compaction, a number of computer programs and associated subroutines were programmed. Since many of the numerical methods used are applicable to more than one portion of the study, and in fact are generally applicable to many other data processing problems, a set of general purpose subroutines were programmed to implement these methods. The subroutines are tailored to emphasize the methods which are most useful in analysis of the C-Band radar data, but are written so as to be generally applicable to many frequency analysis problems. Reference 2 describes the subroutine package in detail and Reference 1 discusses the theory involved.

A.1.1 Subroutine Functional Descriptions

Five of the subroutines are used to apply the fast Fourier transform algorithm to data arrays. The finite Fourier transofrm, implemented by the fast Fourier transform algorithm, is a component of most programs for power spectral density estimation, digital filtering and autocovariance estimation. The subroutines are as follows:

FP 6 Factors a composite (non-prime) number into prime factors and computes partial products of the factors for use in the fast Fourier transform (fFT). The fFt algorithm used is not limited to a number of points which is a power of two. It is applicable to any composite number for which the prime factors are available.

FP 7 Computes the fast Fourier transform of a complex data array. Either the direct or the inverse transform can be computed.

FP 8 Re-orders the output of FP 7, stored in digit inverted order, into normal order.

FP10 Computes the array of complex exponentials used in FP 7.

FP15 Used to economize on computing time and array storage, by allowing the transform of real arrays "packed" into complex arrays. FP15 unscrambles the transform of the packed array to produce the transform of the real array.

These five subroutines, called in the appropriate sequence, will perform any desired finite Fourier transform operation.

FP 1 Computes the coefficients of a non-recursive digital filter over N points, to obtain a high-pass, low-pass, band-pass or band stop filter.

FP 2 Applies the Lanczos sigma smoothing as a lag window function to a non-recursive digital filter array, to minimize the Gibb's effect oscillations.

FP 3 Computes the frequency response function (transfer function) of a symmetric non-recursive digital filter.

FP 4 Applies a non-recursive digital filter to a data array.

FP 5 Modifies the coefficients of a non-recursive digital filter so that the gain of the filter is unity at a specified frequency and zero at another specified frequency.

FP18 Applies a non-recursive digital filter to a data array by using the finite Fourier convolution property. The filter and the data to be filtered are Fourier transformed and the product of the transforms is inverse transformed to obtain a filtered array.

Subroutine FP11 applies a recursive three point notch filter to a data array, to remove isolated frequency spikes from the spectrum.

Four subroutines are used to generate test data, of known frequency content and statistical properties, to provide test cases for the other subroutines.

FP12 Computes a sequence of pseudo-random numbers from a uniform distribution, zero to one, by the multiplicative congruence method.

FP13 Filters a sequence of pseudo-random numbers to obtain pseudo-white noise with specified amplitude and cutoff frequency.

FP14 Constructs a data array to simulate s signal with up to ten frequency spikes (pure sinusoids), of specified amplitudes and frequencies, added to white noise.

TDATA Computes simulated radar tracking data (range, azimuth, and elevation) from a simplified orbital tracking model to provide idealized error free, data inputs to the subroutines.

Since the theory underlying all of the methods used is based on equally spaced data, and since the data contains wild points which must be edited out, an editing subroutine is used. The editing subroutine is FP16, which takes the Fourier transform of the array, deletes high frequency components, then inverse transforms to obtain a smooth function. The smooth function is compared point by point with the original data, and all data points differing from the corresponding smoothed value by more than an error limit are edited and replaced by the smoothed value.

Subroutine FP20 is used to subtract a double precision quadratic function from an array X, store the coefficients of the quadratic, then add the same quadratic to the modified array. This is used to remove the large magnitude data component from data before filtering, and to restore it after filtering, in order to minimize the effects of truncation error in the computation.

Subroutine FP 9 computes the periodogram and autocovariance function of a real data array.

Subroutine FP19 computes the cross spectrum and cross-covariance of two real arrays.

Subroutine FP17 computes an estimate of the power spectral density of a real data array. The spectral estimate is obtained by computing the discrete Fourier transform of the data, then averaging and squaring to obtain smoothed spectral estimates.

Three types of averaging are used:

1) The data is segmented, before transforming, into KSEG aubarrays of NSEG points each. After transforming and squaring to obtain raw periodograms, the spectral estimates (periodogram values) from corresponding frequency points are averaged.

2) The Fourier transforms of the data segments are averaged, before squaring and averaging, by applying the hanning spectral window KWIND times.

3) The squared estimates from each segment are averaged over KAVG points, and only the midpoint of each KAVG points is stored.

A.2 SPECDEN PROGRAM

The SPECDEN program was developed to compute estimates of power spectral density of radar measurement data.

A.2.1 Fucntional Description

The SPECDEN program either accepts as inputs radar measurement data in the Wallops PASS1 tape format or on an input option, generates test data internally for the purpose of program testing. If the PASS1 tape is used as input, any word from the data record can be read into storage for

of estimating the power spectral density. The start and stop times of the data input are also specified on input option. If sporadic gaps occur in the input data, zeroes are substituted into the stored array. An editing subroutine (FP16) is used to substitute smoothed data points in for these missing points, and to edit out wild points and substitute smoothed data in their place.

Three types of internally generated test data are available, on input option.

a) Simulated noise free radar measurement data, from a simplified satellite tracking model.

b) Up to ten sine and cosine functions with amplitudes and frequencies as input options.

c) White noise with a specified input r.m.s. value, filtered to a specified cutoff frequency.

These three input options can be used in any combination.

The data, once read in (or generated internally) and edited, can be filtered, if desired, on input option, as follows:

a) Up to 12 recursive notch filters with specified center frequencies and bandwidth can be applied to the data, using FP11.

b) A non-recursive high-pass, low-pass or band-pass filter can be applied to the data using FP18.

These filters can be used to remove known frequency components from the data before estimating the spectral density.

The spectral density estimation is done by FP17. This subrouitne obtains the spectral density by taking the finite Fourier transform of the data to obtain the spectrum of the data, then squaring each spectral component to obtain the periodogram of the data. Three types of spectral averaging, or smoothing can be applied to the data to obtain an estimate of power spectral density.

a) Linear smoothing of the Fourier transform of the data, performed before squaring or averaging, obtained by applying the hanning spectral window. This smoothing improves the resolution of the spectral estimate by decreasing spectral leakage from non harmonic components.

b) Quadratic smoothing of the periodogram, performed after squaring, by averaging a number of adjacent values of the periodogram. This quadratic smoothing improves the variance of the spectral estimates of random noise.

c) Ensemble averaging of the periodogram, obtained by segmenting the data, transforming each segment and obtaining the periodograms, the averaging corresponding frequency components.

The effects of these three types of smoothing on sample data are discussed in the next section.

The theory of linear and quadratic smoothing of spectral estimates is discussedin Lecture 5, Reference 1.

The output of SPECDEN is a listing and printer plot of the estimated power spectral density of the input data.

A.2.2 Test Data Output

The data presented in Figures A-1 through A-7 demonstrates the use of linear smoothing of the periodogram to obtain spectral estimates. For each test 200 data points were generated at a simulated time increment of 1/second. The result is 101 spectral points from 0 to 0.5 hz, at a spacing of .005 hz. All the periodogram from 0 to 0.5 hz is symmetric with that from 0 to 0.5 hz, and in accordance with convention, the total power is presented in the positive portion of the spectrum.

All spectral data are presented in decibels, obtained by taking 10 log 10 of the spectral points.

Test 1 data consisted of a steady state component and periodic components at .1, .2, .3, .4 and .5 hz, all with amplitude 1. Figure 1 shows the resulting spectra, with spikes at the input frequencies at 0. db for the steady state component and -3 db for the periodic components. This test demonstrated that the program performs correctly on idealized periodic, harmonic data.

The computational noise level, caused by truncation in the 27 bit mantissa of the floating point word in the computer, is about -140 db, so the dynamic range of the spectral estimates if 140 db.

FIGURE A-1

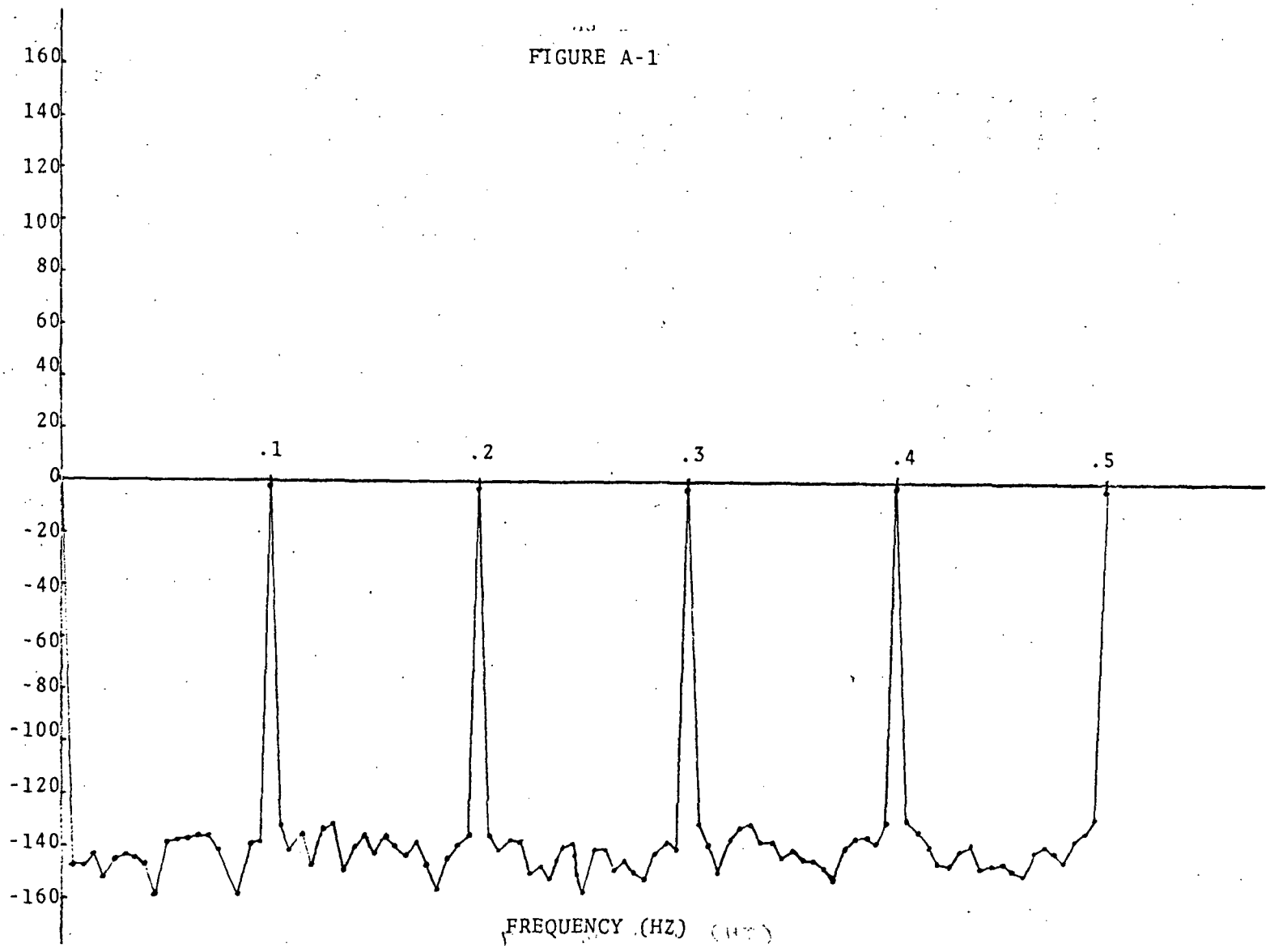
SPECTRAL DENSITY (DB)
160
140
120
100
80
60
40
20
0
-20
-40
-60
-80
-100
-120
-140
-160
.1
.2
.3
.4
.5
FREQUENCY (HZ)

FIGURE A-2

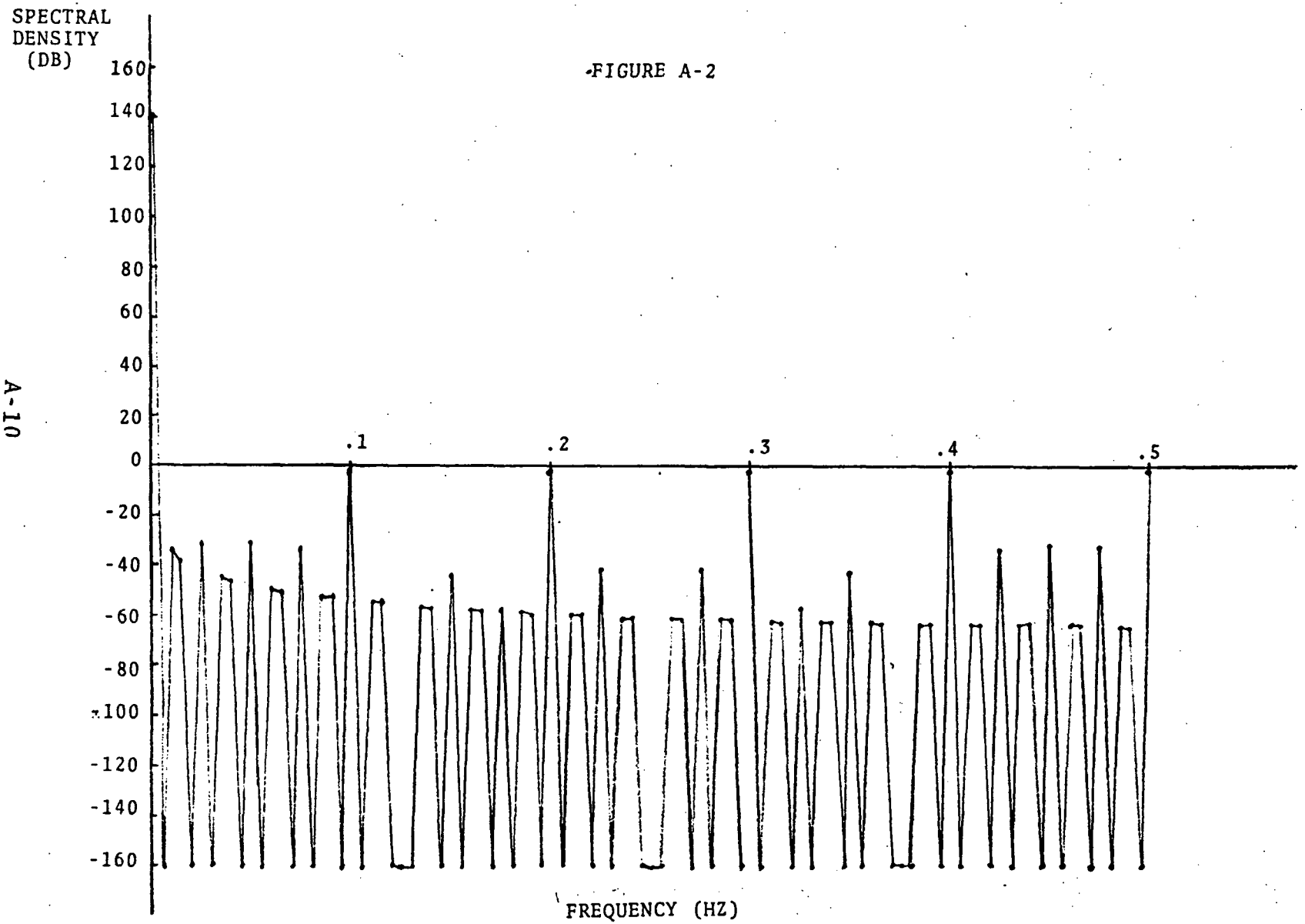
SPECTRAL DENSITY (DB)
160
140
120
100
80
60
40
20
0
-20
-40
-60
-80
-100
-120
-140
-160
.1
.2
.3
.4
.5
FREQUENCY (HZ)

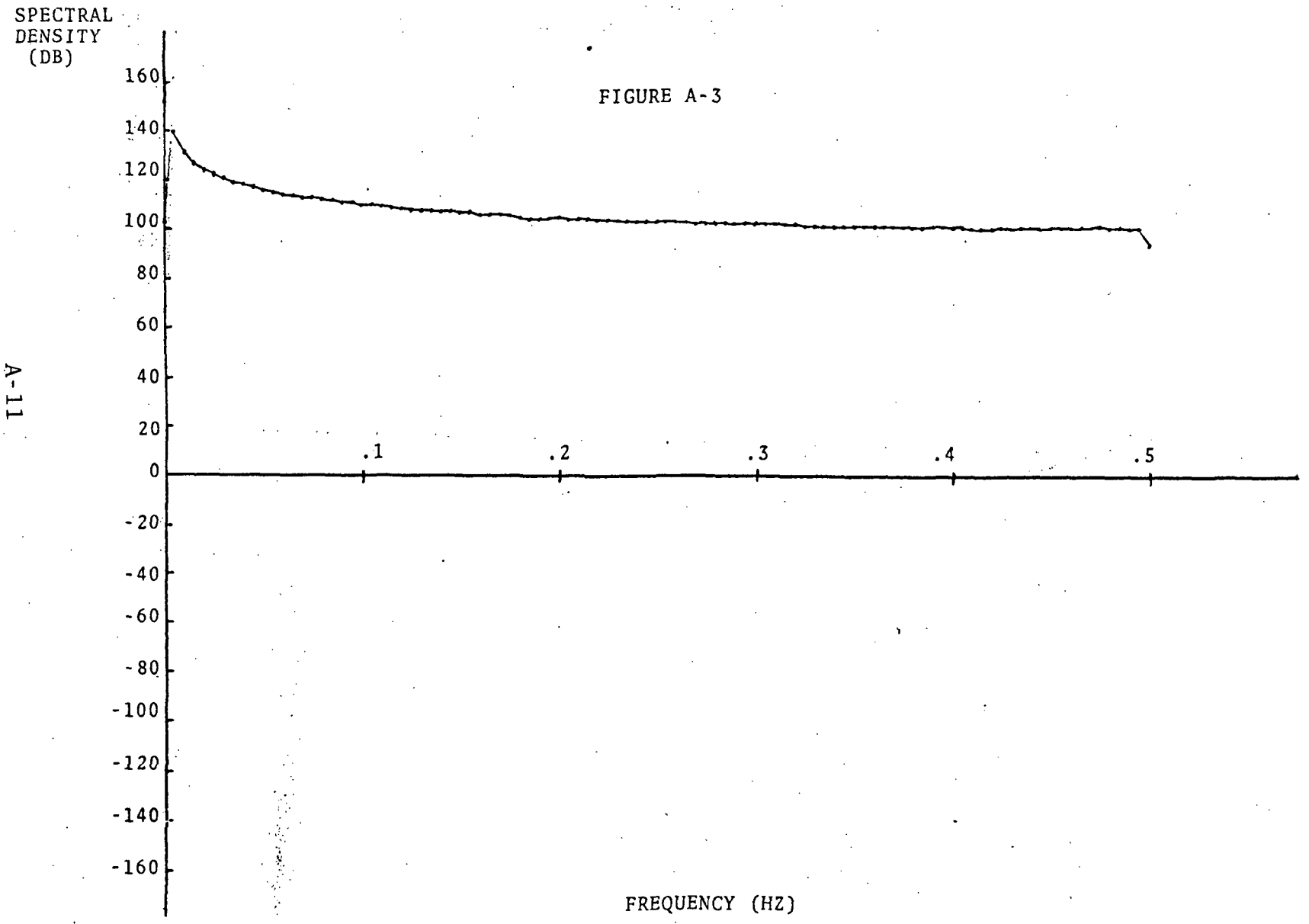
SPECTRAL
DENSITY
(DB)
160
140
120
100
80
60
40
20
0
-20
-40
-60
-80
-100
-120
-140
-160
.1
.2
.3
.4
.5
FREQUENCY (HZ)

FIGURE A-3

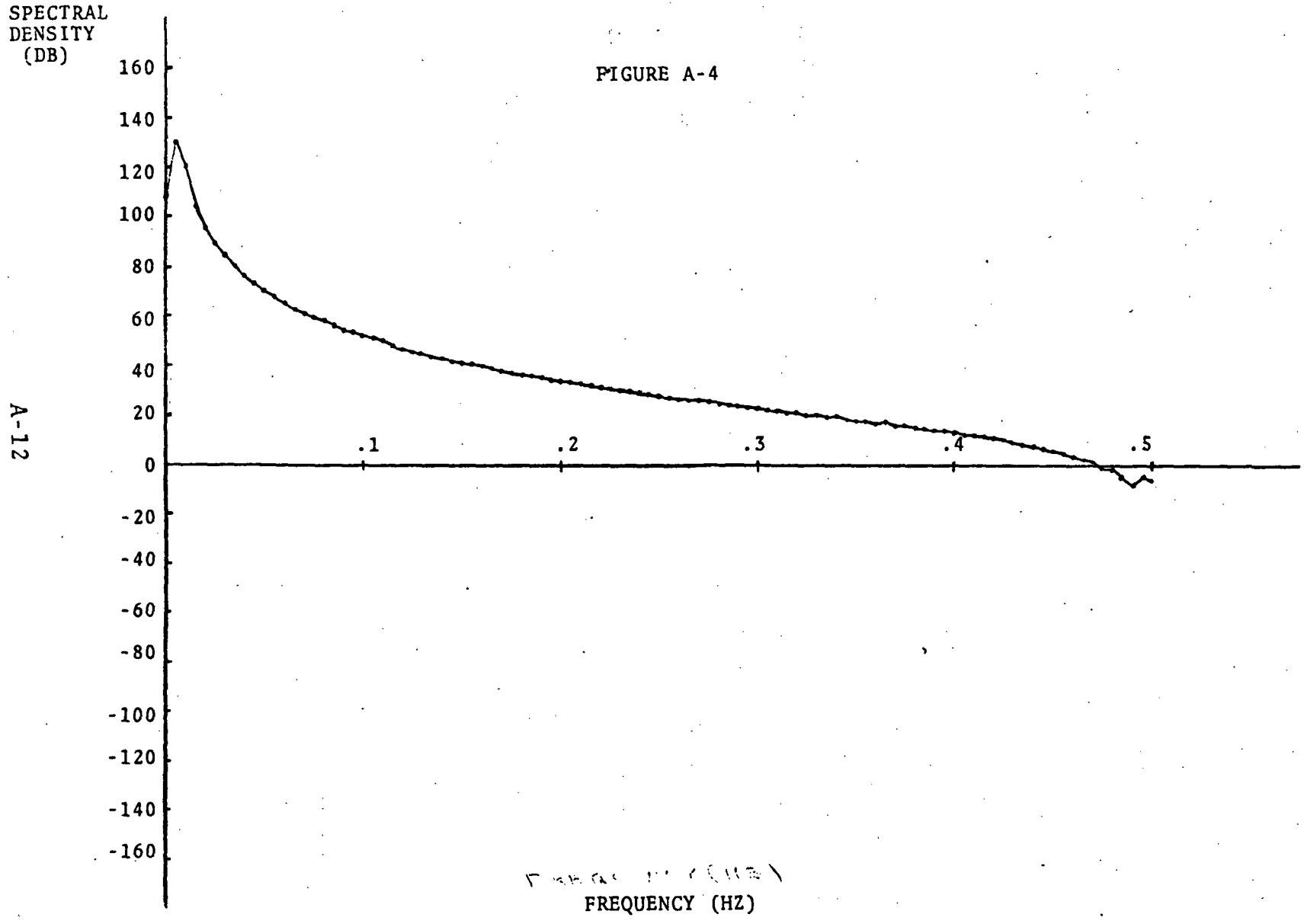
SPECTRAL
DENSITY
(DB)
160
140
120
100
80
60
40
20
0
-20
-40
-60
-80
-100
-120
-140
-160
.1
.2
.3
.4
.5
FREQUENCY (HZ)

FIGURE A-4

FIGURE A-5

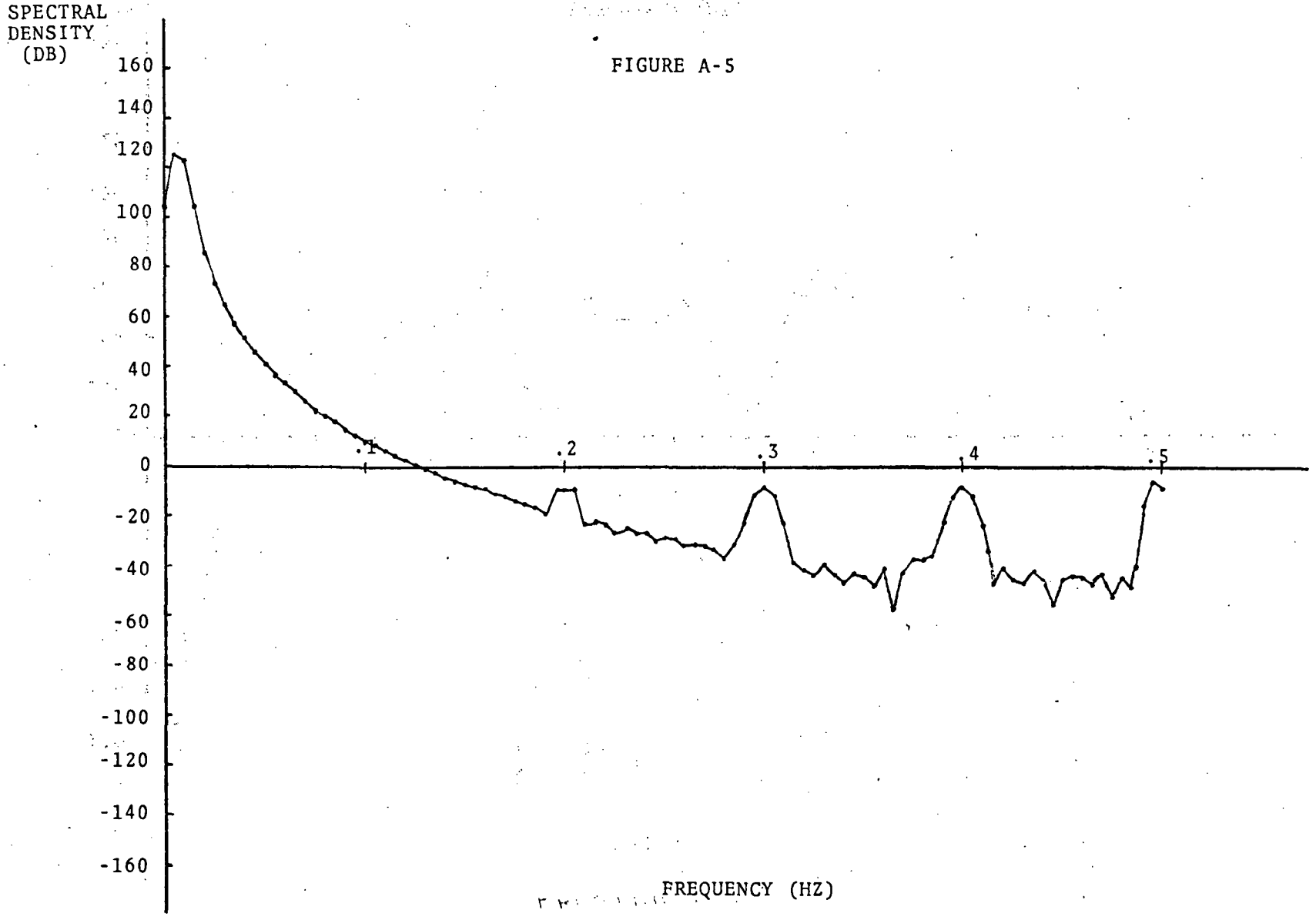
SPECTRAL
DENSITY
(DB)
160
140
120
100
80
60
40
20
0
-20
-40
-60
-80
-100
-120
-140
-160
.1
.2
.3
.4
.5
FREQUENCY (HZ)

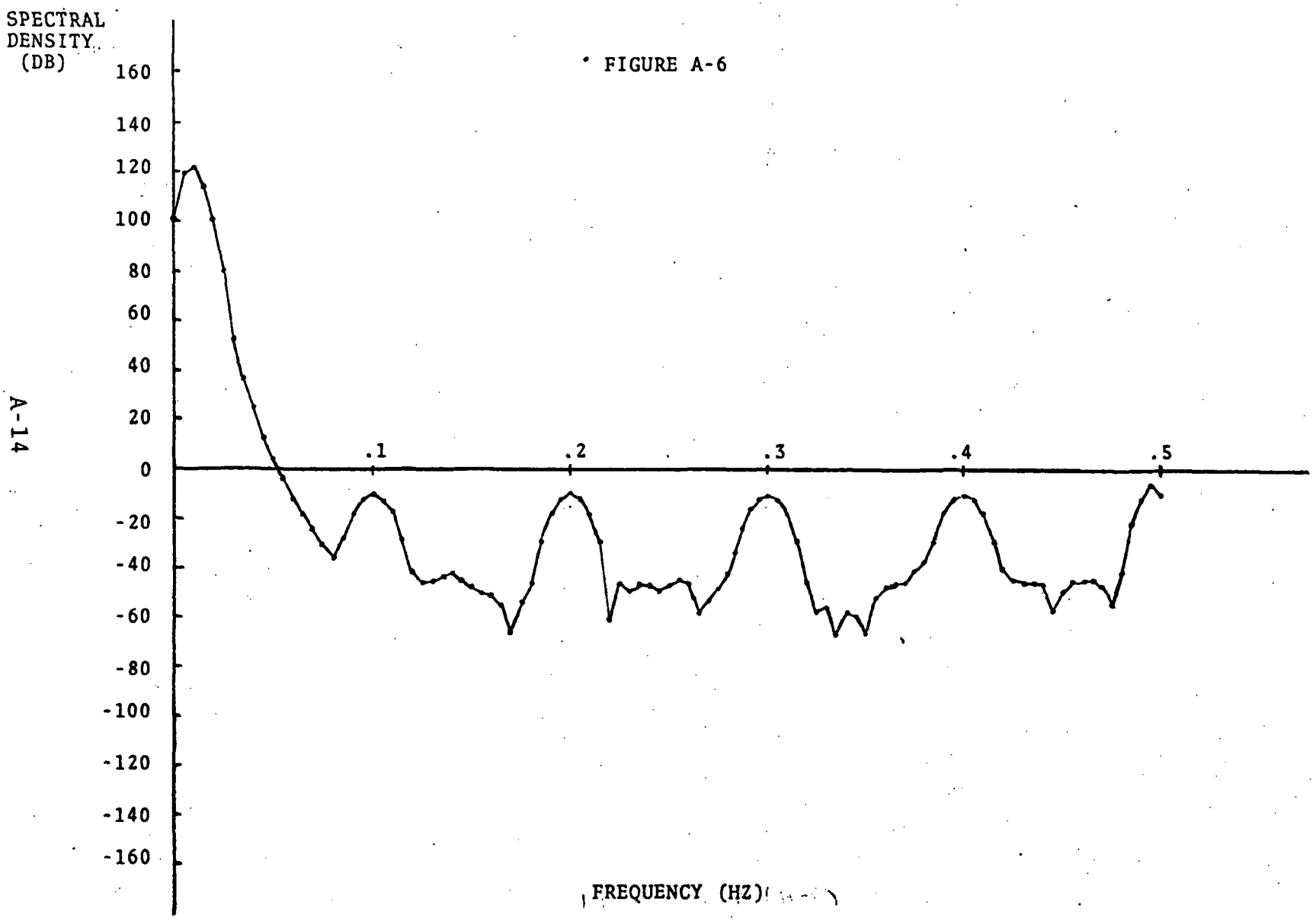
SPECTRAL DENSITY (DB)
160
140
120
100
80
60
40
20
0
-20
-40
-60
-80
-100
-120
-140
-160
.1
.2
.3
.4
.5
FREQUENCY (HZ)

FIGURE A-6

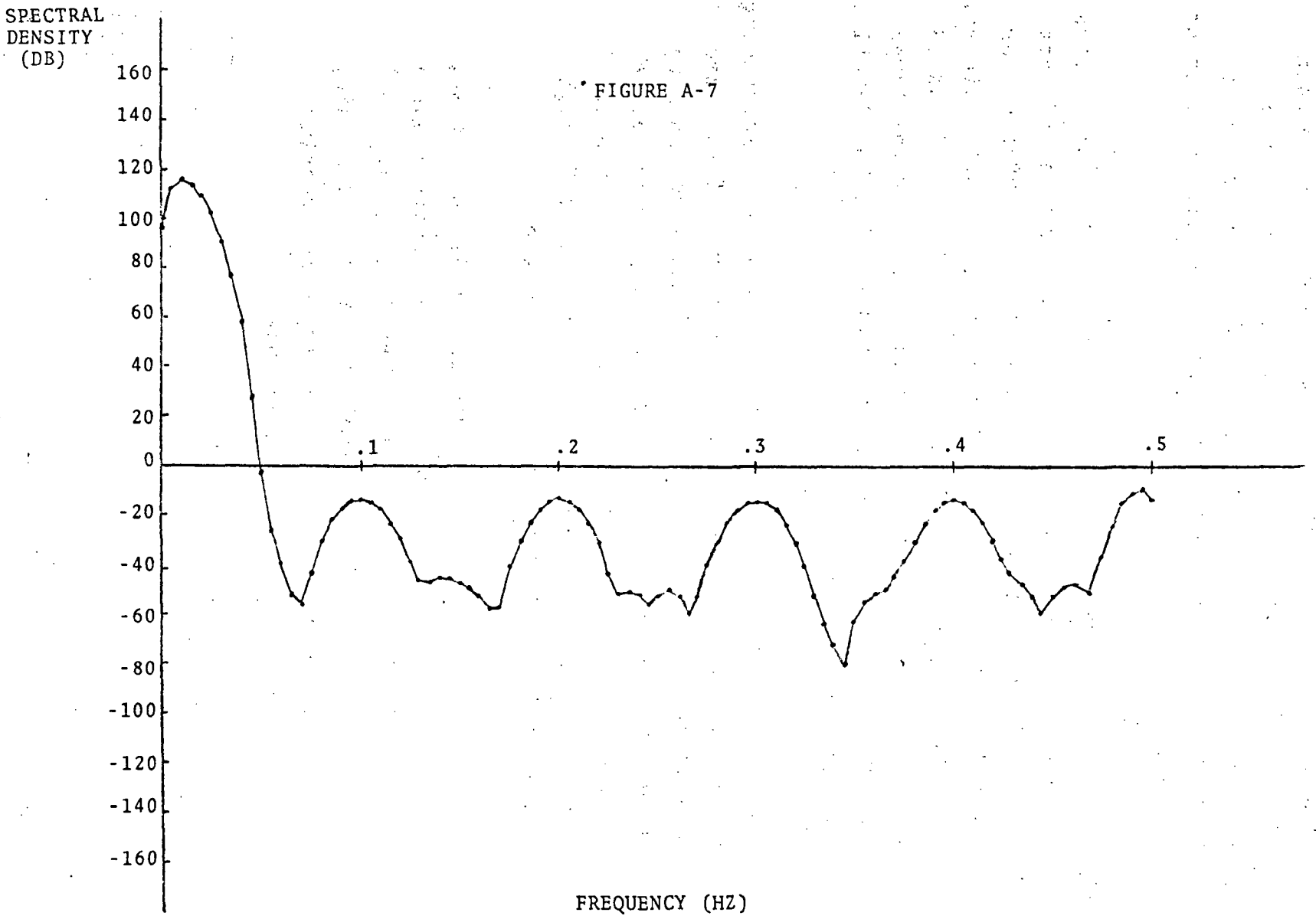
SPECTRAL
DENSITY
(DB)
160
140
120
100
80
60
40
20
0
-20
-40
-60
-80
-100
-120
-140
-160
.1
.2
.3
.4
.5
FREQUENCY (HZ)

FIGURE A-7

Test 2, with results shown in Figure 2, used the same periodic components, with a steady state component of 10^7. The truncation error increased to about -50 db, the steady state spike increased to 140 db, as it should, and the periodic component spikes stayed constant at -3 db.

Test 3 presents a graphic demonstration of spectral leakage caused by a large non-harmonic component of data. The input was a component with amplitude of .0025 hz, or one half of the fundamental frequency of the data interval, and components with amplitude 1 at .1, .2, .3, .4 and .5 hz, as before. The spectral leakage caused by the large non-harmonic component completely hides all other detail in the spectral estimate.

Figures 4, 5, 6 and 7 show the effect of increasing amounts of linear smoothing on the spectrum of the same data as presented in Figure 3. In Figure 4 the hanning window was applied to the transformed data once before squaring. In Figure 5 the hanning window was applied twice, in Figure 6, four times, and in Figure 7, eight times. The effects to be noticed are these:

a) As the hanning window is applied more times, the peak near zero hertz gets sharper until Figure 7, where it is broader. It appears that about four applications of the hanning window is optimum, for improving resolution of peaks of this magnitude.

b) The signals at .1, .2, .3, .4 and .5 hertz emerge from the frequency leakage, but are broadened and decreased in amplitude by the effects of the window.

The data presented in Figures A-8 through A-14 present the effects of quadratic smoothing on spectral density estimates computed from random noise. The input data for all of the these results were computed by generating a set of random numbers with a uniform distribution, then applying a linear filter with cutoff at .25 hz. In addition, a frequency spike, consisting of a cosine function with frequency 0.1 hz and amplitude 1 was added to the data. A data sampling rate of 1/second was used, resulting in a frequency range from 0. to 0.5 hz in the output spectral estimates.

The power spectral density estimates shown were arrived at by computing the periodogram over N data points, then averaging over M frequency intervals. The numbers N and M are given below:

Figure	N	M
A-8	100	1
A-9	200	2
A-10	500	5
A-11	1000	10
A-12	2000	20
A-13	5000	50
A-14	10000	100

100 DATA POINTS
NO SPECTRAL AVERAGING

FIGURE A-8

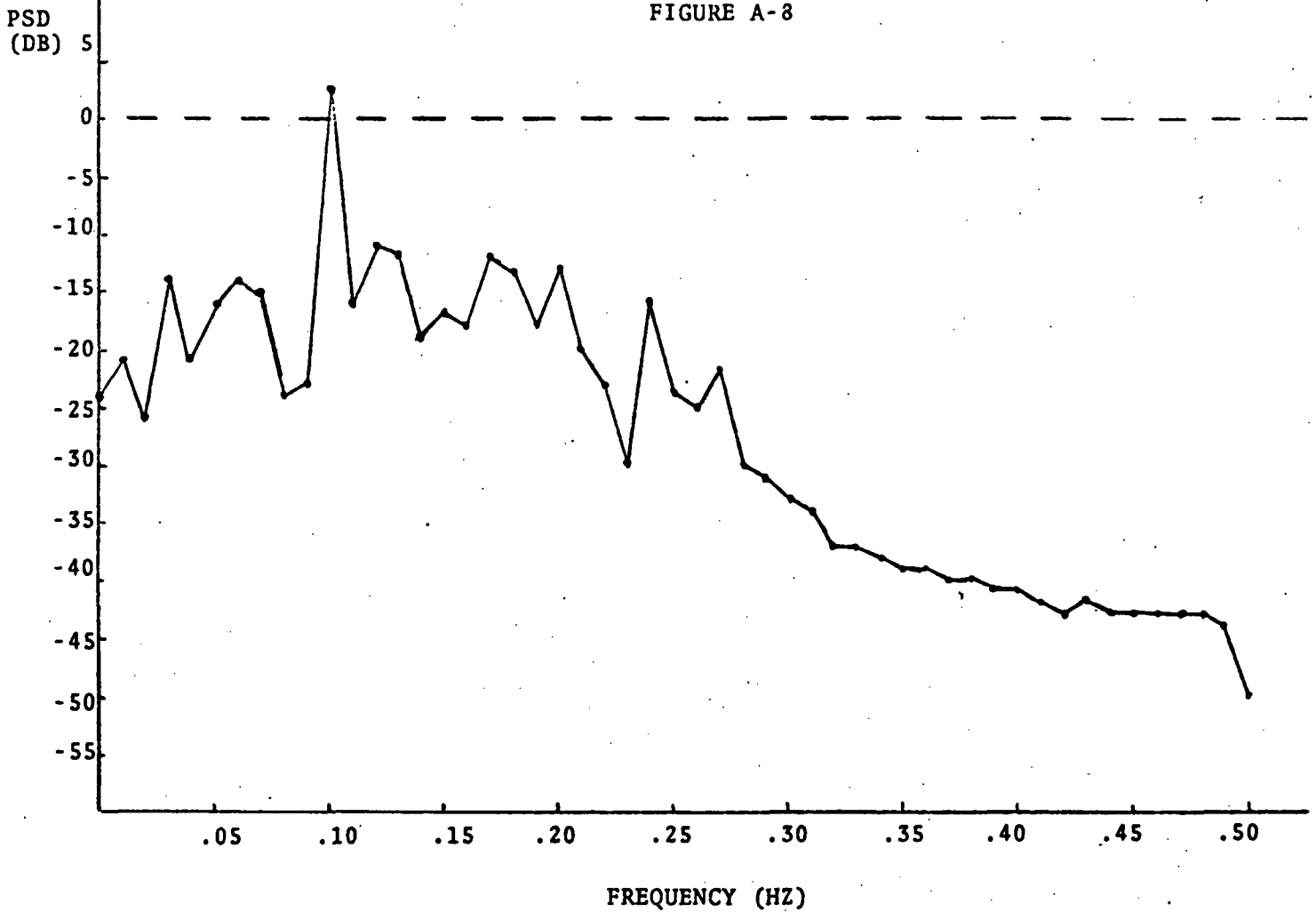

200 DATA POINTS
SPECTRUM AVERAGED OVER 2 POINTS

FIGURE A-9

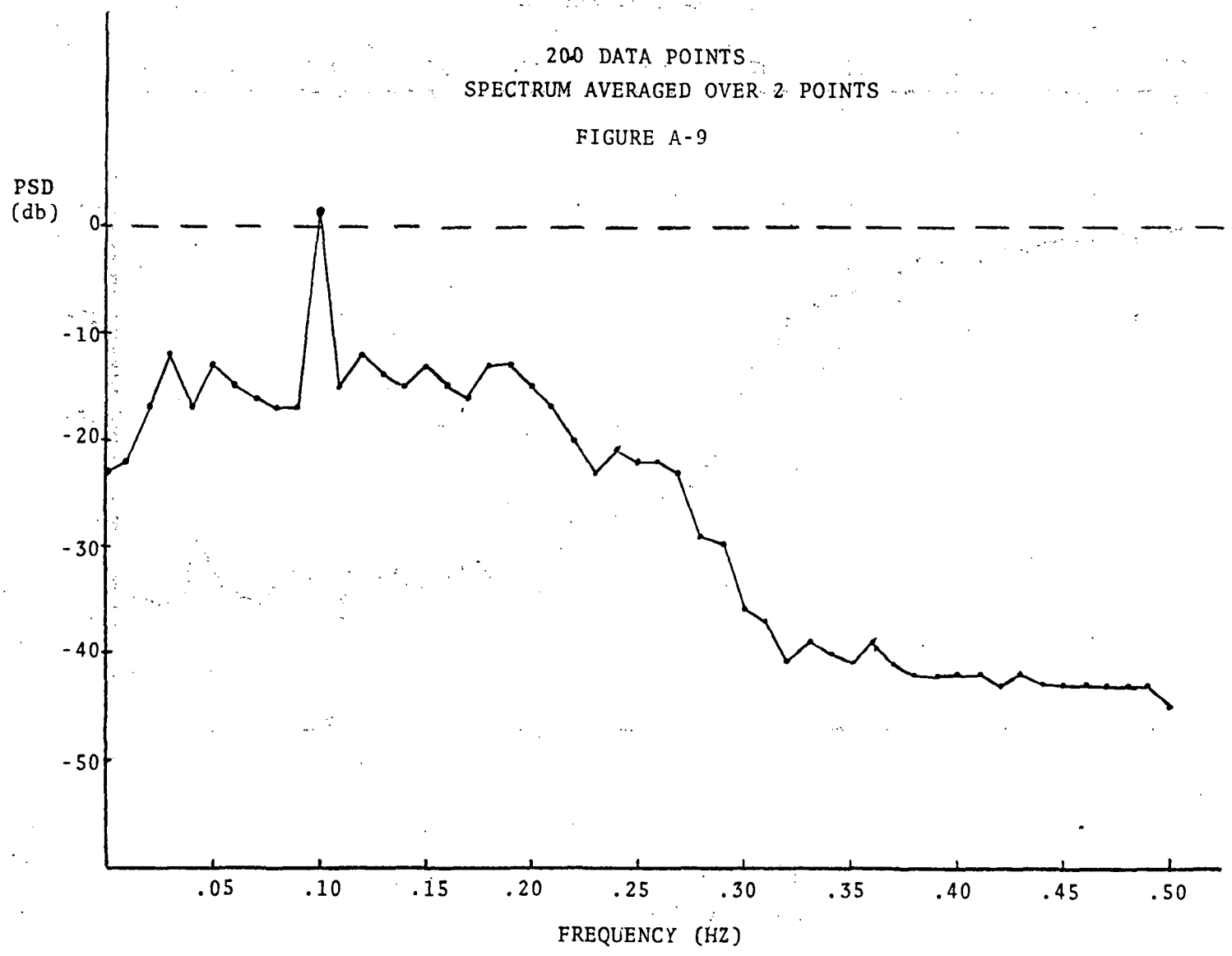

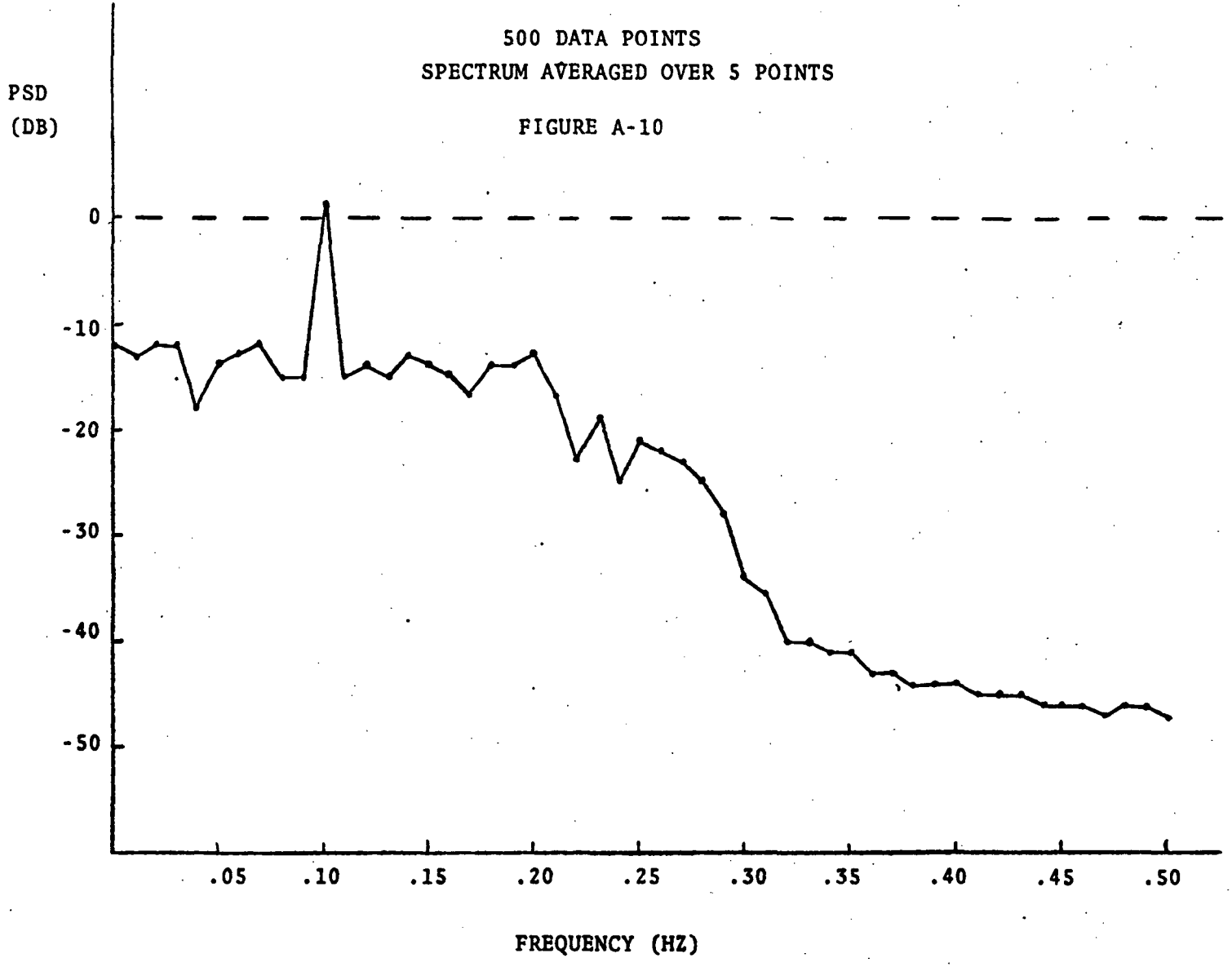
500 DATA POINTS
SPECTRUM AVERAGED OVER 5 POINTS
PSD
(DB)
0
-10
-20
-30
-40
-50
.05
.10
.15
.20
.25
.30
.35
.40
.45
.50
FREQUENCY (HZ)

FIGURE A-10

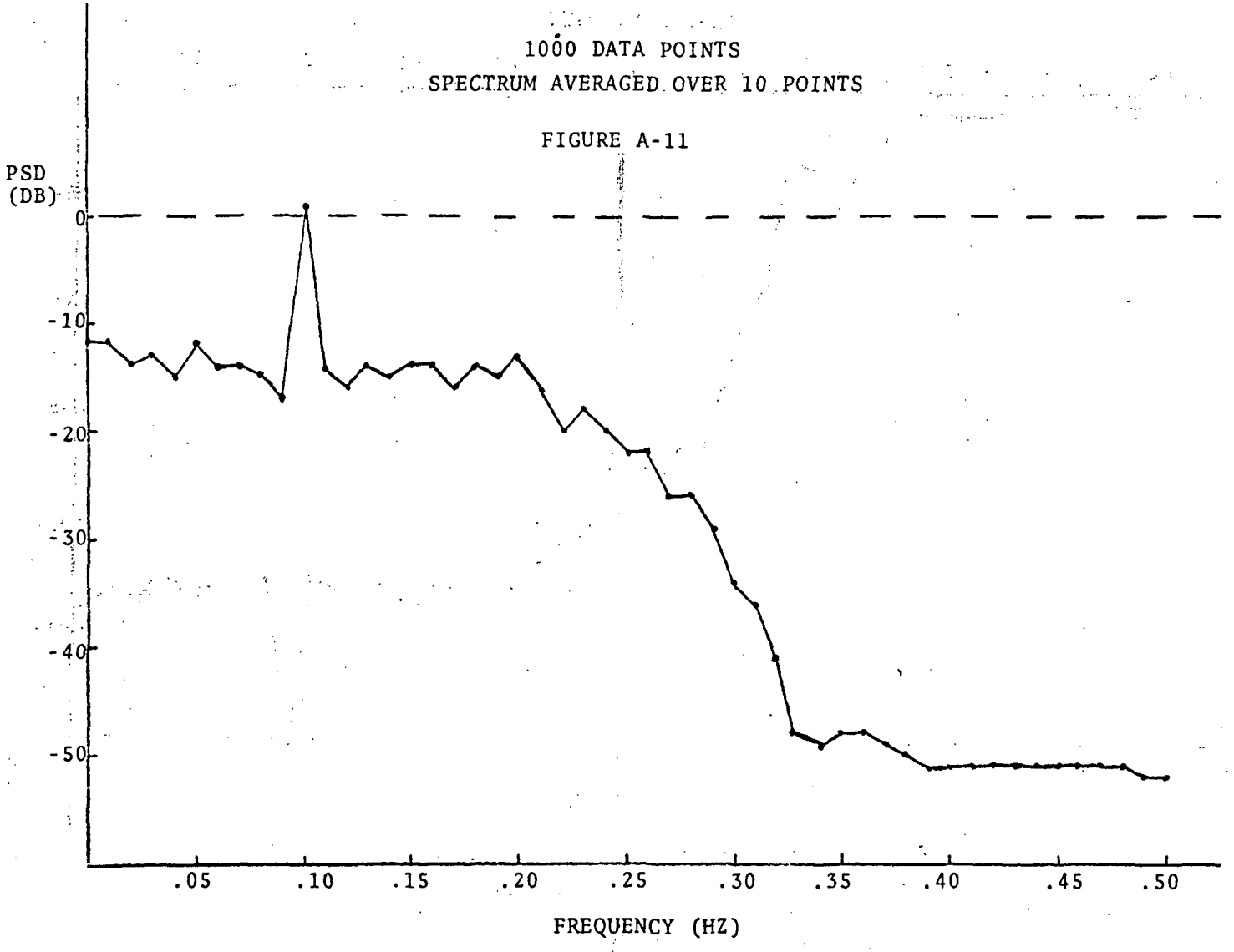
1000 DATA POINTS
SPECTRUM AVERAGED OVER 10 POINTS
PSD
(DB)
0
-10
-20
-30
-40
-50
.05
.10
.15
.20
.25
.30
.35
.40
.45
.50
FREQUENCY (HZ)

FIGURE A-11

2000 DATA POINTS
SPECTRUM AVERAGED OVER 20 POINTS

FIGURE A-12

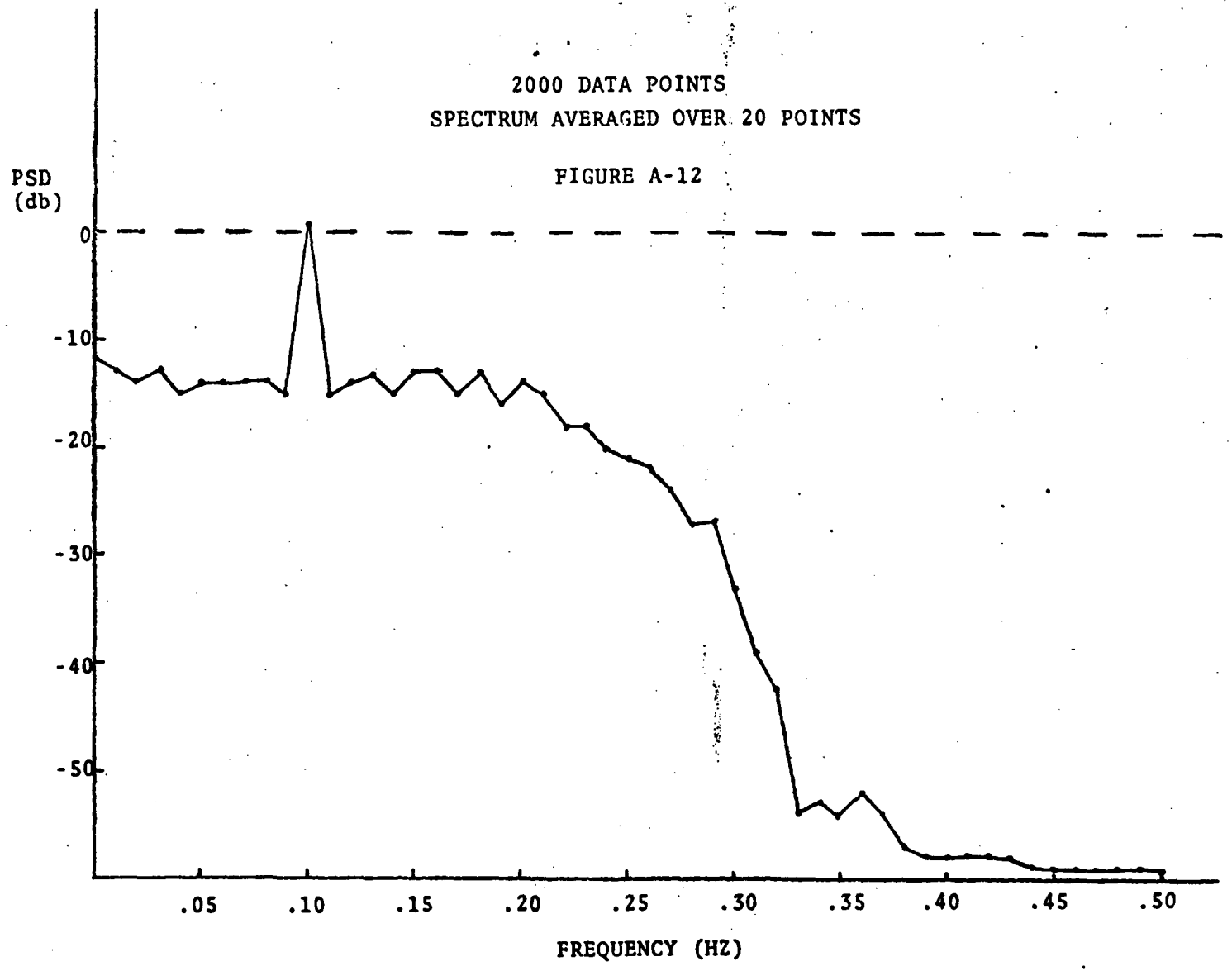

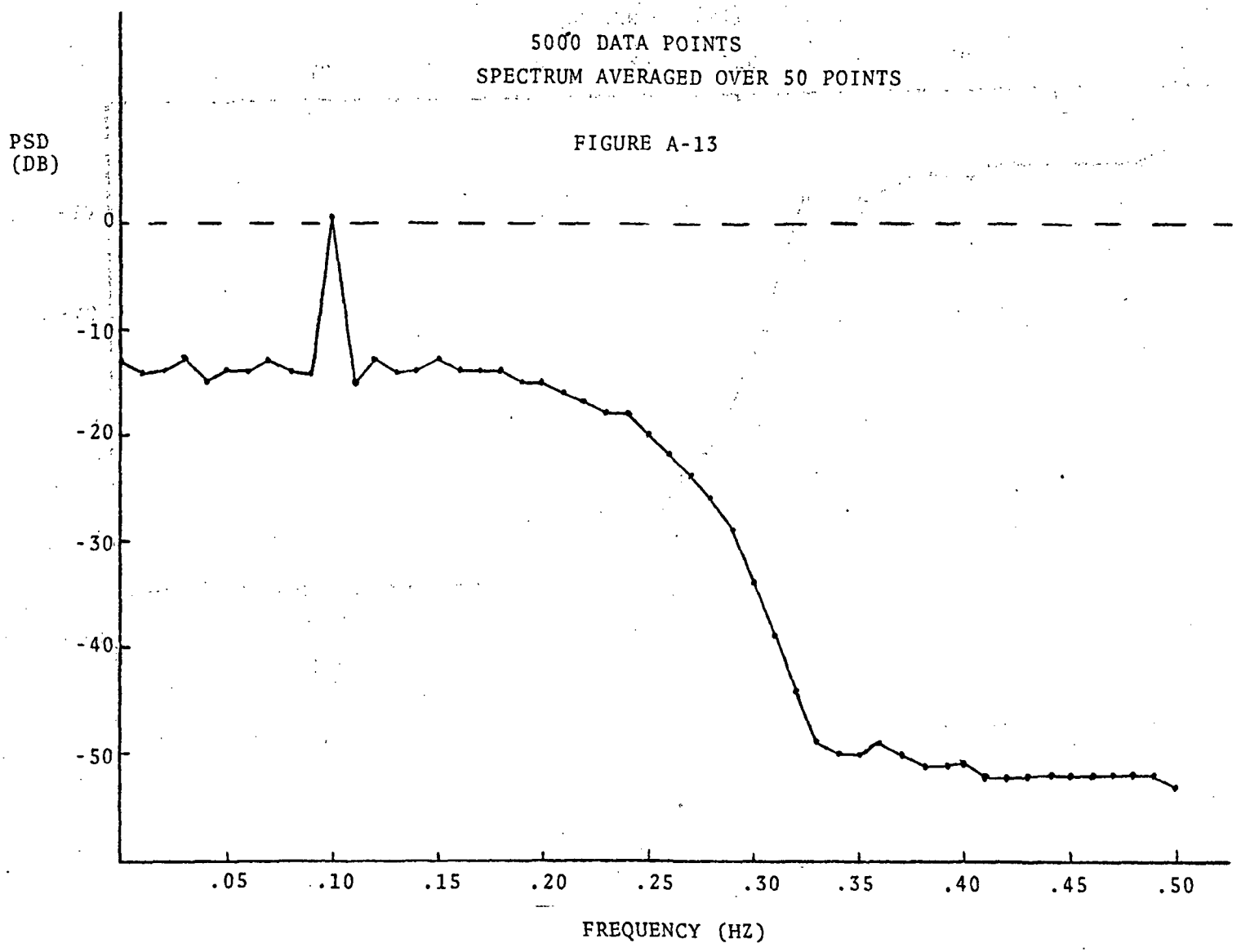
5000 DATA POINTS
SPECTRUM AVERAGED OVER 50 POINTS
PSD
(DB)
0
-10
-20
-30
-40
-50
.05
.10
.15
.20
.25
.30
.35
.40
.45
.50
FREQUENCY (HZ)

FIGURE A-13

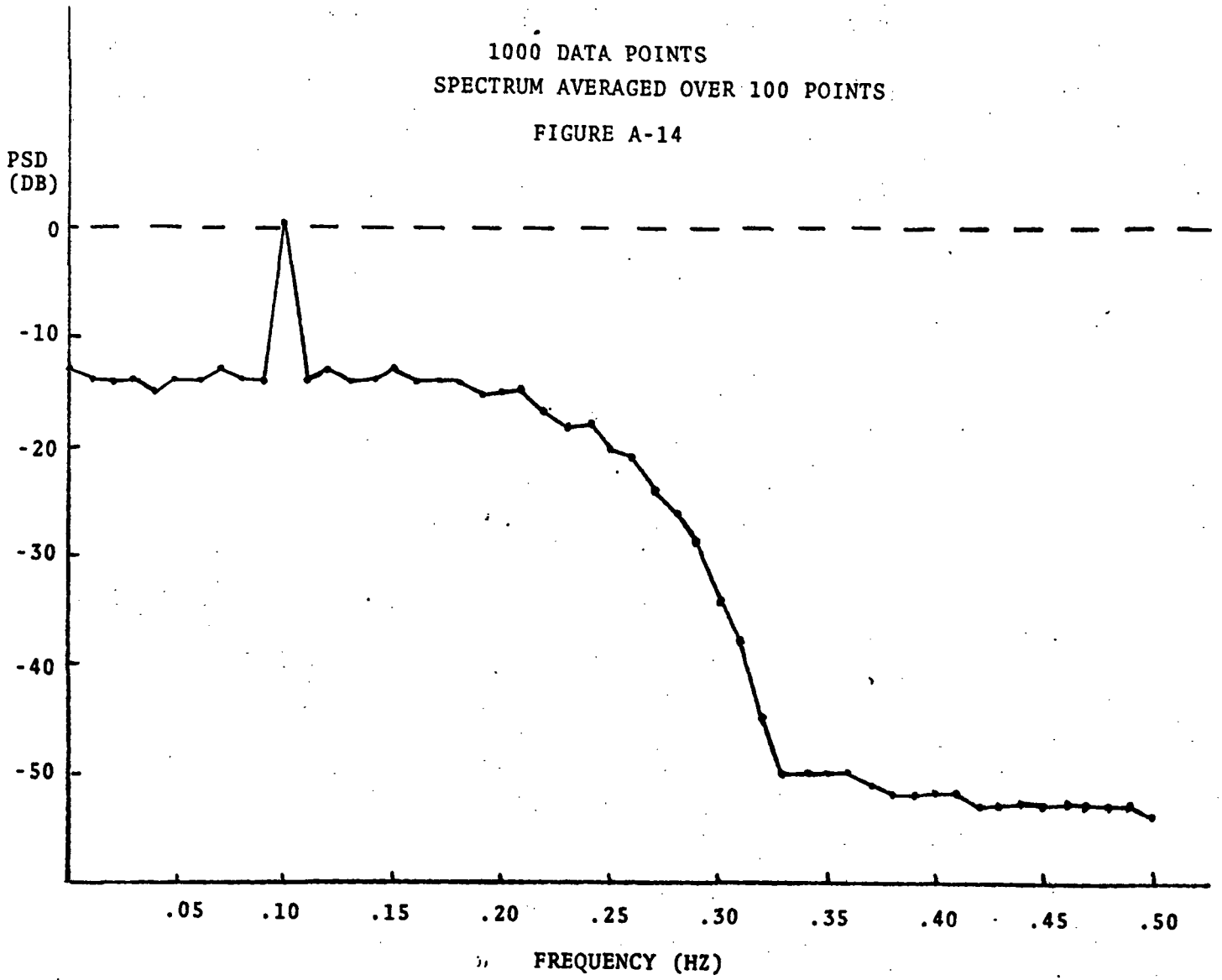
1000 DATA POINTS
SPECTRUM AVERAGED OVER 100 POINTS
PSD
(DB)
0
-10
-20
-30
-40
-50
.05
.10
.15
.20
.25
.30
.35
.40
.45
.50
FREQUENCY (HZ)

FIGURE A-14

The result, in each case, is 51 spectral points, with a frequency interval of .01 hz. The decrease in spread of the points with increased smoothing is evident. The data spread, or variance, according to theory should be inversely proportional to the number of points, M, used in smoothing. The results are in agreement with this. The frequency spike at .1 hz is not affected by the smoothing, also in agreement with theory.

These results were presented to demonstrate the effects of the linear and quadratic filtering used in obtaining the spectral density estimates and to demonstrate that the SPECDEN program performs correctly on artificially generated input data, for which the results are known from the theory. Other tests, not presented here, were conducted to validate the editing methods, the filtering methods, and the accuracy of the spectral density estimates on other combinations of artificially generated test data.

A.3 COMPACT PROGRAM

The COMPACT program has the function of preparing compacted radar data from the PASS1 raw data tapes.

A.3.1 Functional Description

The COMPACT program accepts as input a magnetic tape in the Wallops PASS1 format as given in Table A-1. The output of the COMPACT program is a tape in the same format, with filtered and compacted data. The design philosophy was that the COMPACT Program would fit into the satellite data reduction operation without requiring any change in any of the other computer programs used. The program, and its use, satisfy this philosophy. If data compaction is desired, the PASS1 raw data tape is used as input to the COMPACT Program, and an output PASS1 filtered data tape is prepared, which is used as input to the ELPRO program. If data compaction is not desired, the PASS1 raw data tape is used as input to the ELPRO program. In order to accomplish this, the following operations are performed:

a) The pre-mission calibration is written on the the output tape unchanged.

b) All tracking data before an input start time and after an input stop time are deleted.

c) The data is first filtered with a digital low pass filter.

Tape Format (output)
Mode of Writing: Binary Density: 800 BPI
Words/Record: 34
Explanation of Record:

Each word consists of 36 bits:

1	I	Run Number
2	A	Radar Number (0-11); Model Number (12-35)
3	A	Radar Mode (0-5)
4	A	Control Mode
5 & 6	DP	Time (hours)
7 & 8	DP	Azimuth (degrees)
9 & 10	DP	Elevation (degrees)
11 & 12	DP	Slant Range (feet)
13 & 14	DP	Delta Azimuth (degrees)
15 & 16	DP	Delta Elevation (degrees)
17 & 18	DP	Delta Slant Range (feet)
19	I	Azimuth Error (bits or Temp bits)
20	I	Elevation Error (bits) or Humidity (bits)
21	I	Range Rate (feet per sec x 10000)
22	I	Roll (bits) or Velocity of Propagation (feet per sec)
23	I	Pitch (bits) or Doppler Freq Counter (Megahertz)
24	I	Yaw (bits) or Transmitter Freq (Hertz)
25	I	Ship Velocity (knots) or Temp Δ
26	I	Ship Latitude (degrees x 1000) or Humidity Δ
27	I	Ship Longitude (degrees x 1000)
28	I	AGC (bits) or Calibration Number (bits)
29 & 30	DP	Elapsed Time (hours)
31	0	Milgo Aux Bits Recorded Only (0-32); R bits (33-35)
32	0	FPQ-6 Status Bits (0-29); Milgo Aux Bits Recorded and Transmitted Bits (31-35)
33	A	Azimuth Lag Correction Bit (bit 5) or Calibration Data
34	A	Elevation Lag Correction Bit (bit 5)

I = Integer
A = Alphanumeric
DP = Double Precision
O = Octal

TABLE A-1

PASS1 RECORD FORMAT

d) Every NSELth point is then selected from the filtered data and written on an output tape.

e) Each output record consists of a PASS1 record. All unfiltered (auxillary) data from the PASS1 are recorded unchanged. The items to be filtered are specified by input option, and any word on the record can be specified. Range only, or range, azimuth and elevation will usually be selected.

f) The post-mission calibration is written on the output tape unchanged.

The result is a simulated PASS1 tape, complete with calibrations, with the selected tracking data filtered and compacted.

Several secondary functions are performed on the data, as follows:

a) If a data glitch has caused the "model number" on pre-mission calibration to erroneously show post mission status, the model number is corrected.

b) The data is edited for wild points by testing the residuals of filtered data from the raw data, rejecting all data for which the residual exceeds an input multiple of sigma, and substituting the filtered data point.

c) The power spectral densities of the raw data and of the filtered data are computed and output on a printer plot, for use as a check on data quality.

d) The data residuals, filtered minus raw data, are computed and output as a printer plot.

e) A histogram of the data residuals is computed and output as a printer plot.

f) On an input option, FP9 is used to compute the periodogram and the autocovariance function of the residuals, and to output printer plots of the results.

The data selected is filtered by a non-recursive low pass digital filter. The number of filter weights (NFILT) is input, as is the cutoff frequency (TH2) in hertz. The filtered output Y, corresponding to unfiltered data input X, with filter coefficients a, is given by

$$Y_j = \sum_{i=-N}^{N} a_i \; X_{j-i}$$

where N = (NFILT-1)/2.

Using this type of filter, N points at the beginning of the data and N points at the end are lost in the filtering process. A study was made to determine the number of filter

coefficients necessary for the low-pass filter functions to be performed. The following general conclusions were reached. The details of the theory are given in Lecture 2, Reference 1.

a) Every low-pass filter has a finite transition region on the plot of gain vs frequency, between the pass-band, in which the gain is essentially unity and the stop-band, in which the gain is essentially zero.

b) The width of the transition region is inversely proportional to the number of points in the filter.

c) The cutoff frequency (the frequency at which the gain is 0.5) is the center of the transition region.

d) The number of points in the filter, NFILT, which determines the amount of data lost at each end, is inversely proportional to the cutoff frequency of the filter and to the data interval T.

data interval T.

NFILT = 6.0/(T*TH2) +1

Table A-2 summarizes the relations for T = .1 second, or 10/second data.

Cutoff Frequency (Hz)	Number of points in the filter	Data lost at each end of the filter (seconds)
1.	61	3
.5	121	6
.25	241	12
.15	401	20
.1	601	30
.05	1201	60
.0167	3601	180

TABLE A-2

RELATIONSHIP BETWEEN CUT-OFF FREQUENCY, LENGTH OF FILTER AND DATA LOST